Universitetet
i Stavanger

FACULTY OF SCIENCE AND TECHNOLOGY

MASTER'S THESIS

Study program/specialization: Petroleum technology/Reservoir technology	Spring semester, 2009 Open
Author: Andreas Byberg	…… (signature author)

Instructor: Svein Magne Skjæveland

Supervisor(s): Mailin Seldal

Title of Master's Thesis:

"Importance of Fault Communication for Predicted Snorre Performance"

ECTS: 30

Subject headings: Reservoir simulation Eclipse 100 Faults Fault seal	Pages: 144 + attachments/other: 5 Stavanger, 15.06.2009 Date/year

Importance of Fault Communication for Predicted Snorre Performance

Table of contents

List of tables

List of figures

1 Preface

The work of this thesis was performed at StatoilHydro's offices at Forus Vest in Stavanger. I want to thank StatoilHydro and the Snorre RFUT department for giving me the opportunity to write this thesis.

I want to thank Professor Svein Magne Skjæveland, who has been my professional supervisor at the University of Stavanger, for good guidance and comments during the work of this thesis.

I also want to thank Steinar Ekrann in Snorre RFUT for always taking time to answer my questions and for giving me useful comments during the work.

Finally, I would like to thank Mailin Seldal, who has been my advisor in Snorre RFUT, for contributing to the work performed in Irap RMS and for helping me with problems experienced during the simulations.

Andreas Byberg

June 2009

2 Abstract

The reservoir in the Snorre Field contains numerous faults making the reservoir very complex and challenging to model and produce. In the new models made of the field in 2006 a fault seal analysis was performed in Irap RMS. The analysis was based on fault rock properties estimated in a study undertaken by the Rock Deformation Research Group in Leeds. The aim of the analysis was to get a more realistic representation of faults in the simulation model. The models were improved, but fault transmissibility multipliers must still be applied to some of the faults to achieve a satisfying history match.

Two simulation studies were performed to investigate the impact of faults on the dynamic behaviour of the Snorre reservoir. The history matched A-Lunde reservoir simulation model was used as basis for both studies. The model's sensitivity when dividing and multiplying all modelled faults by different factors was tested. The impact on the different fault blocks in the model was evaluated. It was revealed that it is possible to obtain a satisfactory history match for RFT pressures, oil production, water production and gas production in different areas of the model, when applying different fault transmissibility multipliers. This indicates that there is large uncertainty associated with the fault communication in the model today, which will impact the predicted performance of the field. The difference in predicted oil production was largest for NCFB. In the Eastern Fault Block there were small differences in predicted performance when the fault transmissibility was multiplied by a factor 5. A prediction run until 2030 for an alternative case with modified multipliers gave an increase in oil production of 1.4 million Sm^3 for the fault blocks tested, compared with the official model.

In order to investigate the impact of different parameters affecting the flow across a fault a small segment was cut out from the A-Lu model. A qualitative sensitivity study was performed on different fault seal parameters. In addition, different geological realizations, increased throw of the fault, two algorithms for calculating fault zone permeability and the use of fault transmissibility multipliers were tested. Increasing the fault throw had major impact on the performance of the segment. Much of the oil located at the footwall side of the fault became unavailable when increasing the fault throw. The geological realization used in the model also had large effect on the oil production from the segment. One of the two realizations tested had an alternative distribution of sand in the channels and made the segment too tight in terms of communication. The other realization, where an alternative direction of the channels was used, gave dramatically reduction in the oil prodcution. The Manzocchi algorithm, used for estimation of fault zone permeability, gave the lowest pressure drop across the fault compared with the SGR-curve method and the Sperrevik algorithm. This indicates that this algorithm gives the highest fault zone permeability for the fault tested.

All parameters changed in the fault seal analysis in RMSfaultseal gave the expected effect, except the oblique slip angle and the cementation factor. Calculations performed on the oblique slip angle showed that very large fault throws and high oblique slip angles are needed to get a thicker fault zone and reduced transmissibility across the fault. Applying a value of zero for the cementation factor in the RMSfaultseal module is supposed to make the fault sealing. Simulations performed in this study revealed that this adjustment had the opposite effect and made the fault more open.

3 Introduction

Fluid flow through porous medium can be influenced by factors like faults, sedimentological facies and diagenesis. Faults are one of the most common forms of heterogeneities in a petroleum reservoir and have major impact on both reservoir performance and recovery. Faults can be restrictions to or transmitter of fluid flow and divide the reservoir into compartments having different pressure regimes and fluid properties. Faults are often modelled based on limited amounts of data. This makes the modelling of faults very uncertain and this must be taken into consideration when using the reservoir models. Collection of fault data can be done from seismic data and by studying cores drilled through faults. In addition, evaluation of analogous outcrops can give useful information about the fault rock properties.

The Snorre Field contains a very complex reservoir with numerous of faults affecting the fluid flow. A total number of 240 faults are interpreted from seismic and 129 of these faults are incorporated into the reservoir model. The large number of faults present in the Snorre Field makes the reservoir very complex and challenging to model. For the reservoir models to achieve optimal predictions of the reservoir performance, faults were given particular focus when making the new reservoir models of the field in 2006. In the previous reservoir simulation models built on Snorre the history matching was performed by adjusting fault transmissibility multipliers in the model, until a satisfactory history match was achieved. A large amount of work has been performed in order to incorporate the faults in the reservoir model in a more realistic way.

In the new reservoir models of the Snorre Field it was decided to use a more sophisticated treatment of faults in the simulation model. Rock samples from the Lunde and Stafjord formations on the Snorre and Vigdis fields were studied by the Rock Deformation Research Group (RDR) in Leeds in order to estimate the fault rock properties. The data was used as input in a fault seal analysis performed in the Irap RMS sofware to calculate fault transmissibility multipliers. These fault transmissibility multipliers were incorporated into the reservoir simulation model built in the simulation software Eclipse.

Although the fault seal analysis is giving a better history match of the model there are a lot of uncertainties associated with the analysis. Estimation of factors like fault permeability, fault throw and distribution of clay along the fault planes is difficult. Still fault transmissibility multipliers must be applied in order to obtain a satisfying history matching of the models.

A simulation study has been performed on the history matched A-Lu model to investigate the sensitivity on history matching and predicted performance of the field, when applying different fault transmissibility multipliers to the faults. In addition, a small segment was taken out of the large scale A-Lu model to investigate how different fault seal parameters affect the performance of the segment. SGR – curves, brittle factor, increased fault throw and changing geological realization were some of the parameters tested.

4 The Snorre Field

4.1 Introduction

The Snorre Field was discovered in 1979 by the exploration well 34/4-1, and is located in blocks 34/4 and 34/7 in the Norwegian North Sea (Figure 4-1). Two drilling and production facilities, Snorre A and Snorre B, are installed at the field today. Production start of the field was in 1992 when Snorre A was set into production. In 2001 Snorre B was also set on stream. After being operated by both Saga Petroleum ASA and Norsk Hydro ASA, Statoil became the operator of the Snorre Field at year-end in 2002 in a process where Statoil became sole operator in the Tampen Area [25].

The producible part of the Snorre reservoir consists of the Lunde Formation and the Statfjord Formation comprising more than 1000 m of fluvial sandstones. Volume estimates indicate that there are 513 MSm^3 Stock Tank Oil Original In Place (STOOIP) and associate Gas Initial In Place (GIIP) of 52 GSm^3. The reservoirs at the Snorre Field contain light under saturated oil and the main reservoir drainage strategy of the field is water injection, gas injection and water-alternating-gas injection. Currently, a total number of 120 wells (13 exploration and 107 production/injection wells) have been drilled at the Snorre Field [25]. The field is containing the largest remaining reserves of the fields operated by StatoilHydro on the Norwegian Continental Shelf.

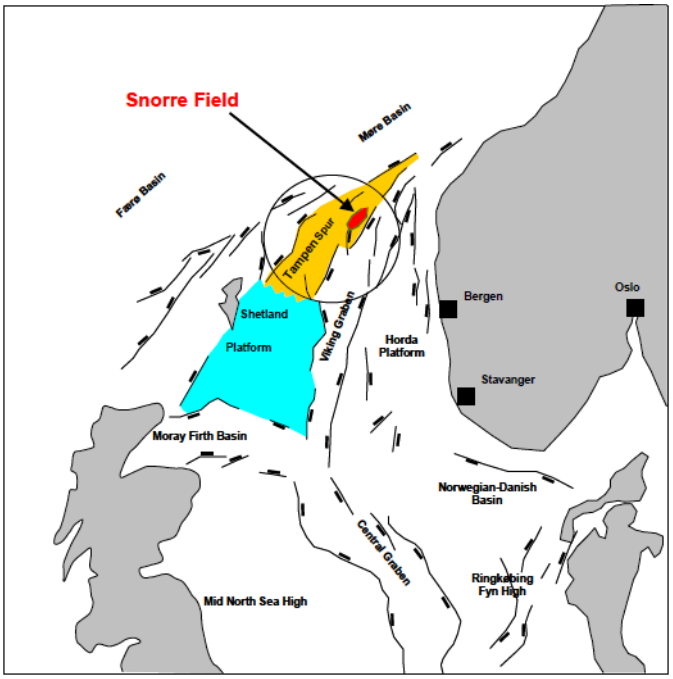

Figure 4-1 Location of the Snorre Field [25]

4.2 Reservoir Location

The Snorre reservoir is located in the north-eastern part of the East Shetland Basin, or more specific, within the northern crest of the Tampen Spur (Figure 4-1). The Tampen Spur is a major structural height at age from Jurassic to early Cretaceous and it consists of many large west to north-westward rotated fault blocks located between the Viking Graben to the east and south-east and the Møre Basin in north and north-west. Other giant fields, like Statfjord and Gullfaks, are also situated at the Tampen Spur. The Snorre Fault Block includes both the Snorre Field and the Tordis and Vigdis fields [25].

4.3 Structural Setting

A series of major faults following a NNE-SSW structural trend characterizes the Snorre structure. These major faults are the Murchison Fault, the Outer Snorre Fault (OSF), the Central Snorre Fault (CSF) – delineates the WFB and CFB fault block and the Inner Snorre Fault (ISF). There are numerous of E-W and SE-NW striking faults within the Snorre Field that makes the reservoir very complex. “These faults, together with a third set striking N-S and NNW-SSE, with throw towards the east, divide the NNE-SSW trending fault-blocks into minor fault compartments. This is shown in the geological structural cross-section for the southern part of the field (Figure 4-2)” [25]. The Snorre Field consists of a total number of nine rotated faults blocks. All of the fault blocks are eroded by the Base Cretaceous Unconformity (BCU) [32].

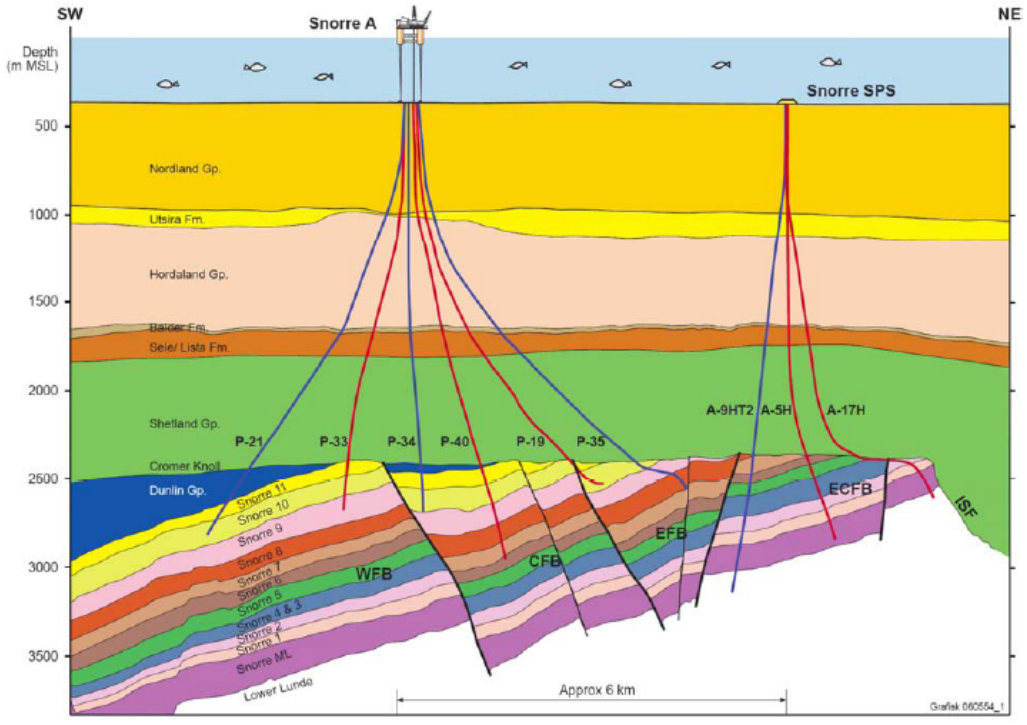

Figure 4-2 SW to NE cross -section through the southern part of the Snorre Field [23]

4.4 Reservoir Description

The reservoir rock in the Snorre Field consists of the Triassic Lunde Formation (Lunde Fm.) and Triassic-to-Early-Jurassic Statfjord Formation (Statfjord Fm.). The Middle and Lower Lunde Fm. do not contain hydrocarbons on the Snorre Field. Both the Upper Member of the Lunde Fm. and the Statfjord Fm. are present in the western, southern and central parts of the Snorre Field. In the northern and eastern part of the field the Base Cretaceous Unconformity (BCU) truncates the Upper Member of the Lunde Formation and the Statfjord Formation [25].

The Upper Member of the Lunde Fm. (SN1-SN10.3)
This formation is built up of interbedded, medium grained, white, pink or grey channel belt sandstones. The sandstones are again interbedded with red brown to green caliche-rich siltstones and mudstones of continental origin. In the stratigraphic model of the Snorre reservoir the Upper Member of the Lunde Fm. is divided into 10 main reservoir zones (SN1-SN10.3). These zones are divided into smaller subzones. The Upper Lunde Member shows a general decreasing trend of the net/gross value upwards [25].

The Statfjord Fm. (SN10.3-SN11)
This formation consists of more carbonaceous silt and mudstones, which implies a more coastal plain depositional setting. In the stratigraphic model the Statfjord Fm. is divided into one main reservoir zone (SN10.3-SN11). In the Statfjord Fm. there is an increasing net/gross upwards with dominantly meandering fluvial sequences passing upwards into braided stream deposits. The sandstones in the Statfjord Fm. have in general coarser grains than observed in the Upper Lunde Member [25]. There are changes in lateral thickness in the middle to upper part of the Statfjord Fm. This is assumed to be a result of renewed minor pulses of tectonic activity and differential subsidence and uplift with local incision [9].

Figure 4-3 illustrates the depositional environment in the different zones.

4.4.1 SN1-SN7: Braided Channel Systems on Upper Alluvial Plain

The zones SN1-SN7 consist of channel sandstones that are, most likely, deposited in braided shallow channels. The sandstones have varying size vertically but most of them are in the fine to medium range. Fining upwards units, vertically stacked sandstone bodies and coarse grained channel – lags are common in these zones. Some of the sandstone bodies have thicknesses of more than 20 m as a result of vertical stacking of channel bodies. Individual sandstone bodies deposited in a channel can have thickness in the range of 8 – 10 m, although a thickness range of 4 – 7 m is the most common [25].

4.4.2 SN8-SN10: Meandering Channel and Distributary Channels on Lower Alluvial Plain.

The channel sandstones in SN8 – SN10 are interpreted to be deposited in an environment dominated by meandering and distributary channels. The meandering channels have high sinuosity and deposit much of the bed load at the inside of the meander loops, where point bars are formed. Point bars form the most important sandstone depositional element on an alluvial plain where meandering rivers are flowing. Lateral migration of the channel will cause a characteristic fining up log profile of a point bar. Sandstones deposited as point bars will have thicknesses of more than 7 meters, but thicknesses exceeding 13 meters are also common [25].

The main channel on the lower alluvial plain tends to split into several distributary channels when it is approaching the upper delta plain. The distributary channel sandstones are characterized by low sinuosity and have thicknesses in the range 4 – 8 m. The distributary channels occur frequently in the upper part of SN9 (SN9.3 and SN9.4) and SN10 (SN10.2, SN10.3 and SN10.4) [25].

4.4.3 SN11: Coastal Plain

The Statfjord Formation (SN11) consists of high permeable lateral extensive sandstones. The sandstones are expected to be deposited on the coastal plane, with a depositional environment including embayment deposits, coastal plain channels, crevasse splays and paleosoils. It is assumed that both fluvial and tidal processes deposit and rework the sediments [25].

The sediments have a dominating grain size range from medium to coarse grained. The upper parts of the Statfjord Formation (SN11.3 – SN11.4) contains the coarsest sandstones. In the lower Statfjord Formation (SN10.4, SN11.1 and SN11.2) the sediments have finer grained paleosoil sediments [25].

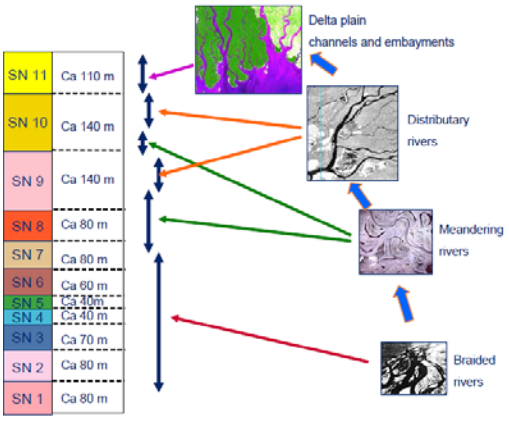

Figure 4-3 Depositional settings in the different Snorre zones [modified 25]

4.5 Reservoir Properties

In Table 4-1 and Table 4-2 the initial reservoir conditions and the average petrophysical properties of the Snorre reservoir is given. Figure 4-2 reveals the high differences in reservoir properties for the different zones.

Initial reservoir condtions			
Statfjord/Lunde	Datum depth	2475 m TVD MSL	
	Datum pressure	383 bar	
	Datum temperature	90 Deg. C	
	Oil gradient	0.065 bar/m	

Table 4-1 Initial reservoir conditions of the Snorre Field [modified 25]

	NTG (%)	*PHID (%)*	*PERM* (Aritm. avg) mD	*PERM* (Geo. avg) mD
SN 11	36	24	2423	327
SN 10	21	24	193	33
SN 9	27	25	189	38
SN 8	42	24	na	na
SN 7	44	24	620	139
SN 6	47	23	346	43
SN 5	47	25	1110	120
SN 4	52	24	178	16
SN 3	56	25	694	155
SN 2	54	25	817	125
SN 1	64	25	914	251
SN ML	21	21	134	40

Table 4-2 Petrophysical properties of the Snorre Field [modified 25]

5 Reservoir Simulation

5.1 Introduction

Today, models are widely used to describe processes and obtain a better understanding of physical phenomena. In reservoir engineering both *physical* and *numerical* models are used. Physical models are based on measurements performed on rock and fluid samples from small parts of the reservoir. Such models will have their limitations because they cannot represent a whole petroleum reservoir. To model such a large-scale system as a petroleum reservoir usually a mathematical approach must be applied to give a representative picture. Mathematical equations are used to model the physical system and numerical methods are used to solve the equations. These kinds of models are often referred to as numerical models. By using large computers and advanced software most of the processes in a reservoir can be modelled. A reservoir simulator is a computer program written to solve the fluid flow equations in a reservoir [15].

A reservoir simulator is the most important tool for a reservoir engineer to predict the performance of a reservoir. The simulation model integrates disciplines like geology, geophysics, production and drilling, petrophysics and surface facilities to give the most representative results. The reservoir simulator can be used to plan the target of new wells, forecast production and pressure depletion and make long term strategies [15]. It is important for a reservoir engineer to be aware of the limitations of the reservoir simulation model. The model consists of a large amount of input data, each associated with uncertainty. It is important to take this into consideration when analyzing the results of the simulations.

History matching is performed on the reservoir simulation model to ensure that it matches the reality. Modifications must often be performed to the model in order to match measured data like production rates, pressures, etc [15].

Reservoir simulators are categorized after the type of reservoir they are intended to simulate. The most common model in the petroleum industry is the *Black Oil model*. The reservoir simulation model of the Snorre reservoir is a Black Oil model. A Black Oil model is based on the following assumptions:

- Three phases; oil, gas and water
- Three components; oil, gas and water
- No mass transfer between water and hydrocarbons
- A part of the gas component can exist in the oil phase and flows together with the oil component
- No oil component exist in the gas phase, which means that all of the oil component will exist in the oil phase

- Constant temperature [15].

Other types of reservoir simulators like compositional models, chemical flood models and thermal models will not be given further comments in this thesis.

The basic equations in a reservoir simulator are differential equations for mass balance and numerical techniques must be applied to solve the equations. The solution will give vital information about the reservoir performance. In order to solve the differential equations some transformations of the differential equations must be performed. By using difference approximations the reservoir is divided into grid blocks and the basic differential equations are replaced by algebraic equations for each grid block. These algebraic equations are not linear and linear approximations are used to linearize them. The Newton-Raphson method is often used in this linearization process. When all these steps are performed both direct and iterative techniques can be used to solve the linear equations [15].

Deduction of the mathematical equations behind a Black Oil model can be found in references 3 and 15.

5.2 History Matching

5.2.1 Introduction

The history matching process is maybe the most important part in a reservoir simulation study. The main objective with the history matching of a reservoir simulation model is to make the model satisfy measured data within some specified uncertainties. In this way it is possible to maintain the model updated. If there is difference between measured data and predicted data from the simulator, input data (seismic interpretation, geological model, fault seal, relative permeability, PVT, etc.) must be changed in order to obtain a satisfactory history match [1].

Matching predicted results from the reservoir simulation model with historical performance is the only practical way to check the validity of the model. The history matching can be a time consuming task and often manually adjustments of data through a trial-and-error method are required. A general rule is to change the parameters which will have the largest uncertainty and at the same time largest influence on the solution [3].

According to StatoilHydro's "*Best practice 3D reservoir modelling*" a history matching process can be divided into the following steps:

- Preparation of input data with uncertainty
- History matching procedure
- Quality control of results

A successful history match results in an improved quality reservoir model which is of fundamental importance in predictions, well planning, reservoir uncertainty analysis and reservoir management studies [1].

5.2.2 Input data

History matching requires data from many different technical disciplines like geologists, petrophysicist, geophysicist and production engineers. Petrophysical properties, SCAL data, well completion details, production data and fault properties are some of the data that are modified to achieve a satisfactory history match. Some of the historical data typically used in history matching are listed in Table 5-1 [1].

Data type	*History match to*
Pressure data	Formation pressure versus depth (RFT,MDT)
	Flowing bottom-hole and well-head pressures
	Shut-in pressure (pressure build-up)
	Average reservoir pressure
Log data	PLT measurements (production logs)
	Open-hole logs
	Fluid saturation profiles from well logs
Production data	Historical production/injection rates and cumulatives
	Well tests (DST, production test)
	Well productivity data
Well chemistry data	Scaling/contamination data
	Ion concentrations (formation or injection water?)
	Tracer data
Seismic data	Time lapse (4D seismic)
Rock mechanics	Compaction of the reservoir

Table 5-1 Historical data typically used in history matching [modified 1]

5.3 Prediction

When a satisfying history match is achieved the model can be used to run predictions for future behaviour of the reservoir. These predictions are extremely important because many major decisions, like planning new wells, upgrading facilities and the lifetime of a field are based on them. It is important to be aware of the limitations of a reservoir model. The model is based on input data associated with high uncertainty and only represents an approximation of what is most likely to happen in the reservoir. It is not possible obtain the “correct” model. Often different predictions of the model are run, based on different sensitivities of important parameters like fault communication or geological realization. There are then run predictions for the “best” and the “worst” case in order to find the limits of the uncertainty.

6 Faults and Fault Seal

6.1 Introduction

In its simplest form a fault can be defined as a planar fracture in rock where the rock on one side of the fracture has moved with respect to the rock on the other side of the fracture [37]. Such movements are initiated when rock or rock layers are subjected to tectonic stress. Faults are one of the most common forms of heterogeneities in a reservoir. A fault can influence several processes in the reservoir, like being a transmitter of or barrier to fluid flow and pressure communication [5].

Since faults in most cases are restrictions to fluid flow they often cause reduced petroleum production. Faults can be classified as static or dynamic, depending on the sealing capacity [9]. The fluid conductivity across faults can have a major effect on the oil and gas recovery from a reservoir. A sealing fault will prohibit fluid flow and pressure communication with other regions. Conductive faults can give pressure support by allowing fluid transfer along and across their planes [14]. A fault that has the capacity to maintain a pressure drop over million of years (geological time scale) is classified as static, while faults that can maintain a pressure drop only over the life-time of a field (5-100 years) are classified as dynamic [9]. The permeability in the fault zone can differ from the host rock with several orders of magnitude. In most reservoirs faults will have so much impact that they must be taken into consideration for evaluation, production planning and reservoir modelling [31].

In some cases sealing faults can transform large and continuous hydrocarbon reservoirs into smaller compartments. Each of these compartments can behave as a reservoir and may have their own pressure regime and fluid properties. Such complex reservoirs can be extremely challenging to produce in an effective way with regards to recovery and economics. Also in-fill drilling of new wells can be very challenging in complex reservoir because different parts of the reservoir can have very large differences in pressure [5].

To generate a representative model of fluid flow in a reservoir it is very important to gain detailed insight into the evolution, structure and properties of faults [18]. The most common way to incorporate fault-rock properties in a reservoir flow simulator is to apply fault transmissibility multipliers. The use of transmissibility multipliers will cause a great uncertainty in the estimation of reserves in the reservoir. Transmissibility multipliers are numerical devices based on properties, like fault permeability and fault thickness, that are very difficult to get good estimates of [21].

6.2 Basic Fault Material

This section provides some basic background material to fault terminology and fault processes.

The two sides of a non-vertical fault are often called the *hanging wall* and the *footwall* (Figure 6-3), where the *hanging wall* is positioned above the fault plane and the footwall below the fault [37].

Slip can be defined as “the relative movements of geological features present on either side of the fault plane” [37]. Faults can be divided into different types based on the type of slip [37].

The fault *throw* is simply the vertical movement, while the *heave* is the measured horizontal offset (Figure 6-1) [37]. The *displacement* of the fault is movement along the fault plane (Figure 6-1).

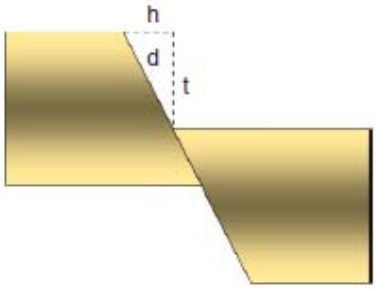

Geometry of a dip-slip normal fault displacement:
h - heave
t - throw
d - displacement

Figure 6-1 Illustration of heave, throw and displacement [1]

When a fault is slipping a zone of deformation referred to as the *fault zone* is developed along the fault plane. The *fault zone* will contain *fault rocks* with properties that differ from those of the host rocks [14]. The zone of deformation will also have a measurable thickness called *fault zone thickness.*

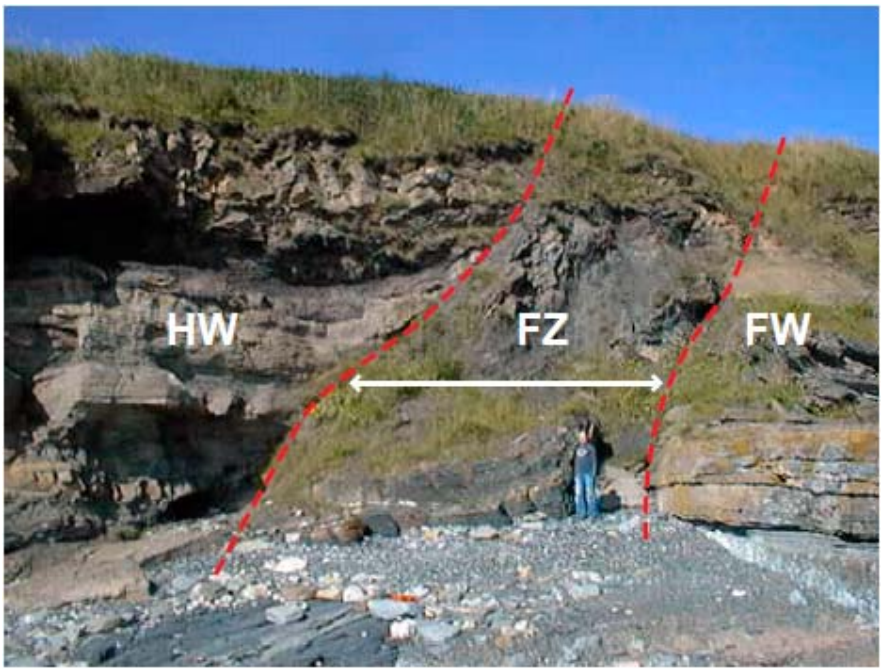

Figure 6-2 Outcrop showing the fault zone (FZ) [1]

6.3 Fault types

Faults can be divided into three different groups based on the sense of slip. The three groups are *dip – slip faults*, *strike slip faults* and *oblique-slip faults* [37]. A short introduction to the three fault types will be given in the next sections.

6.3.1 Dip – Slip Faults

In dip – slip faults the main sense of movement on the fault plane is in the vertical direction. Dip – slip faults can be divided into *reverse faults* and *normal faults*. Normal faults are created when the crust is extended and the hanging wall will move downward relative to the footwall (Figure 6-3) [37]. These types of faults are the most common in hydrocarbon reservoirs.

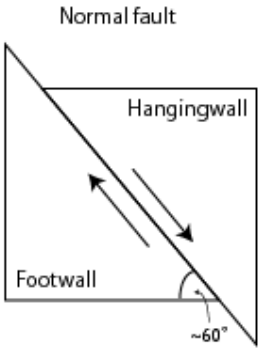

Figure 6-3 Illustration of a normal fault [37]

Reverse faults are the opposite of normal faults and the hanging wall moves relative to the footwall (Figure 6-4). Reverse faults occur when the crust is shortened and will have relatively steep dips (more than 45°) [37].

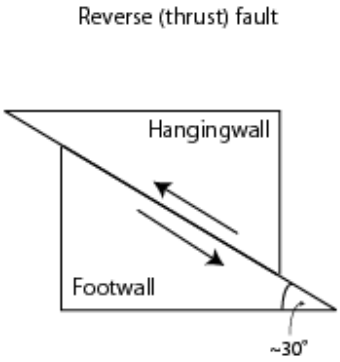

Figure 6-4 Illustration of a reverse fault [37]

6.3.2 Strike – Slip Faults

A *strike – slip fault* has a fault surface that is nearly vertical. The footwall move either left or right or laterally and the displacement in vertical direction is close to zero. Strike – slip faults with left lateral motion is often called *sinistral* faults, while those with right lateral movement are called *dextral* faults (Figure 6-5) [37].

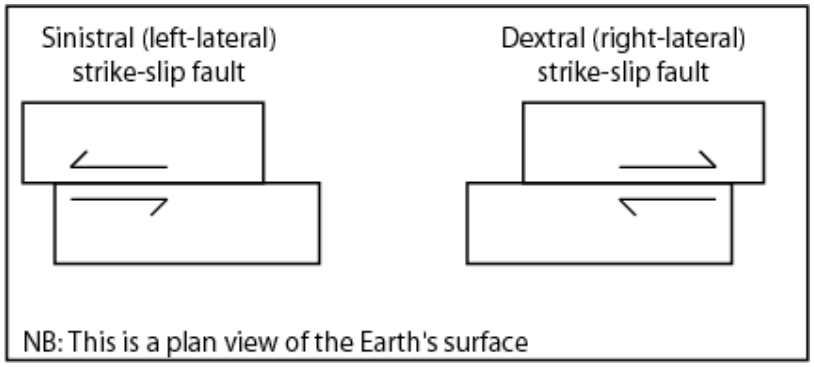

Figure 6-5 Illustration of the two types of strike-slip faults [37]

6.3.3 Oblique – Slip Faults

An *oblique – slip fault* has both a component of dip – slip and a component of strike – slip. Almost all faults will have some component of both dip – slip and strike – slip. For this reason it is required that both components are of significant magnitude when defining a fault as an oblique – slip fault [37].

6.4 Fault Seal

Fault seal is a fault's ability to prevent fluid from flowing across it. When a fault is created a zone of complex deformation is developed along the fault plane. This zone of deformation has properties that differ from those of the host rocks and is often referred to as the fault rock. The fault rock has often reduced petrophysical properties, like permeability and porosity, compared to its host rock [14].

Many factors like fault architecture, throw distributions, lithologies, fault rock distributions and properties will influence the fault seal. Also the fault history like the burial history, deformation timing and hydrocarbon charge history is important when predicting the sealing capacity of a fault [5].

Fault seals can be characterized as membrane seals or hydraulic seals, depending on their likely failure mode. Membrane seals are fault rocks with high capillary entry pressure, caused by factors like smear, cementation and cataclasis, and will fail when the capillary entry pressure (pressure required for hydrocarbons to enter the largest interconnected pore throat of the seal) of the rock is reached [12, 35]. When a fault has hydraulic seal the entry pressure must exceed the strength of the rock to break the seal [35].

Many mechanisms have been recognized whereby fault planes can act as seals. The two most common are juxtaposition seal, where reservoir sand are juxtaposed against a non-

reservoir rock and clay smear where impermeable clay/shale is incorporated to the fault plane (Figure 6-6) [33, 35]. It is important to be aware of that the sealing capacity of a fault is not constant over the entire area of the fault surface. The sealing capacity tends to vary as the juxtaposed stratigraphy changes laterally and vertically along the fault plane [16].

Today fault seal analysis is often performed in order to predict the sealing properties of faults in a petroleum field. Different data like seismic, structural and micro structural information from high resolution core analysis and wellbore and production data are utilized in these analyses [5]. Often sophisticated modelling software, like RMS for instance, are used to give a best possible representation of the sealing properties of the fault.

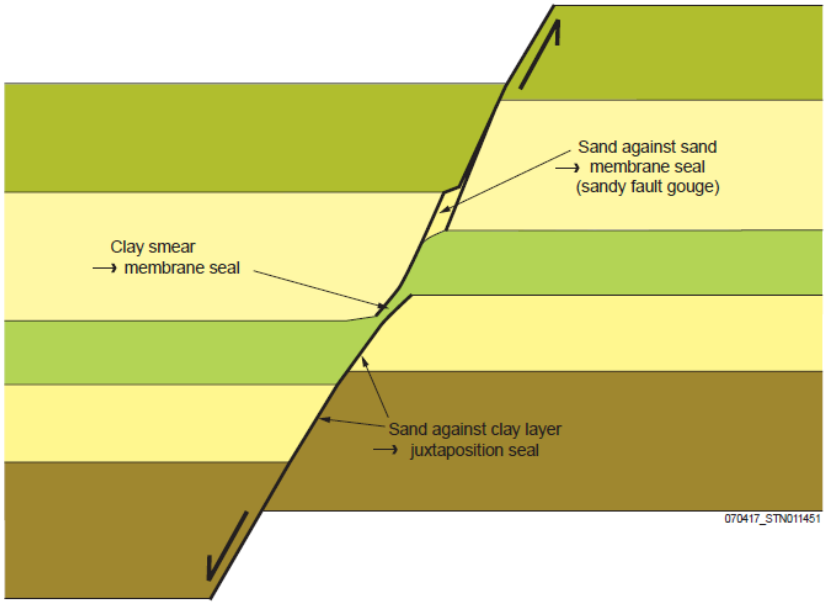

Figure 6-6 The two most common fault seal types [1]

6.4.1 Clay or Shale Smear

Incorporation of clay or shale into fault zones is one of the most common forms of fault seals in clastic sequences [14]. Shale or clay contains very small pore throats and forms an extremely good capillary seal and permeability barrier to fluid flow [13]. Clay smear may occur when a shale layer is offset by a fault throw larger than the vertical thickness of the layer [31]. The clay is smeared along the fault plane possibly making a membrane seal or hydraulic seal [35].

It is very difficult to estimate the presence of and distribution of clay smear along fault and the estimation is associated with very high uncertainty. The smears are below seismic resolution and cores and logs from wells drilled through faults are often of limited quality [31].

There are mainly three ways in which shale can be incorporated in the fault zone. The three ways are shearing, abrasion and injection, where abrasion smears are the most common. Abrasion smears are created when a shale layer slips past a sandstone unit. Then a thin and uniform shale veneer will be created on the sandstone surface. Shearing occurs when shale layers are dragged normally towards the fault. Injection takes place when variable displacement along the fault results in volume changes adjacent to the fault. Lithified clay can be injected into these volumes [31].

The likelihood of clay/shale smear is controlled by some factors like the thickness of the source bed, distance from the source layer and throw. A thick source bed will give a thick clay smear. Also the distance from the source layer will have impact because shear-type smears have reducing thickness with the distance away from the source bed. Abrasion-type smears will decrease in thickness with increasing throw [31]. A study of faults in the North Sea from 1993 concluded that the great majority of faults with a throw larger than the thickness of the reservoir interval were sealing faults [19].

6.4.2 Algorithms for Predicting Clay Smear

6.4.2.1 Introduction

Estimation of the clay content/distribution along the fault plane is very important in a fault seal analysis. This parameter gives information about the sealing properties of the fault. Different algorithms have been developed to estimate the clay distribution. They are often divided into two categories:

- Algorithms that estimate the continuity of clay smears
- Algorithms that estimate the actually clay content of the fault gouge [9].

The two most used algorithms for estimation of continuity of clay smears are the *Clay Smear Potential (CSP)* and the *Shale Smear Factor (SSF)*. For estimation of the actual clay content the *SGR (Shale Gouge Ratio)* is the most used [9]. Gouge ratios can actually be calculated for any impermeable material that can be incorporated into the fault zone. This impermeable material is often clay or shale and is thereby referred to as the shale gouge ratio [10]. The three algorithms for prediction of clay smear are not completely independent since all of them relate to the amount of clay in the sequence [34].

Deciding which algorithm to use for fault seal prediction depends on the available lithological data and the format of the input data. CSP and SSF require define of each individual shale

bed [31, 34]. The SGR method can in addition to this use zonal average of volumetric shale fraction and give a prediction of the fault zone composition [34].

6.4.2.2 Shale Smear Factor (SSF)

The SSF can be defined by the following relationship (Figure 6-7)

$$SSF = \frac{Throw}{Thickness(\Delta z)}.$$

The shale smear factor is based on studies of lithified shales. Empirical studies of shale smear has concluded that continuous clay smear can be expected if SSF<7 and is most likely to occur if SSF$\leq$ 11. If SSF>30 a composite type of smear is expected [31]. Figure 6-8 shows a general rule, established based on a field study, to determine if the clay smear is continuous or discontinuous.

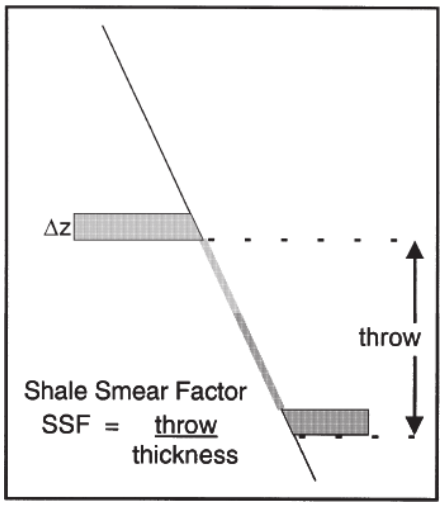

Figure 6-7 The SSF algorithm [35]

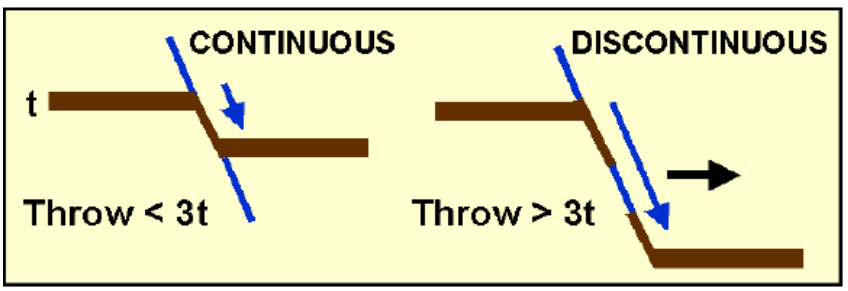

Figure 6-8 General rule for determination of where a clay smear is continuous or discontinuous [9]

6.4.2.3 *Clay Smear Potential (CSP)*

The CSP is be defined by the following relationsship (Figure 6-9)

$$CSP = \sum \frac{Thickness^2}{movement}$$ [35].

CSP is based on study of ductile clays and is a similar method as the SSF for estimation of clay smear potential [31, 34]. The clay smear potential represents “the relative amount of clay that has been smeared from individual shale source beds at a certain point along a fault plane” [11]. CSP will increase with the shale source bed thickness and decrease when the fault throw becomes larger. The larger the number of source beds displaced past a particular point along a fault plane, the larger the CSP will be [11].

The values of SSF and CSP can be calibrated by examining fault rocks or production data in the field to determine when the clay smears are becoming discontinuous. A specified value is used as a limit to differ between continuous and discontinuous clay smears [9].

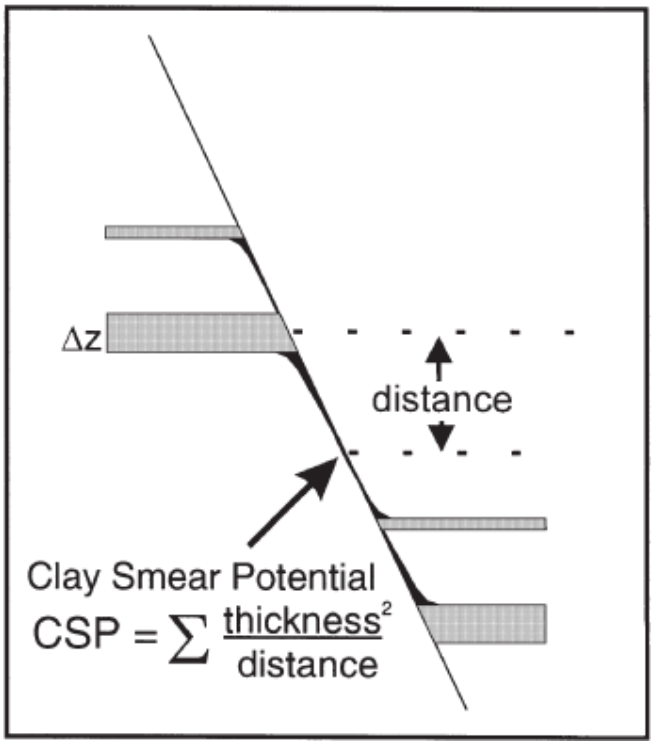

Figure 6-9 The CSP algorithm [35]

6.4.2.4 Shale Gouge Ratio (SGR)

The shale gouge ratio algorithm is a method to predict the proportion of shale material in the fault zone. SGR method calculates the net content of shale/clay in the volume of rock that has slipped past that point on the fault (Figure 6-10). The calculation is performed on each point of the fault. The SGR algorithm is based on the implicit assumption that “material is incorporated in the fault gouge in the same proportions as it occurs in the wall rocks in the slipped interval”. This assumption means that the SGR can provide a direct estimate of the up scaled composition of the fault zone and be converted to permeability by using experimental data on permeability for fault gouges with varying clay content and geological history [31,34].

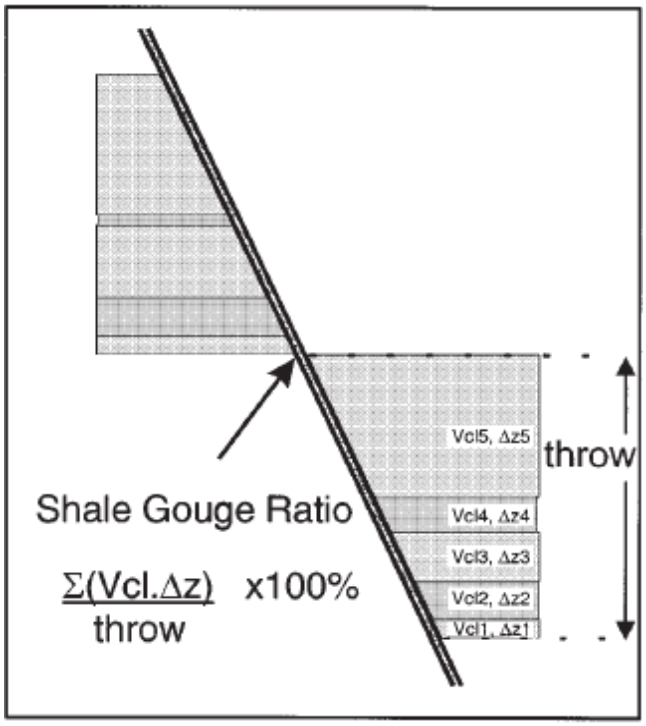

Figure 6-10 The SGR algorithm [35]

6.4.3 Fault Zone Architecture

Faults rarely occur as single slip-surfaces. The fault zone architecture is often very complex. The complexity depends on many factors like the lithology of the host rock, the deformation history (temperature, pressure, stress conditions and strain rate) and deformation mechanisms. The fault zone will have different structural, mechanical and petrophysical properties compared to those of the host rock [31]. Many of the factors that determine the sealing properties of the fault occurs at sub seismic scales and within the fault zone [5]. The

fault zone often consists of several sub-parallel and interconnecting closely spaced fault surfaces. Spatial and temporary variations are also occurring rapidly along the fault [31]. By studying fault zones in outcrops it is possible to get a better prediction of how faults affect subsurface fluid flow. Such outcrop studies can be of fundamental importance in modelling fault seals [5].

The fault zone is constructed by a *fault core* surrounded by a *damage zone*. Most of the displacement takes place in the fault core. The fault core has a complex architecture where features like multiple slip surfaces, gouges, breccias, cataclasites, clay smears and lenses of rock are common [31]. The damage zone has high density of small-throw faults. These small throw faults often maintain the same orientation as the principal fault segment [5].

The static geometry and the fault rock properties are the main factors controlling the flow across a fault. Another phenomenon called fault reactivation will also influence the fluid flow along the fault. A fault can be reactivated over geological time when changes in tectonic stress regimes are occurring. This can create new pathways that did not exist earlier and allowing hydrocarbons to leak. During the life-time of a petroleum field changes in the pore pressure regimes caused by production or injection can also result in fault reactivation and loss of seal. These changes in pressure will have major impact on production, enhanced oil recovery (EOR) and pressure maintenance [5].

6.4.4 Fault Zone Permeability

The permeability is a measure of the capacity of a porous medium to transmit fluid and the porosity the volume fraction of the rock which is porous [2, 6]. When a fault is slipping a zone of deformation, referred to as the fault rock, is developed. In sandstone reservoirs this zone of deformation tends to have lower porosity, lower permeability and higher capillary entry pressure compared to their surrounding host rock [27, 29]. The changes in the fault zone properties are caused by porosity collapse, grain size reduction and mixing of phyllosilicates with framework grains and grain fragments. The proportion of phyllosilicates in the fault-zone material will have great impact on the hydraulic properties of the fault zone and results in lower fault zone permeability. A large content of phyllosilicates will reduce the pore throat and lead to higher capillary entry pressure [36]. Often there are observed increased mineralization effects in the fault zone. In addition, many fault rocks experience increased quartz cementation or grain contact quartz dissolution [27].

Different methods have been developed to in order to relate known host rock properties to the fault rock permeability, k_f. Most commonly the fault permeability is estimated from the shale-gouge ratio [27].

Fluid flow properties of fault rocks are mainly controlled by the ensemble properties of the pore network. This is again related to geometric properties like the size of the pore throat radii, and the tortuosity. The grain mineralogy, grain size, grain sorting and extent of lateral diagenetic alteration are all factors that will effect the geometric properties [27]. In the next

sections two of the most used methods (Sperrevik and Manzocchi) for calculating fault zone permeability will be outlined.

6.4.4.1 Manzocchi

Manzocchi et al. made an empirical prediction of fault zone permeability as a function of shale content and displacement. The prediction was based on the assumption that SGR is equivalent to the shale content of the fault gouge. The trend in the data showed a general decrease in fault zone permeability with increasing shale content. In addition, there were large variations in permeability at a particular shale content value. The following equation was derived based on a relationship between plug and probe permeability data for various reservoirs, out-crop fault-rock samples and volumetric shale fraction of the core plugs

$$\log k_f = -4SGR - \frac{1}{4}\log(D)(1-SGR)^5$$

where

k_f : Fault zone permeability
D : Fault displacement in metres
SGR : Shale Gouge Ratio [21].

Tests show that this method is is not able to predict fault zone permeability larger than 10 mD. In addition there is large difference (as much as four orders of magnitude) between calculated and measured values of k_f. A probable explanation to this is that the equation is based on relatively limited amount of data in addition to inconsistent method of measurement. The data used are from fault rocks occurring in different geological setting, where both normal and strike-slip faults are present [27].

Figure 6-11 shows a comparison of the two methods.

6.4.4.2 The Sperrevik algorithm

This subchapter is based on reference 27.

Sperrevik et al. used data from faults in cores to derive an empirical equation for estimating fault rock permeability. The data showed that there exist a relationship between fault rock clay content, V_f, and fault rock permeability. The fault rock permeability tends to decrease when the fault rock clay content increases. This relationship is dependent on both the deformation mechanism and the maximal burial depth (z_{max}). For a specific fault rock type the relationship between fault rock clay content and fault rock permeability will change as the maximal burial depth is changed. The fault permeability will be reduced when z_{max} increases as a result of increasing overburden stress and temperature.

For a specific maximal burial depth the relationship between fault rock clay content and fault rock permeability varies for different fault rock types. For a specific fault rock clay content the fault rock permeability is strongly dependent of the type of deformation mechanism.

In the Sperrevik algorithm it is assumed that fluid flow properties of fault rocks are mainly controlled by fault rock clay content, maximum burial depth and depth at time of deformation (z_f). The following equation was established based on measured fault rock permeability data

$$k_f = a_1 \exp\left\{-\left[a_2 V_f + a_3 z_{\max} + (a_4 z_f - a_5)\left(1 - V_f\right)^7\right]\right\}$$

where the constants have the values

a_1 = 80000
a_2 = 19.4
a_3 = 0.00403
a_4 = 0.0055
a_5 = 12.5.

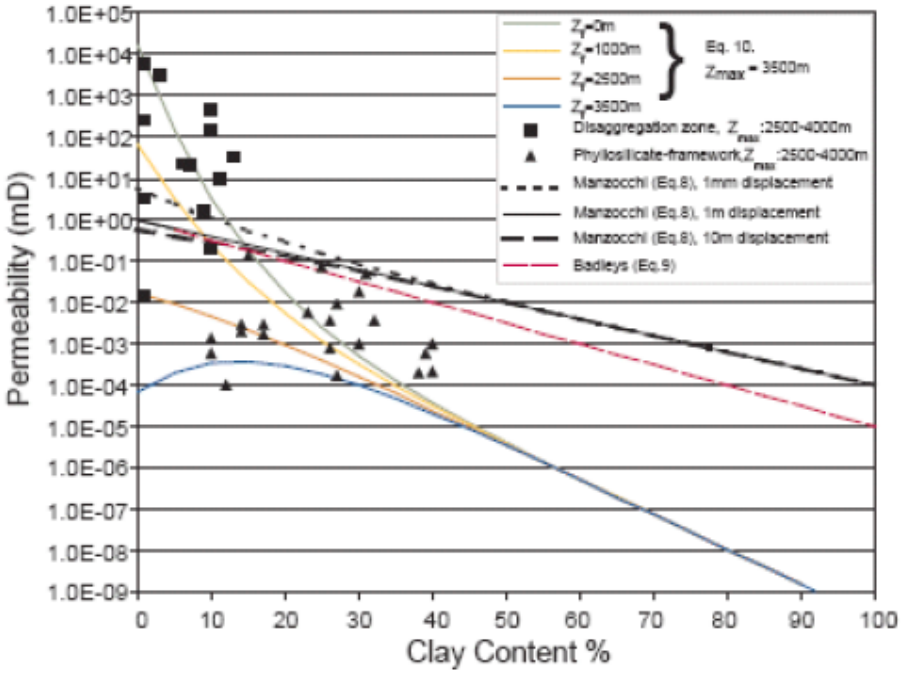

Figure 6-11 Comparison between the Sperrevik and Manzocchi algorithms [24]

6.4.5 The Capillary Entry Pressure

The sealing capacity of a fault is not only dependent of the reduced permeability of the fault rock compared to the host rock. The fluid that occupies the pores in the fault rock will also influence the fault sealing [29]. The capillary entry pressure of the fault, P_t, is important when estimating the sealing capacity of a fault. In water-wet rocks the capillary entry pressure can be defined as: "the lowest capillary pressure, P_c, at which hydrocarbons form a continuous path through the largest interconnected pore throats in the fault rock" [5].

The two most likely barriers to fluid flow in rock over a geological timescale are *membrane* and *hydraulic* seals. A membrane seal can be described as the boundary of a layer of smaller pore throats. Fluid can flow across this boundary under certain pressure conditions and the capillary entry pressure will determine the effectiveness of membrane seals. Hydraulic seal contains no interconnected pore space and the rock strength will be exceeded before the capillary entry pressure is reached [13].

Capillary pressure concepts have numerous applications in the petroleum industry. It can for instance be used to evaluate reservoir rock quality, pay versus non pay, expected reservoir fluid saturations, depth of the reservoir fluid contacts and the seal capacity (height of hydrocarbon column a seal can hold before it leaks). Estimation of the capillary pressure is very important when evaluating the potential of a petroleum reservoir. The capillary pressure controls the static distribution of fluids in the reservoir at initial state and distribution of the remaining hydrocarbons after primary production [30].

In its simplest form the capillary pressure can be defined as: "the difference in pressure across the meniscus in the capillary tube" [30]. The following formulas are often used to express the capillary pressure

$$P_c = (\rho_w - \rho_{nw}) \times g \times h$$

and

$$P_c = \frac{2\sigma \cos\theta}{r_c}$$

where

ρ_w: Specific gravity of the wetting phase
ρ_{nw}: Specific gravity of the non-wetting phase
g: Gravitational constant
h: Hydrocarbon height
σ: Interfacial tension
θ: Contact angle between fluid and the capillary tube
r_c: Radius of the capillary [30].

If the capillary entry pressure of different fault rocks, generated under different conditions is known, it is possible to calculate the sealing capacity of the fault rock. The capillary pressure has a value equal to zero at the free water level (FWL) and increases upwards in the hydrocarbon column. A membrane seal can prevent migration across the fault for a hydrocarbon column height until P_c equals P_t. The effective permeability to hydrocarbons will be zero when P_c has a value less than P_t. When the hydrocarbon column is high enough to give a P_c greater than P_t the hydrocarbons will slowly flow across the fault [5].

Most of the faults that segment the Snorre reservoir are assumed to be water wet. This assumption is based on the fact that faults in Snorre field were created prior to any hydrocarbon migration into the reservoir. In addition, the permeability of the fault rock is very low. If the buoyancy difference between hydrocarbons and water was less than the capillary entry pressure, fault zones with low permeability may be water filled after the migration of the hydrocarbons [29]. This means that the capillary entry pressure will most likely cause restrictions to fluid flow in the Snorre reservoir.

6.4.6 Fault Rocks

The properties of fault rocks that develop in the fault zone will influence the fault's ability to seal. Factors like local facies, reservoir-fluid types and saturations, pressure difference across the faults, fault-zone architecture, burial and fault histories and juxtaposition of the lithologies across faults are all affecting the fault rock properties [5].

Faults present in porous sandstones with low clay content (less than 15%) may develop low-permeability seals. This follows from porosity reduction as a result of mechanical crushing of the quartz grains. These fault rocks are called *cataclastic*. When a fault is created in porous sandstone, without the associated reduction in porosity and grain crushing, the fault rocks are called *disaggregation bands* [5]. It has been assumed that all clean sandstones deformed in the Snorre field have become cataclasites [9].

Faults created in impure sandstones (clay content from 15-40%) form *phyllosilicate-framework* fault rocks. These fault rocks will have reduced porosity and permeability as a result of compaction and mixing of the clay particles and quartz grains [5]. Phyllosilicate – framework fault rocks investigated in the RDR – study on Snorre had permeabilities in the range 0.0005 – 1.3 mD [9].

Faults occurring in sandstones with clay content greater than 40 % will form fault rocks called *clay smears*. Clay smears are formed when clay or shale layers are dragged and deformed along the fault plane. There will then be created a low-permeability barrier to fluid flow [5]. Studies undertaken by the RDR showed that permeabilities are likely to be 0.0001 mD or less in clay smears [9].

Cementation can also occur along a fault plane. This will result in nearly impermeable barriers to fluid flow. Cemented zones are rarely continuous, though they can be continuous if a regional change is occurring. A regional change like an increase in temperature above 90 °C, will increase the rate of quartz precipitation [5]. In the cores tested from the Snorre and Vigdis fields there were little cemented deformation features [9].

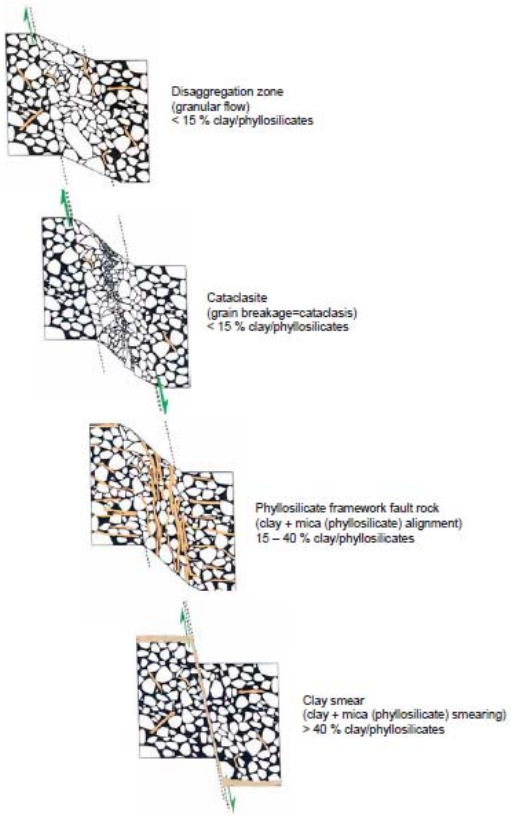

Figure 6-12 Different fault rock types [1]

6.5 Incorporating Faults into Reservoir Simulation Models

6.5.1 Definition of Fault Transmissiblity Multiplier

Transmissibility in a reservoir simulation model depends on the grid block geometry, permeability and transmissibility multipliers applied to the faces of the grid blocks [9]. The transmissibility between two adjacent cells can be defined in the following way

$$T = \frac{C_{Darcy}}{\frac{1}{T_1} + \frac{1}{T_2}}$$

where

$T_i = K_i R_i D_i S_i$
T : The transmissibility value
C_{Darcy} : A constant
T_1 and T_2 : The cells specific transmissibility values
K : The cell permeability
R : The net-to-gross ratio
D : The distance between cell center and the interface
S : The contact area [20].

In a reservoir simulation model the effect of faults on fluid flow can be modelled by using so called fault transmissibility multipliers. To calculate the fault transmissibility multipliers some fault zone properties like fault zone thickness, fault zone permeability and properties of the grid blocks to which they are assigned are required [13].

By applying a transmissibility multiplier, T_{mult} , the transmissibility between any two cells in the grid can be modified. If faulted cells are occurring in the grid the fault transmissibility multiplier is used to incorporate the fault seal. The fault transmissibility multiplier, T_{mult} , is defined as the faulted transmissibility, T_f , divided by the unfaulted transmissibility, T . The following equation shows the relationship between fault transmissibility and unfaulted transmissibility

$$T_{mult} = \frac{T_f}{T}$$ [20].

Earlier the transmissibility multipliers were often used as a tuning parameter to achieve a history match [9]. Adjusting fault transmissibility without any serious scientific justification can result in use of totally unrealistic fault rock properties and the history matches will be non-unique [8, 9]. Wrong results can occur if transmissibility multipliers are used to compensate for problems within the reservoir simulation model that are not caused by the presence of faults. Experiences show that the extent of sedimentary heterogeneities is often underestimated within the geological models. To compensate for this sealing faults that may not even exist are incorporated into the simulation model. Even though a history match is achieved the result may not be useful for predicting future production behaviour. A model that is history matched at these assumptions should be used with great caution [8].

Availability of fault permeability, fault thickness and capillary entry pressure characteristics of fault rocks have made the incorporation of fault rock properties into production simulation models more sophisticated. In addition, information about how the permeability of fault rocks is

affected by clay content or post-deformation diagenesis is available. This increased understanding of fault rock properties has resulted in a more realistic treatment of faults in reservoir simulators. It has become more common to calculate transmissibility multipliers based on real fault rock data. These transmissibility multipliers are applied to grid block faces adjacent to faults in order to model how the faults will affect fluid flow [9].

6.5.2 RMSfaultseal

Sophisticated software and visualization tools have been developed for modelling reservoir geometries in 3D. This is a useful tool for geoscientists and reservoir engineers working in the petroleum industry. It is very important to be aware of the limitations of a modelling tool and that the model can never be more accurate than the accuracy of the input data [22].

Several geological modelling softwares have developed modules in order to calculate fault transmissibility multipliers. The RMSfaultseal module in the Irap RMS (developed by ROXAR software solutions) is used to determine the fault sealing properties of the Snorre faults. The faultseal module uses published algorithms to calculate fault transmissibility multipliers. Fault rock properties are used as input to transmissibility multiplier calculations. The following equation is used to calculate fault transmissibility multipliers

$$T_{mult} = \frac{\frac{L_{fw}}{K_{fw}} + \frac{L_{hw}}{K_{hw}}}{\frac{L_{fw} - W_{fz}}{K_{fw}} + \frac{L_{hw} - W_{fz}}{K_{hw}} + \frac{2W_{fz}}{K_{fz}}}$$

where

T_{mult} : Fault transmissibility multiplier

K_{fw} : Permeability of footwall cell

K_{hw} : Permeability of hanging wall cell

W_{fz} : Fault zone thickness

L_{fw} : Grid cell dimension for footwall

L_{hw} : Grid cell dimension for hanging wall

K_{fz} : Fault zone permeability [24].

K_{fw}, K_{hw}, L_{fw} and L_{hw} are obtained directly from the 3D grid properties. The two parameters W_{fz} and K_{fz} require some extra input to be determined. The fault zone thickness W_{fz} can be determined by using the displacement-thickness ratio

$$W_{fz} = \frac{D}{X}$$

where

D : Displacement obtained directly from the 3D grid
X : Thickness [24].

For normal faults the displacement-thickness ratio will be in the region from 50 to 200 (Figure 6-13) [24].

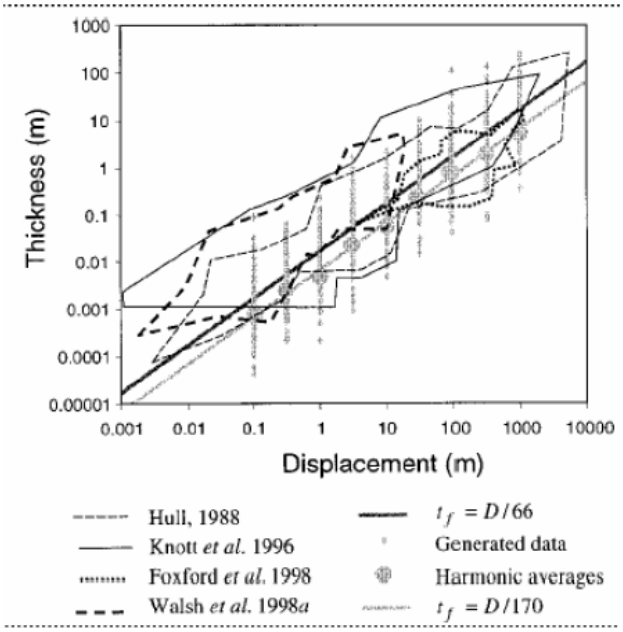

Figure 6-13 Published relationships between fault displacement and fault zone thickness [24]

The fault transmissibility multipliers calculated from RMSfaultseal are incorporated into the Eclipse reservoir simulation model using the keywords *TRANX*, *TRANY* and *EDITNNC*. The TRANX and TRANY keywords specify the transmissibility explicitly and are replacing those calculated by the program. When faults are modelled with a throw in the simulation grid non – neighbour connections may be generated. This means that cells that are not index – neighbours in the grid can become neighbours. The EDITNNC keyword can be used to modify the transmissibility between non – neighbour connections. The fault transmissibility multipliers across the faults (calculated in RMS and exported to Eclipse) can be modified by using the Eclipse keyword MULTFLT [7].

6.5.2.1 Oblique Slip Angle

It is possible to obtain a more exact value of the displacement, D, by using the oblique slip angle. A fault can often have significantly larger displacement than recorded caused by some component of oblique movement [5]. By specifying the angle between the dip and the oblique slip vectors a more accurate relationship (Figure 6-14) can be derived

$$D = \frac{Displacement}{\cos(\alpha)} \quad (6\text{-}1)$$

where

α : angle, degrees [24].

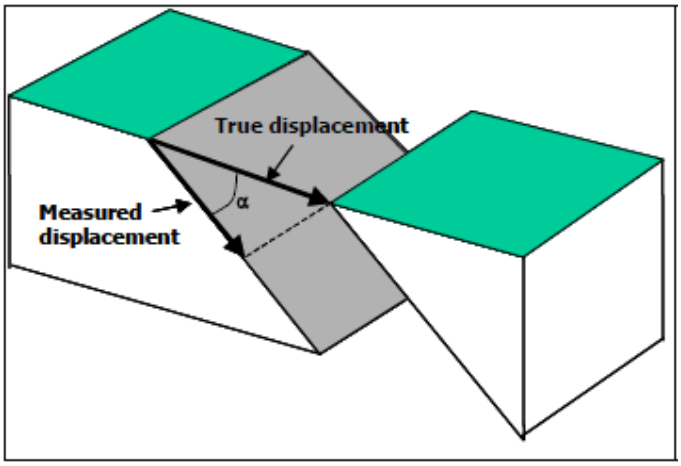

Figure 6-14 True displacement of an oblique slip fault [24]

6.5.2.2 Brittle Factor

The fault zone permeability can be modified by using the *Brittle factor*, the *Cementation factor*, the clay smear potential and the shale smear factor. Not only permeability changes caused by shale/clay smear will affect the fault zone properties. Factors like brittle deformation and cementation will also have an impact. The pore volume of sediments and the permeability can increase as a result of brittle deformation by cataclasis and/or brecciation. A *Brittle factor* can be used to compensate for effects like this [24].

6.5.2.3 Cementation Factor

Cementation will reduce the transmissibility across the faults. Cementation occurring along an originally permeable fault plane can partially or completely remove the porosity and creating hydraulic seal [35]. The *Cementation factor* can be used to open or close a fault and can be given values between 0 and 1. A value of 0 indicates that the fault is sealing [24].

6.5.2.4 Calculation of SGR and Fault Zone Permeability

The values of shale gouge ratio calculated in RMSfault seal vary between 0 and 1. The same equation as presented in chapter 6.4.2.4 is used in the calculation of SGR. The SGR for a particular point is calculated for both sides of the fault due to the fact that lithology may change across faults. Input in the equation comes from the properties of the contributing cells along both the hangingwall and footwall side if the fault. SGR is then given by the arithmetic average beween SGR^{fw} and SGR^{hw} [24].

$$SGR = \frac{\left(SGR^{fw} + SGR^{hw}\right)}{2}.$$

Based on SGR^{fw} and SGR^{hw} the fault zone permeability are calculated for the hangingwall (K_{fz}^{hw}) and footwall (K_{fz}^{fw}) side of the fault. Fault zone permeability is given as the harmonic average between the footwall and the hangingwall values

$$K_{fz} = \frac{2}{\left(\frac{1}{K_{fz}^{fw}} + \frac{1}{K_{fz}^{hw}}\right)}.$$

The fault zone permeability can be calculated by using the Sperrevik or Manzocchi algorithms. It is also possible to define relationships between SGR and fault zone permeability and apply this in the fault seal analysis. This is done in the Snorre reservoir model. The calculated SGR value then gives a corresponding fault zone permeability value predefined by the user [24]. The SGR curves on the Snorre Field are based on a fault rock study performed by Rock Deformation Research Group in 2006 and experience from the Tampen area.

7 Snorre Reservoir Model

7.1 Introduction

In 2006 a new geological model of the Snorre Field was finalized. Flow pattern maps were used to build a geological model that would reflect the dynamic behaviour of the reservoir. The flow pattern maps are based on pressure and front information and tracer observations. Based on this work a new reservoir simulation model was made in 2007. The new models were built in order to improve geological and dynamical reservoir understanding. Some of the main objectives for making new models were to update in-place volume estimates, forecast production with uncertainty, optimizing field development (new wells, IOR potential) and make a reservoir management tool for decision making. The most important input data to the models were seismic interpretation, well data, production data and communication maps [23, 26].

7.2 Geological Model

A new fault and stratigraphic modelling was performed on the Snorre Field in 2006. The aim of the model work was to construct new 3D grids for the Snorre geological and reservoir simulation models. The model is based on a 3D seismic survey of the Snorre Field where nine reservoir horizons were interpreted. The nine horizons cover the interval from the top of Lower Lunde Fm. to the Base Cretaceous Unconformity (BCU) and are referred to as: SN LL, SN ML4, SN 3.4, SN 6.4, SN 9.3, SN 10.1, SN 10.4 and SN 11.4 [4].

7.2.1 Fault Modelling

In the fault modelling a total number of 240 faults were interpreted on the Snorre Field. The complex nature of the about 1000 meter thick Snorre reservoir makes it impossible to incorporate all of the faults. One reason is the limitation of the grid size, because the grid resolution is coarser than the distance between some of the faults. A multidisciplinary team including geophysicist, geologist, reservoir engineer and production engineer made a prioritizing of the faults. Main faults with large throws were first incorporated in the model. Secondly the smaller faults and staircase faults were prioritized. There exist three different ways to incorporate faults in a reservoir model:

- Linear faults are the most common faults. These faults are incorporated as stiff pillars and need to intersect the whole model (Figure 7-1).
- Staircase faults do not follow a pillar but a staircase along the faults in the vertical direction (Figure 7-1).
- Multipliers are incorporated in the reservoir grid without throw (Figure 7-2) [4].

The final result of the fault modelling was 109 linear faults and 20 staircase faults. The remaining 111 faults can be included in the 3D grid as multipliers. In comparison, the previous model developed in 2000 had 84 faults incorporated [4].

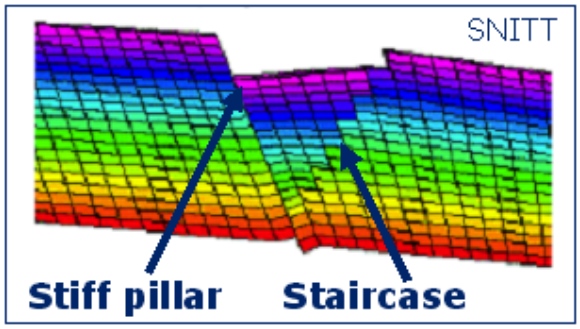

Figure 7-1 Illustration of linear fault and staircase fault [4]

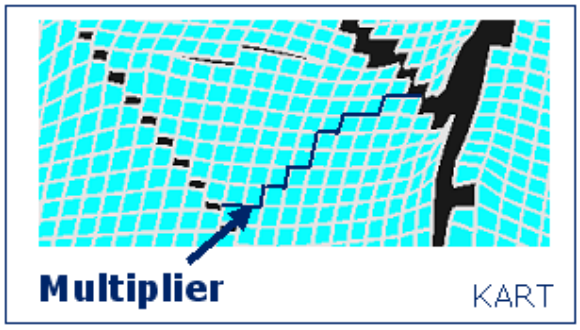

Figure 7-2 Illustration of a multiplier incorporated into the grid [4]

7.2.2 Fault Seal Analysis

In the new reservoir models of the Snorre Field from 2006/2007 it was decided to model faults in a more sophisticated way using the RMSfaultseal module in RMS (Chapter 6.5.2). In the earlier models the flow through faults was modified by applying fault multipliers in order to obtain a history match. The lack of good match indicated that using fault transmissible multipliers was a too simplistic approach [32].

Fundamental to a successful fault seal analysis is the estimation of petrophysical properties of the different fault rocks present in field evaluated. The critical properties which need to be quantified are permeability, fault rock thickness, capillary entry pressure, transmissibility, and the strength of the fault rocks. Earlier the absence of these data made the fault seal analysis difficult [17]. Now there exist more data available, but still there is uncertainty associated to the estimation of the parameters.

A detailed description of the fault seal calculations are given in an earlier chapter. Here an introduction to the different input parameters in the fault seal analysis at the Snorre Field will be given.

In order to capture the static properties of fault zones by applying fault transmissibility multipliers, knowledge of both the permeability and thickness of the fault rock is needed. In addition, knowledge about the undeformed reservoir adjacent to the fault is required. The Rock Deformation Research Group (RDR) performed a study of the fluid flow properties of fault rocks in the Snorre Field. Microstructural and petrophysical properties were estimated from 25 rock samples collected from the Statfjord Fm. and Lunde Fm. on the Snorre and Vigdis Fields. Based on the measurements and observations representative fault related properties, like fault thickness and SGR curves, were established for the Snorre faults. These data together with volume fraction of shale and permeability from the 3D grid were used as input in the RMSfaultseal [32]. The SGR-curve method was used in the calculation of fault transmissibility multipliers [28].

Different cases were constructed containing different parameters for fault seal modelling. The different cases (included input parameters) are listed in Table 7-1, where P90 is the most tight case and P10 the most open case. It was decided to use the P70 case in the official reservoir models. This case gave the best match to historical data.

INPUT PARAMETERS FOR FAULTSEAL MODELLING					
	base	open	tight		
	P50	P10	P90	P30	P70
Displ/thickness	100	200	50	200	50
Oblique slip angle	0	0	0	0	0
Brittle factor	1	1	1	1	1
Cementation factor	1	1	1	1	1
Shale Smear factor limit	5	7	3	4	6
VSH cut off limit	0,55	0,55	0,55	0,55	0,55

Table 7-1 Input parameters used in the fault seal analysis (from internal StatoilHydro data bases)

7.3 Reservoir Simulation Model

This chapter is based on reference 26.

Three reservoir simulation models were built in the study in 2007. One model was made for the Statfjord Fm, while the Lunde Fm. was represented by two models (Figure 7-3). This division was based on the assumption that there is no communication between the Statfjord Fm. and the Lunde Fm.

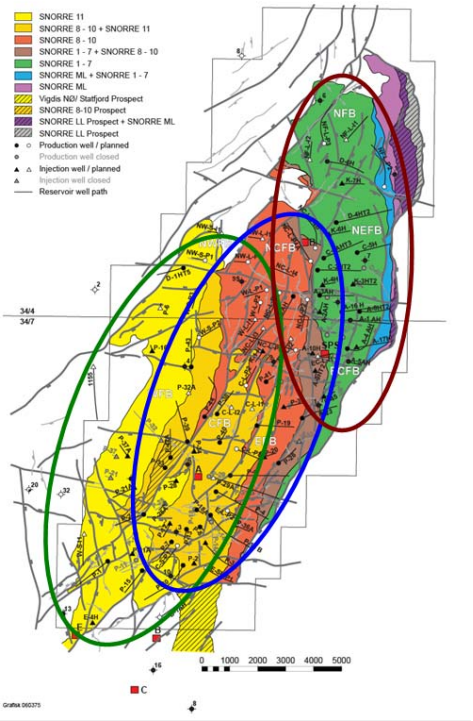

Figure 7-3 The Snorre reservoir models. Green: The Statfjord Model, blue: The A-Lunde Model, red: The B-Lunde Model [26]

The Statfjord represents the Statfjord Fm. and includes zones SN11-SN10.4 within the Western (WFB), Central (CFB) and Eastern (EFB) fault blocks.

The A-Lu model includes the upper part of the Upper Lunde Fm and consists of SN10.3-SN6.4 in the Western (WFB), North Western (NWFB), Central (CFB), North Central (NCFB) and Eastern (EFB) fault blocks.

The two Lunde Models are split along the fault MNSF_2. In the northern part of this fault there is assumed to be no communication. In the southern part on the other hand, communication is proven. To solve this problem the wells of interest were split between

the two models. The P-22 well has been included in both models, while only the upper part of well P-23 is included in the A-Lunde model.

The B-Lu model represents the lower part of the Upper Lunde Fm. and the Middle Lunde Fm. These formations include zones SN8.2-SNML1 within the East Central Fault Block (ECFB), North Eastern (NEFB) and Northern fault blocks (NFB).

Table 7-2 shows the grid dimensions and number of active blocks for the three models.

Model	*Grid dimensions*	*Gridblocks*	*Active grid blocks*
Statfjord	79x155x31	~ 380000	~ 120000
A-Lu	70x156x71	~ 775000	~ 340000
B-Lu	107x149x98	~ 1560000	~ 240000

Table 7-2 Grid dimensions, number of grid blocks and active grid blocks [modified 26]

7.4 The A-Lu Model

All reservoir simulations performed in this thesis are performed on the pre-built A-Lu model. The grid dimensions of the model is 70 x 156 x 71, where 341 413 of the grid blocks are active. Figure 7-3 gives an indication of the area of the A-Lu model. The A-Lu model is complex regarding reservoir communication due to many faults [26]. A list of the faults including the fault transmissibility multipliers incorporated in the model can be found in App A. A total number of 34 wells have been included in the A-Lu model, where 21 of them are producers/injectors. Many of the wells have RFT measurements from the Lunde Fm. In the next sections a summary of the A-Lu model construction (reference 26) is presented.

7.4.1 Grid Properties

The grid is based on a structural framework developed in 2004-2005 and is built with corner-point geometry. The lateral grid layout is regular 100 m x 100 m across the entire model and the grid is regularized along the faults. In order to decrease the simulation time an up scaling of the vertical resolution was performed. Well log data were used to select grid thickness in the up scaling procedure. Table 7-3 shows the geological model layers compared with the simulation model layers. The volume in the grid above the BCU is eliminated by setting the Eclipse keyword ACTNUM to zero for these grid blocks indicating that these grid blocks are inactive [26].

Formation	Geomodel layers	ECLIPSE layers	Thickness top tp bottom
Snorre 10.3	1-30	1-4	7-7-8-8
Snorre 10.2	31-65	5-10	7-8-5-5-5-5
Snorre 10.1	66-105	11-15	6-7-7-10-10
Snorre 9.4	106-150	16-23	3-6-6-6-6-6-6-6
Snorre 9.3	151-200	24-32	2-6-6-6-6-6-6-6-6
Snorre 9.2	201-225	33-36	3-7-7-8
Snorre 9.1	226-260	37-41	3-8-8-8-8
Snorre 8.2	261-300	42-47	5-7-7-7-7-7
Snorre 8.1	301-335	48-52	3-8-8-8-8
Snorre 7.4	336-355	53-56	3-6-6-5
Snorre 7.3	356-375	57-60	3-7-7-3
Snorre 7.2	376-400	61-64	4-8-8-5
Snorre 7.1	401-415	65-68	3-4-4-4
Snorre 6.4	416-430	69-71	3-7-5

Table 7-3 Comparison between geomodel layers and simulation model (A-Lu) layers [modified 26]

7.4.2 Vertical Communication

The vertical communication in the model was modelled by using the following equations

$$PERMZ = PERMX \times 0.7 \times NTG^{\frac{1}{n}}$$

and

$$MULTZ- = NTG^{n}$$

where

n : A parameter representing the degree of vertical communication. The n-value that gave the best model match to production data was selected as a starting point in the history matching.

$PERMZ$: Permeability in the z - direction

$PERMX$: Permeability in the x - direction

$MULTZ-$: Transmissibility multiplier used to modify those vertical transmissibilities calculated by Eclipse. When a MULTZ- value is specified for block (i, j, k) the transmissibility between (i, j, k) and (i, j, k-1) will be modified [7].

7.4.3 Aquifer

In the lower zones in the eastern part of the A-Lu model area the model gives too low pressure support. An aquifer was added below reservoir zone SN6.3 in CFB and EFB to solve this. There is originally no volume included below SN6.3 in the A-Lu model, but the aquifer is added to represent a potential pressure support from these zones. The Eclipse keyword AQUNUM was used to implement this numerical aquifer in the A-Lu model.

7.4.4 Petrophysical Properties

Reservoir properties like net to gross (NTG), permeability, water saturation, shale volume, free water level and fluid contacts were calculated by the petrophysicist and given as input to the geological model. The properties were upscaled in the reservoir simulation grid, which has a lower vertical resolution than the geological model grid. It is important to do the upscaling in a way that preserves the properties of the model.

7.4.4.1 NTG, Porosity and Permeability

When upscaling net to gross (NTG) it is important to maintain both the bulk volume (BV) and the sand volume (SV). The following equations are used in the up scaling process of the NTG

$$BV_{up} = \sum BV_{fine}$$
$$SV_{up} = \sum SV_{fine}$$
$$SV_{fine} = BV_{fine} \times NTG_{fine}$$
$$NTG_{up} = SV_{up} / BV_{up} .$$

In the upscaling process of the porosity the aim was to preserve the pore volume (PV). First a parameter, $PORO \times NTG$ was calculated, upscaled and weighted on total bulk volume. Then the parameter $PORO / NTG$ was calculated for the upscaled grid. The following formulas were considered

$$PV_{up} = \sum PV_{fine}$$
$$PV_{fine} = SV_{fine} \times PORO_{fine}$$
$$PORO_{up} = PV_{up} / SV_{up} .$$

An arithmetic average technique was used to calculate the average permeability-thickness (kh). The following equation was used in the calculations

$$kh_{up} = \sum \left(H_{fine} \times NTG_{fine} \times kh_{fine} \right) / \sum \left(H_{fine} \times NTG_{fine} \right)$$

where H is the gross thickness.

7.4.4.2 Water Saturation

The water saturation model implemented in Eclipse was given by the following relationship

$$S_w = S_{wirr} + (1 - S_{wirr}) \times S_w(J)$$

where

S_w: Water saturation
S_{wirr}: Irreducible water saturation
$S_w(J)$: J – function.

The capillary bound water, $CapillaryS_w$, was given as the difference between the water saturation and the irreducible water saturation

$$CapillaryS_w = S_w - S_{wirr} = (1 - S_{wirr}) \times S_w(J).$$

7.4.4.3 Connate and Critical Water Saturation

For the A-Lu model the connate water saturation was defined by the relationship

$$SWL = 10^{(1.2-7\varphi)}.$$

where SWL is the connate water saturation and φ is the porosity.

The Eclipse keyword TZONE has been applied in the A-Lu model to modify the water mobility in the transition zone due to high water production at production start. This was done by setting the critical water saturation equal the initial water saturation for values less than a certain value. For larger saturations the critical water saturation is set equal the cut-off. A cut-off value of 0.6 was used in the A-Lu model.

7.4.4.4 Capillary Pressure Curve

Two expressions for capillary pressure, P_c, were generated to fit set of capillary pressure curves for different porosities

$$P_c = 0.014 \times S_w^{1.55}$$

and

$$P_c = 0.025 \times S_w^{1.6}.$$

7.4.5 Fluid Properties

The oil in the Snorre Field is highly under saturated and injected gas may be miscible with the oil. There was used a two-phase Eclipse black oil PVT table, and partly swelling of oil contacted by gas was assumed.

7.4.6 Rock Properties

During the history matching process of the A-Lu model it was decided to use a constant value of 6×10^{-5} for rock compressibility.

7.4.7 Relative Permeability

In 2004 there were performed water/oil relative permeability measurements on cores from the Snorre reservoir. It was decided to use Corey shaped relative permeability curves and end point correlations. Different case studies showed that it was not necessary to upscale the relative permeability. The relative permeability is equal in all of the models.

7.4.7.1 Water-Oil Relative Permeability

Normalized oil-water relative permeability was given by the following relationships:
Corey water: $n_w = 2.9$
Corey oil-water: $n_o = 4.25$.

7.4.7.2 Gas-oil Relative Permeability

Normalized gas-oil relative permeability (miscible case) is given by:
Corey gas: $n_g = 1.5$
Corey oil-gas: $n_{og} = 1.2$

7.4.7.3 Residual Oil Saturation

The residual oil saturation to water, S_{orw}, in the A-Lu model was defined as

$S_{orw} = 0.23 - 0.38 \times S_{wi}$, for $S_{wi} > 0.34; S_{orw} = 0.08$.

The residual oil saturation to gas, S_{org}, was set to

$$S_{org} = 0.5 \times S_{orw}.$$

7.4.7.4 Critical Water and Gas Saturation

In the model the critical water saturation (SWCR) was set equal to the connate water saturation (SWL) and the critical gas saturation (SGCR) was given a value of zero.

7.4.7.5 End-points and Scaling Method

The endpoint water relative permeability, $(k_{rw}(S_{orw}))$, was dependant of the connate water saturation.

The following expression was used to calculate endpoints in the A-Lu model:

$k_{rw}(S_{orw}) = 1.3 - 2 \times S_{wi}$, for $S_{wi} > 0.5; k_{rw}(S_{orw}) = 0.3$

7.4.8 Regional Parameters

The A-Lu model has only one PVT region which includes eight RSVD tables. Each RSVD table contains the dissolved gas-oil ratio versus depth.

7.4.9 Selecting Geological Realization

Different geological reference cases have been modelled with different facies realizations. Five different stochastic realizations (#3-7) were made with the same channel direction. One realization was made with an alternative channel direction. The reference cases were evaluated in order to find the model that gave best representation of the dynamic behaviour of the reservoir and the best basis for the history matching. The hydrocarbon pore volume was (HCPV) was modified for each realization, using the Eclipse keyword MULTPV to match the official 2D HCPV. For the A-Lu model realization #3 was selected as the preferred geological realization for the history matching.

7.4.10 History Matching of the A-Lu Model

This chapter is based on reference 26.

History matching of such a large model as the A-Lu model is very difficult and challenging, especially because of the complex structure of the reservoir. History matching of the model has been performed until 1. August 2006 and historical data have been included up to 1. April 2007. A more detailed description of the input data and the parameters tuned in the different fault blocks will be given in the next sections.

7.4.10.1 Wells

All producers and injectors have been implemented in the reservoir simulation model. Exact well paths and perforation intervals are used as input.

7.4.10.2 Production and Reservoir Depletion history

Allocated production and injection data from the Snorre Field are daily stored in a production database called *Oil Field Manager*. A software called *schedule,* has been used to convert the production data into Eclipse input format.

7.4.10.3 RFT/PLT data

Quality controlled RFT-data and PLT-data have been summarized in user files for plotting.

7.4.10.4 Well Pressures and PI

Pressures from shut-ins pressure data from down hole gauges have been used as input. Measured liquid productivity indexes for wells have also been implemented in the simulation models.

7.4.10.5 Saturation Data

Because of the lack of saturation log data and the fact that the available data are not crucial for the reservoir understanding, they have not been prioritized in the history matching.

7.4.10.6 4D – Data

The 4D-data have been important in the history matching of the simulation models. The 4D interpretations have given a better understanding of fault communication and barriers in model as well as contributing to increased overall reservoir understanding.

7.4.11 Parameters Tuned in History Matching of the Different Fault Blocks

This chapter is based on reference 26.

The A-Lu model has been history matched until 1. August 2006, but historical data has been included in the model until 1. April 2007. During the history matching process of the A-Lu model different parameters were tuned to achieve a satisfying history match for the model. In the next sections a summary of the history matching process for the different fault blocks (Figure 7-4) will be given. The summary is based on documentation from the “Reservoir Model of the Snorre Field - Simulation model and history matching” [26].

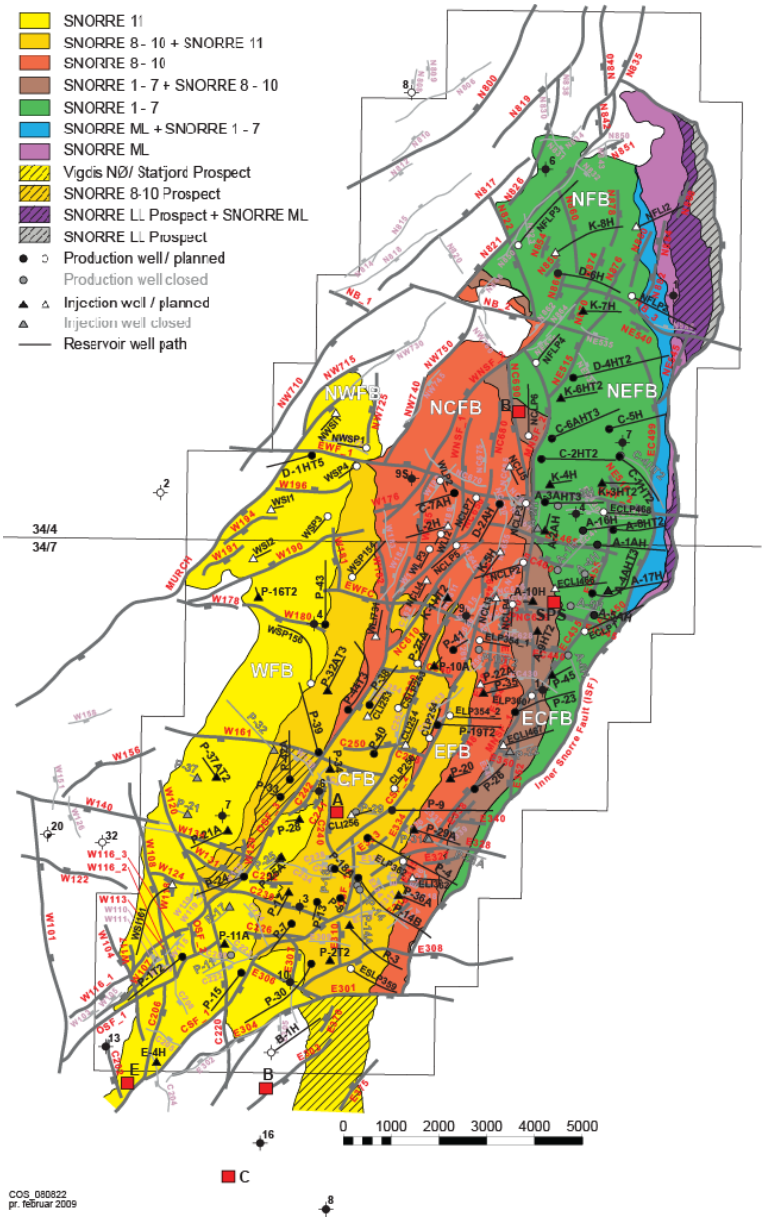

Figure 7-4 Snorre Field map [26]

7.4.11.1 WFB

The Western Fault Block is illustrated in Figure 7-4 including drilled and planned wells. Wells of interest in the WFB are P-44, P-16 and 34/4-9S, where P-44 is the only producer. Simulations revealed that the model gives too high pressure support for WFB, and the pressure decline in P-44 was too low compared with measured pressures. The model also gave higher water production than measured. In order to solve these mismatches manual

modifications of parameters like the size and properties of the aquifer to the west of the fault block, sealing capacities of the faults and elongation of fault *W180,* were performed. The fault *OSF_3* between WFB and CFB was opened to compensate for depletion in P-44 prior to production. 4D seismic indicates water coming in towards the heel of P-44 and barriers were introduced to the west of the well in SN10 to account for this.

7.4.11.2 CFB

The Central Fault Block is illustrated in Figure 7-4 including drilled and planned wells. For CFB the following wells have been taken into consideration: P-18, P-18A, P-8, P-12, P-19 and P-41. P-18 and P-18A are also perforated in the Statfjord formation and have only been produced partly in Lunde. P-19 is perforated in both CFB and EFB, while P-41 produce from the Lunde formation in the northern part of CFB. For the history matching period, P-8 has been the main producer for CFB and P-12 has been the only injector (water).

In the history match of CFB both fault multipliers and transmissibility multipliers have been modified. Transmissibility multipliers have been applied in SN10 in the aquifer and south and north of the fault C230 to control water production in P-8. Transmissibilities south of the fault were increased and transmissibilities north of the fault were decreased, to mimic 4D data showing that water moves mainly from P-12 towards P-8 in the eastern part of C230. The fault C230 was also elongated to CSF_1 in the history matching process. The elongated part of the fault was divided into four parts vertically, with each part having different fault transmissibility multiplier. Also vertical restrictions were introduced in SN10 in CFB. An n value of 10 was used in the calculations of vertical transmissibility (see 7.4.2).

Well P-12 had leakage in a straddle and was shut in for around a year. A cross flow well was introduced during this period to compensate for flow from Lunde to Statfjord.

7.4.11.3 NCFB

The Northern Central Fault Block is illustrated in Figure 7-4 including drilled and planned wells. For NCFB well D-2AH has been the active producer and K-1HT2 the active injector during the history matching period. RFT measurements from D-2H (pilot well of D-2AH) showed varying depletion in the different subzones. To account for this the fault EWFC was divided into four parts vertically. The transmissibility across the upper part of EWFC (SN10.3-9.3) and in SN9.2 was increased. SN9.1-8.2 part of the fault was given decreased transmissibility and in the lower part of the fault (SN8.1 and below) the transmissibility was further decreased.

Transmissibility were increased in the low net to gross (NTG) areas in SN9.3 from EFB towards D-2AH. It was also implemented vertical restrictions between SN9.3-9.2, SN9.2-9.1 and SN8.2-8.1. In addition, the part of fault EWF_1 close to D-2AH was given increased transmissibility.

7.4.11.4 EFB

The Eastern Fault Block is illustrated in Figure 7-4 including drilled and planned wells. History matching of EFB was extremely challenging caused by the very complex geology and the many subzones having low NTG (poor communication between channels). Most of the wells in this fault block produce from both the Stafjord and Lunde formation and PLTs have mainly been used to determine the split. Numerous of modifications have been performed in order to history match EFB. Changing transmissibility and fault transmissibility and introduction of vertical restrictions are some of the modifications done. It will not be given more details of the history matching of EFB in this text.

7.4.11.5 ECFB

The East Central Fault Block is represented in Figure 7-4 including drilled and planned wells. In the history matching of ECFB the injector P-22 and producer P-23 was taken into account. The two wells have been split between the A-Lu model and B-Lu model. The part of P-23 which is west of the fault MNSF_2 has been included in the A-Lu model. RFT pressures in P-23 were influenced by production in P-9 to the east of MNSF_2, production and injection in P-31A and back production in P-22. In the history matching process the fault E352 was opened and a numerical aquifer was created for the area to get enough pressure support.

8 Simulation Study

8.1 Introduction

Two simulation studies were performed during the work of this thesis. The aim of both studies was to investigate the effect on the dynamic behaviour of the Snorre reservoir when changing the fault transmissibility and factors influencing it. The pre-built and history matched A-Lu reservoir simulation model has been used as a basis for both of the studies. First the model's sensitivity to fault communication was tested. It was tested if it is possible to obtain a better history match of the model when modifying the transmissibility by applying fault transmissibility multipliers. This was done by multiplying and dividing the fault transmissibility by fixed values. Predictions were run (until 2030) and compared to the expected case (A-Lu model).

Secondly, a simulation study was performed on a small segment taken out from the A-Lu model to investigate the effects on reservoir performance when changing different parameters affecting the fault transmissibility. This was done to get an indication of what parameters having highest impact on the fault transmissibility. Modification of SGR-curves, alternative geological realizations and the use of different algorithms for prediction of fault zone permeability, were some of the parameters tested in the simulations. The different cases were compared with a reference case, BASECASE_3, which had the same properties as the history matched A-Lu model. All simulations were performed in the *Eclipse 100* reservoir simulation software, while the plotting has been done in Eclipse module *Office*. Eclipse 100 is a black oil reservoir simulation software developed by Schlumberger and is one of the most used reservoir simulators in the petroleum industry today.

8.2 Sensitivity Study of Fault Transmissibility in the A-Lu model

8.2.1 Procedure

In the first study the sensitivity of changing the fault transmissibility multipliers on reservoir performance in the A-Lu model was tested. The history matched A-Lu model was used to run the sensitivities. All faults included in the history matched A-Lu model including fault transmissibility multipliers, can be found in App A. The fault transmissibility multipliers are used to modify the transmissibility values calculated in the RMSfaultseal module. By using the Eclipse keyword *MULTFLT* the transmissibility along the fault trajectory will be modifed. Fault transmissibility multipliers calculated from the RMSfaultseal module in RMS are exported into Eclipse100 by using the keywords TRANX, TRANY and EDITNNC. The MULTFLT keyword will modify the transmissibility along the entire fault. A MULTFLT value of less than one will reduce the transmissibility and a MULTFLT value larger than one will increase the transmissibility. Setting MULTFLT equal to one means that default transmissibility (the fault transmissibility calculated in the RMSfaultseal) will be used.

The faults are divided into different categories based on the way they are incorporated into the simulation model. The large number of interpreted faults (240 faults) on Snorre makes it impossible to include all the faults into the model. One limitation is the grid resolution, which is larger than the distance between some faults. A prioritizing of the faults has therefore been made by a multi disciplinary team including disciplines like reservoir engineers, production engineers and geologist. The faults selected were believed to be important to flow. Faults referred to as *"1st PRIORITY"* faults in App A have been modelled in the 3D grid with a throw. Faults in the category *"3rd PRIORITY"* are possible to include in the 3D grid as multipliers, but they will not have any throw in the grid. The category *"1st PRIORITY taken out from grid generation"* are faults that originally were modelled with throw but now included in the simulation grid as a multiplier without throw. Some of the faults are elongated or divided into smaller parts in order to achieve a satisfying history match of the model. These faults are listed under the category *"Faults elongation/ or division"*. The last category is the *"MEPO Adjusted faults"*. *MEPO* is a software used for assisted history matching. In some areas of the model this software has been used to calculate fault transmissibility multipliers. The use of the MEPO software will not be described in more detail in this thesis.

Different sensitivities were run by multiplying and dividing the multipliers in App A by fixed values in the range 2 - 20. Faults in the *"3rd PRIORITY"* category and the *"1st Priority taken out from grid generation"* category with a multiplier value of 1 (default value) were not adjusted. These faults are modelled without throw and when they are given a value of 1 Eclipse calculates the transmissibility between the grid blocks as for unfaulted grid blocks.

8.2.2 Results and Discussion

8.2.2.1 Field Performance

As described in the previous section different fault transmissibility multipliers were used in order to look at the effect on the field performance and history match. Figure 8-1 shows both the historical production period as well as prediction until 2030 for some of the cases tested in the study. The A-Lu model is also included in the graph for comparison. As expected, changing the fault transmissibility multipliers has large impact on the reservoir performance. An interesting observation is that there is a relatively good match in total oil production from the field within the history matched period for all cases. One must be aware of that there are some changes in the historical period, but in the predicted interval there are large difference in oil production. This is because the observed reservoir volume (oil and water production) from the part of the Lunde formation which the A-Lu model covers has been used as input in the simulations. The model will try to produce this volume and if there is not enough oil available there will be higher water production (if available) to compensate for this and to match the observed reservoir volume produced. This can occur in areas of the model where the fault transmissibility is decreased and there is limited oil flow through the faults.

The trend in Figure 8-1 is that the higher the value of the fault transmissibility multipliers are, the higher the oil production from the field will be. This is due to the fact that several wells are

on pressure control in the predicted period, which means that the wells will produce as long as the BHP is high enough. The wells cannot produce at unlimited rates and an upper limit for oil or liquid production is set, based on expected performance of the well and limitations on the production facilities on the platform. It is clear that altering the fault transmissibility will have significant impact on the predicted performance from the field. The fault transmissibility has been one of the main factors adjusted in the history match of the model. Since there is large uncertainty related to fault communication there is also large uncertainty in the predicted oil production. There is an overall positive effect on oil production when having better communication across the faults. However, this does not mean that increasing the fault transmissibility gives higher oil production in all areas of the model. Some areas may experience pressure depletion faster because of better communication with other areas. The effect of the water and gas injection on the field is also most likely higher with more open faults. Then the fluid injected will flow across the faults and displace the oil easier. When faults are tighter the effect of introducing injectors will be more limited. To investigate these effects it can be useful to perform sensitivity studies on smaller segments in the model.

The two most extreme cases tested, where the fault transmissibility was multiplied and divided by a factor 20 (MULT20 and DIVID20), were studied in detail and compared with field history match. Figure 8-2 through Figure 8-5 show the results of the simulations. The simulations are run from production start of the field until April 2007 (period where historical data are included). Results from the A-Lu case (ALU-OLP-C3-FINAL-3) is also included the figures for comparison.

From Figure 8-2 one can see that the MULT20 case gives an overall good match with the historical data regarding total oil production (light blue line) and oil production rate (green line). The total oil production in the two cases (A-Lu and MULT20) is similar but the MULT20 case gives a better match with historical data. This can indicate that the official A-Lu model is too tight regarding communication, most likely across faults. The DIVID20 case, where the fault transmissibility is reduced, does not match the historical oil production (dark blue line) and oil production rates (red line). There is probably not enough mobile oil or pressure to match the measured oil production when the model becomes too tight.

In Figure 8-3 the total water production and water production rates for the cases are presented. The results reveal that there is a larger mismatch in water production for the two cases (MULT20 and DIVID20) compared with historical data, than in oil production. The A-Lu case gives the best match with historical data, while the two other cases produce too much water. The dark blue curve shows the total water production from the DIVID20 case, which yields the highest water production. This case will produce more water (if available) than the MULT20 case, because of the lack of oil production.

Figure 8-4 represents the gas production and GOR match for the same cases. The figure reveals that there is a relatively good match to historic data for the A-Lu and DIVID20 case. The case with increased fault transmissibility gives too low gas production compared with historical values.

Figure 8-5 illustrates how the pressure in the field develops with time for the A-Lu case (dark blue line), MULT20 case (light blue line) and the DIVID20 case (red line). It is clear that the average field pressure will be higher with increased fault transmissibility. For such a complex reservoir as the Snorre reservoir it will not be representative to use the average pressure on the field because there are many different compartments having different pressure regimes. It can still give an indication of the overall effect when adjusting the fault transmissibility. The increase in field pressure when opening the faults is most likely caused by the combination of larger drainage area and better effect of water and gas injection. With increased fault transmissibility water and gas will be able to flow across the faults and act as pressure support in the reservoir. If faults are fully sealing the effect of injection wells will be less, or in worst case meaningless. When one injector and one producer are located on each side of a fully sealing fault the injection well will not improve the recovery. Even adding a new injector to the injector side of the fault would not help, because no fluid will flow through the fault.

The four figures evaluated above can indicate that there could have been a better match on field level if the fault transmissibility were adjusted in some areas of the model. In the study above only the two most extreme cases (MULT20 and DIVID20) were tested and it seems like increasing the fault transmissibility can give good match when evaluating the field performance. It is evident that multiplying all the fault transmissibilities with a factor 20 is too high, since there is poor match in water production and gas production, but it is possible that fault transmissibility multipliers of 5 or 10 could have given a better match. This kind of study performed here is too simplistic, because the effects on wells in each area of the model must be investigated. It is not sufficient to only history match the oil, water and gas production when adjusting the fault transmissibility. The most important parameter to match when the communication is altered is the pressure in the wells. Repeat Formation Tester (RFT) and measurements of shut-in pressure have been used in the history match of the A-Lu model.

Each of the fault blocks included in the A-Lu model was evaluated when applying different fault transmissibility multipliers. The total oil production from the cases MULT20 and DIVID20 were compared with historical oil production from each fault block to get an indication if the area is too open or too sealing. For each fault block RFT data from a representative well was tested against the different cases. RFT data was taken from wells that were drilled in the fault block some years after production start. This was done to see if the model reflects the dynamic behaviour of the fault block regarding pressure, as RFT from in-fill wells will most likely measure pressure in depleted zones. The case(s) which gave the best match with the RFT data in the well were tested against historical data. One well from each fault block was tested to verify if it was possible to achieve a satisfying history match when changing the fault transmissibility multipliers.

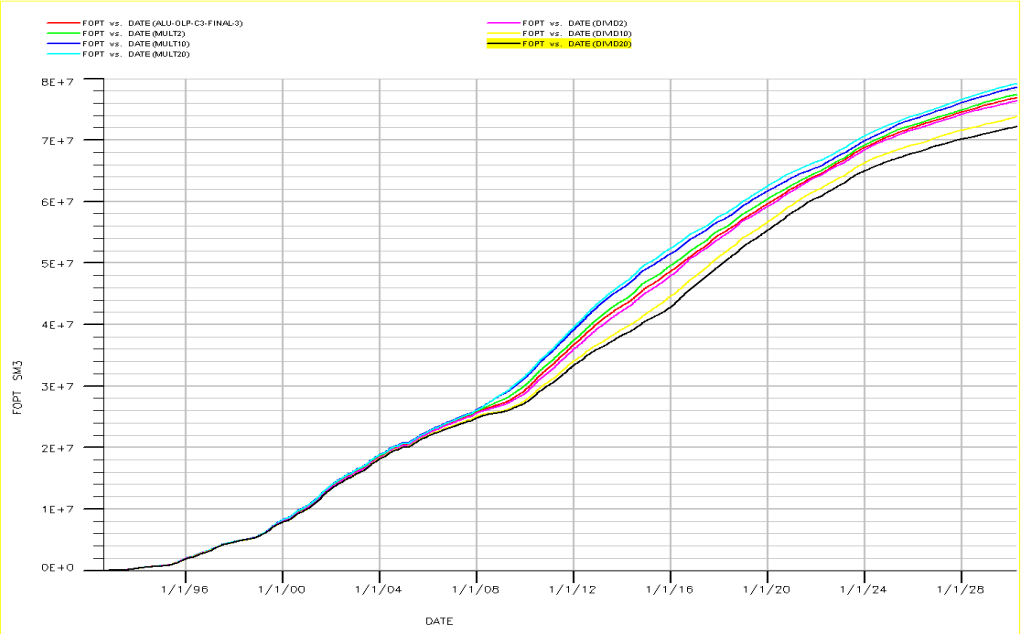

Figure 8-1 Effect of using different fault transmissibility multipliers on total oil production in the A-Lu model

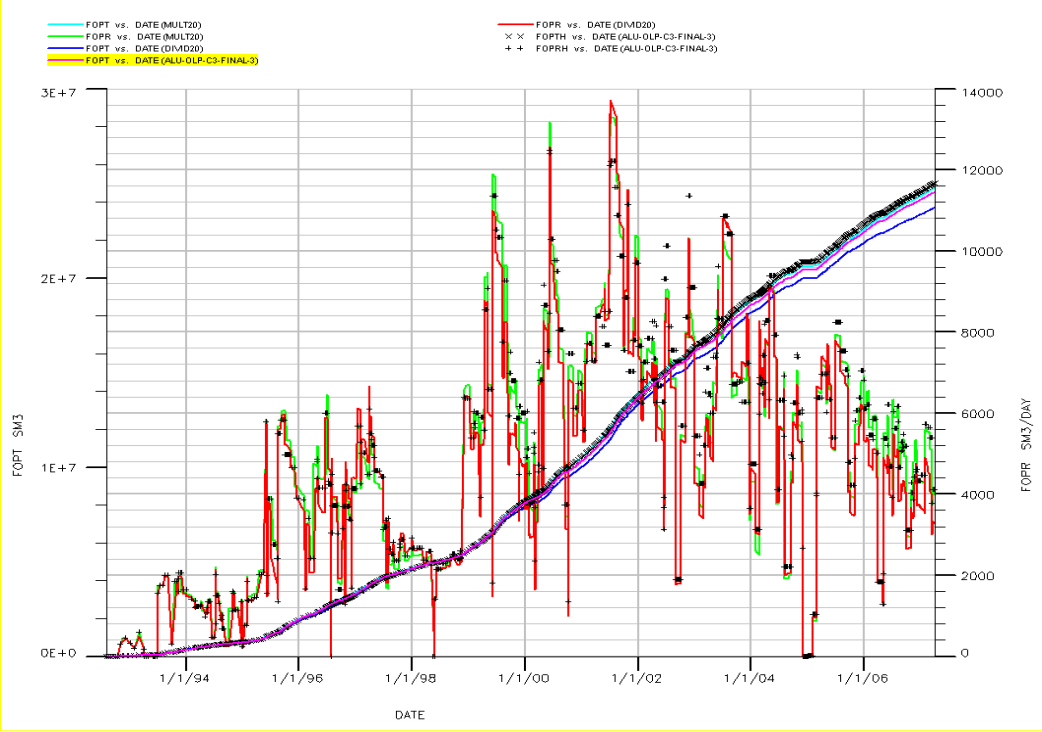

Figure 8-2 Total oil production match and oil production rates match for MULT20 and DIVID20

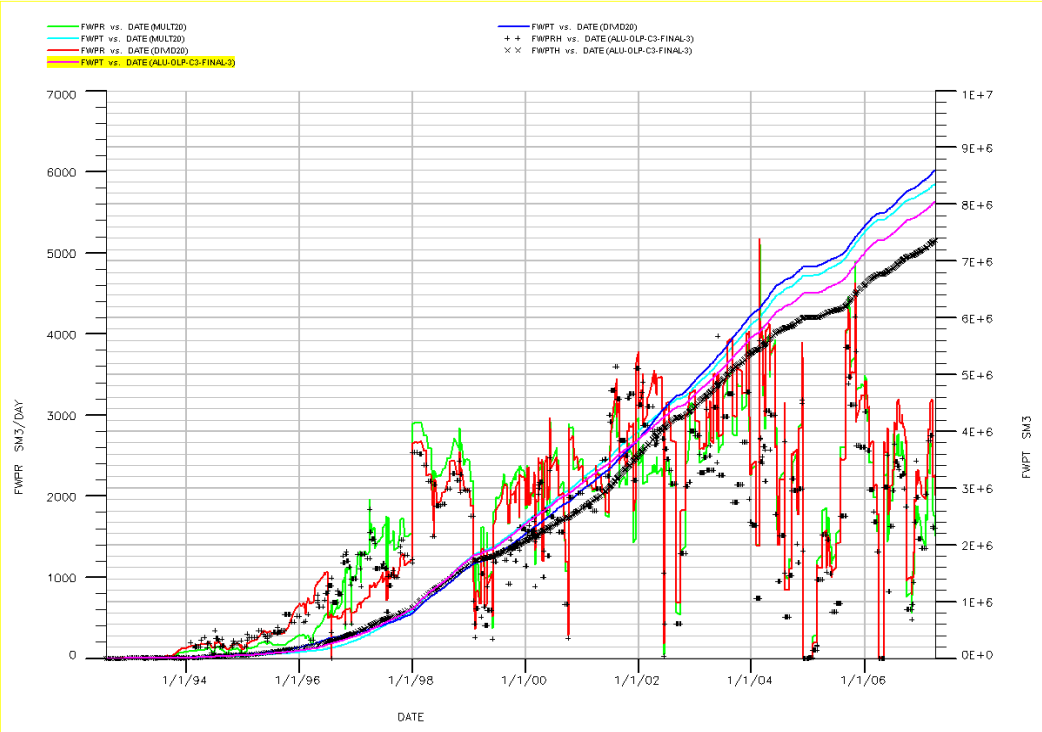

Figure 8-3 Water production match and water production rates match for MULT20 and DIVID20

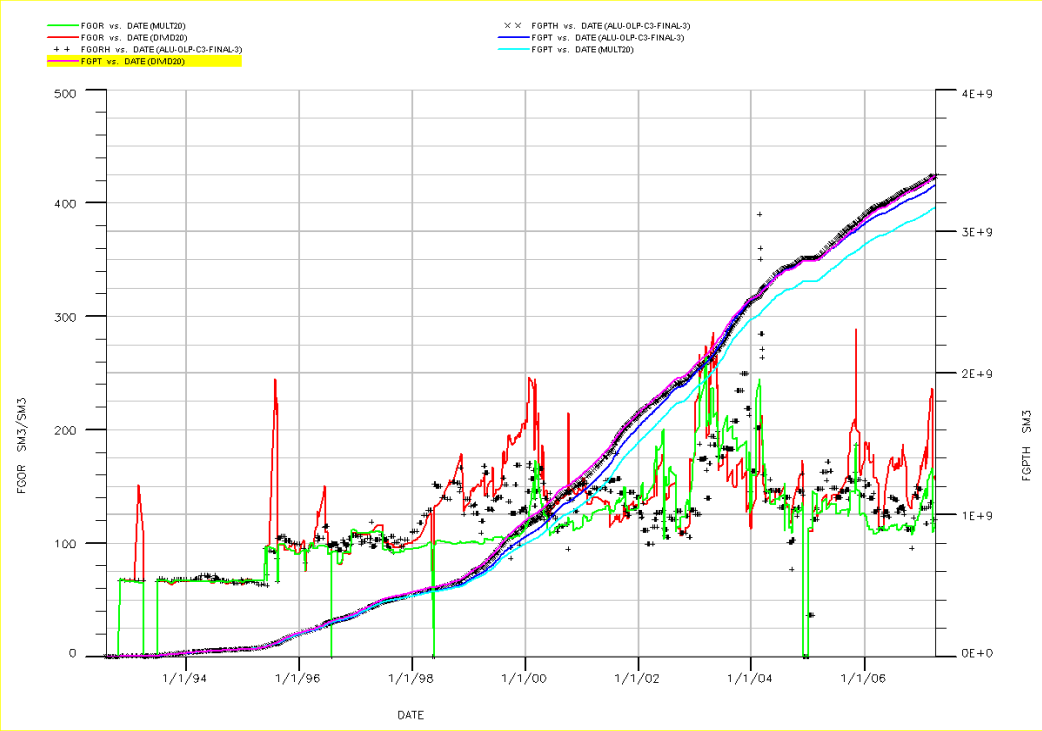

Figure 8-4 GOR match and total gas production match for MULT20 and DIVID20

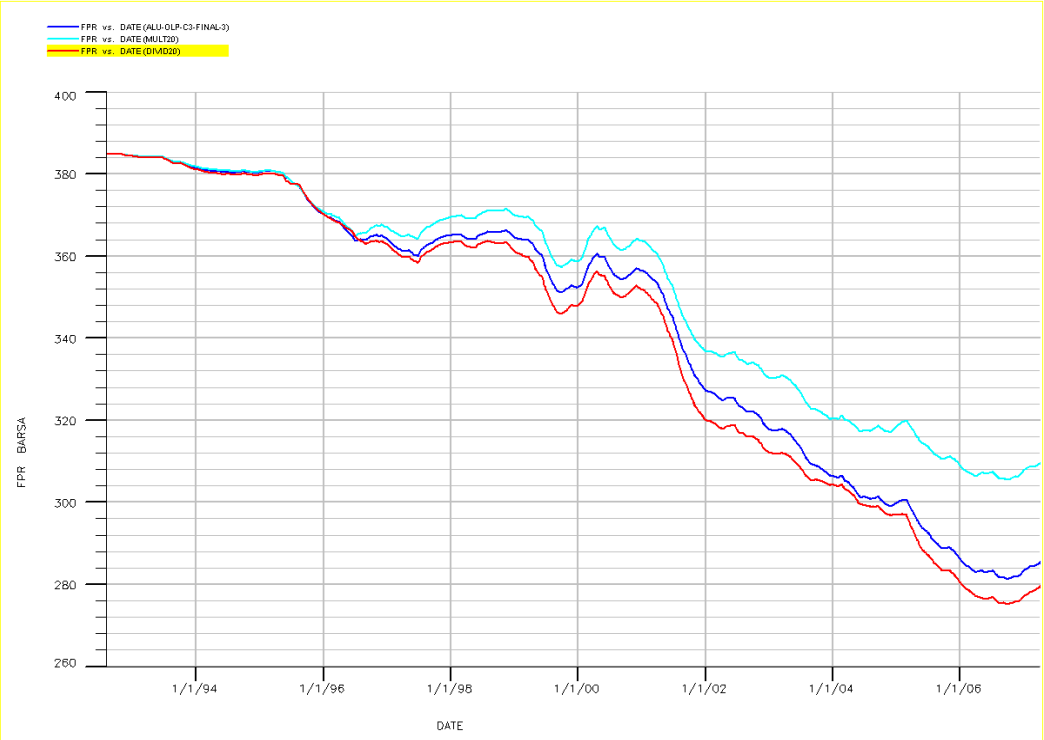

Figure 8-5 Comparison of field pressure in the A-Lu model, MULT20 and DIVID20

8.2.2.2 CFB

Figure 8-6 represents the total oil production for MULT20 (dark blue) and DIVID20 (light blue) compared with historical data from the Central Fault Block. Oil production from the A-Lu case (red) is also included for comparison. The figure reveals that both MULT20 and DIVID20 seem to give a better match with historical oil production from CFB. RFT data from well P-12LW was used to look at the pressure response in the model when altering the fault transmissibility. Well P-12LW was drilled in the CFB more than two years after the first well in the fault block and should be a representative well since depletion in different zones has occurred at this time. The RFT plot shows varying pressure with depth. High pressure “outliers” may be caused by isolated sands that have very little or no communication with other parts of the reservoir. The RFT measurements down to 2550 m TVDMSL are pressures measured in the Statfjord formation and are not included in the A-Lu model. Figure 8-7 and Figure 8-8 represent the RFT match for the cases where the fault transmissibility is increased and reduced. The data referred to as the BASECASE in the RFT plots are the results from the A-Lu model. Figure 8-7 shows that all cases give a relatively good match with the RFT data, though the A-Lu model seems to give the best match. Figure 8-8 shows that the DIVID5 case gives approximately the same RFT pressures as the A-Lu model. Well P-8LP has been the main producer for CFB Lunde and was for this reason used in the evaluation. Simulated performance of well P-8LP in cases MULT5 and DIVID5 was tested against the historical performance of the well.

Figure 8-9 through Figure 8-12 show the results of the study. In Figure 8-9 the water production from P-8LP is evaluated for the two cases. The DIVID5 case water production rate (red) gives too high values compared with historical data. This results in a poor match with total water production from CFB for this case (dark blue line). Case MULT5 seems to give a nearly identical match with historical water production rates (green line) and total water production (light blue line covered by the historical data).

In Figure 8-10 the two cases are compared with historical oil production. The oil production rate from the DIVID5 case (green line) seems to be overall too low. As a result of this the total oil production from case DIVID5 (light blue line) for CFB is too low, especially after 1999. Case MULT5 (red line and dark blue line) seems to give a good match both to the historical oil production rate (red line) and total oil production (dark blue line).

In Figure 8-11 the GOR match for the MULT5 (light blue) and DIVID5 (dark blue) cases is represented. Both cases give approximately the same results and have in general too low GOR values compared with historical data. The high GOR values observed around 1995 is caused by wrong allocation of gas and does not represent a gas breakthrough.

Based on the discussion above the MULT5 case gives the best match to historical data. The results show that it is possible to increase the fault transmissibility in the CFB area with a factor of 5 and still have a good history match. This can indicate that there are too tight faults in the area around P-8LP.

Figure 8-12 illustrates the predicted performance of CFB until 2030 compared with the A-Lu case (expected case). The A-Lu case will give a higher total oil production than the MULT5 case, but the difference is small. This prediction run shows that altering the fault transmissibility in the CFB will affect the forecasted performance of the fault block.

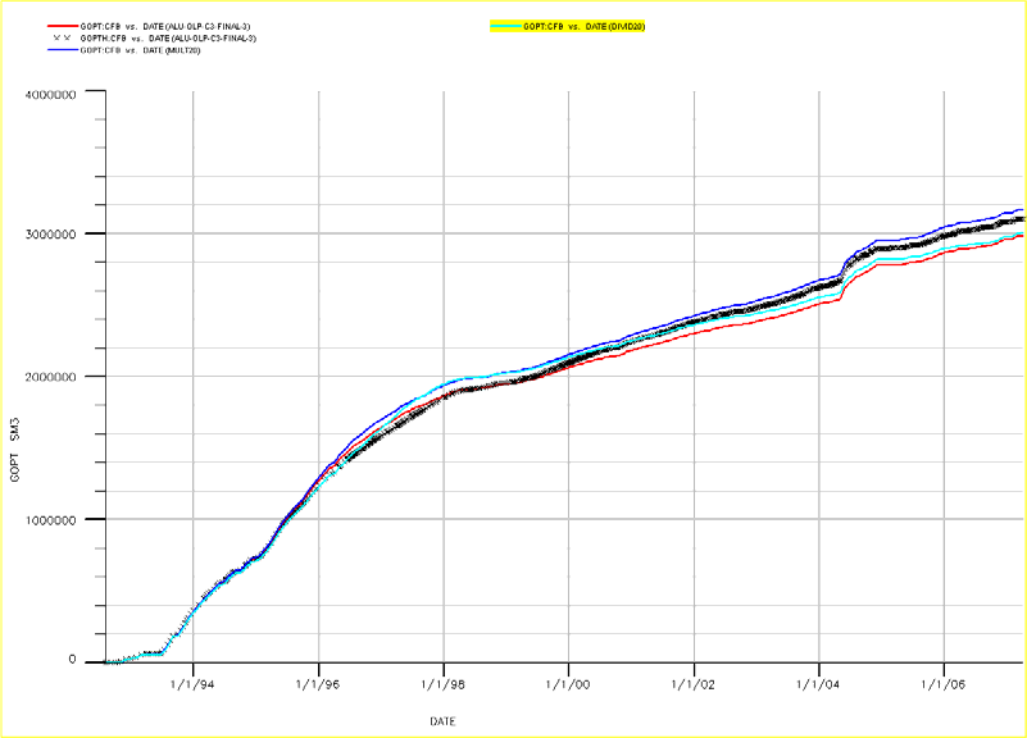

Figure 8-6 Total oil production for the different cases compared with historical oil production from CFB

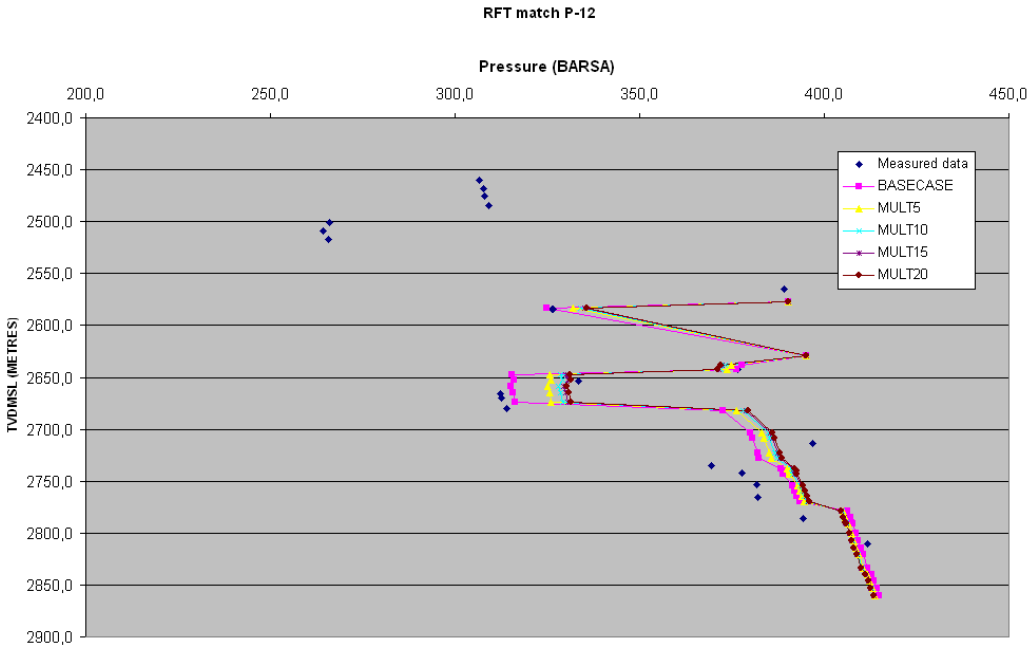

Figure 8-7 RFT match for the different cases where fault transmissibility is increased

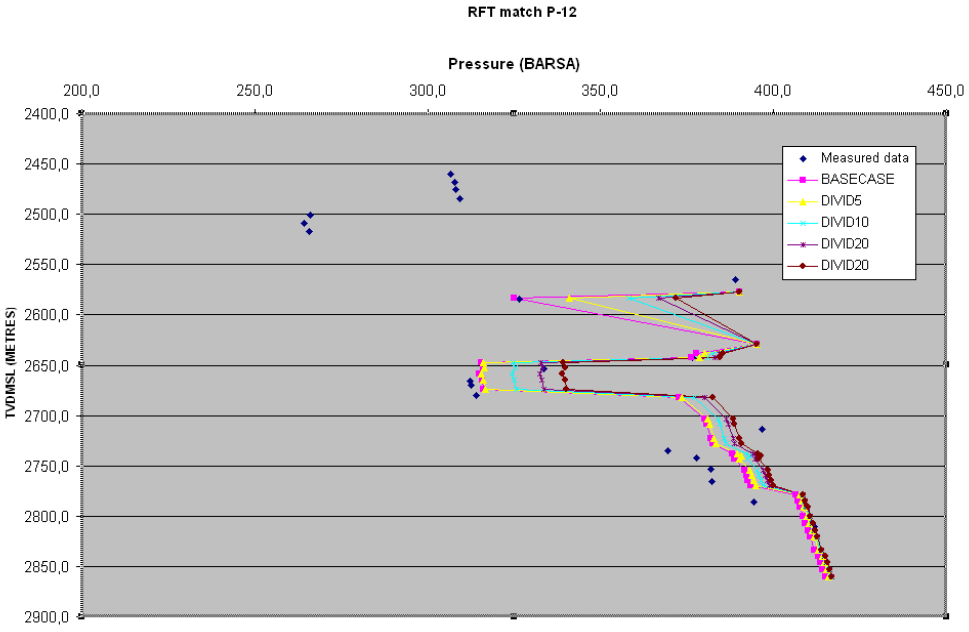

Figure 8-8 RFT match for the different cases where fault transmissibility is decreased

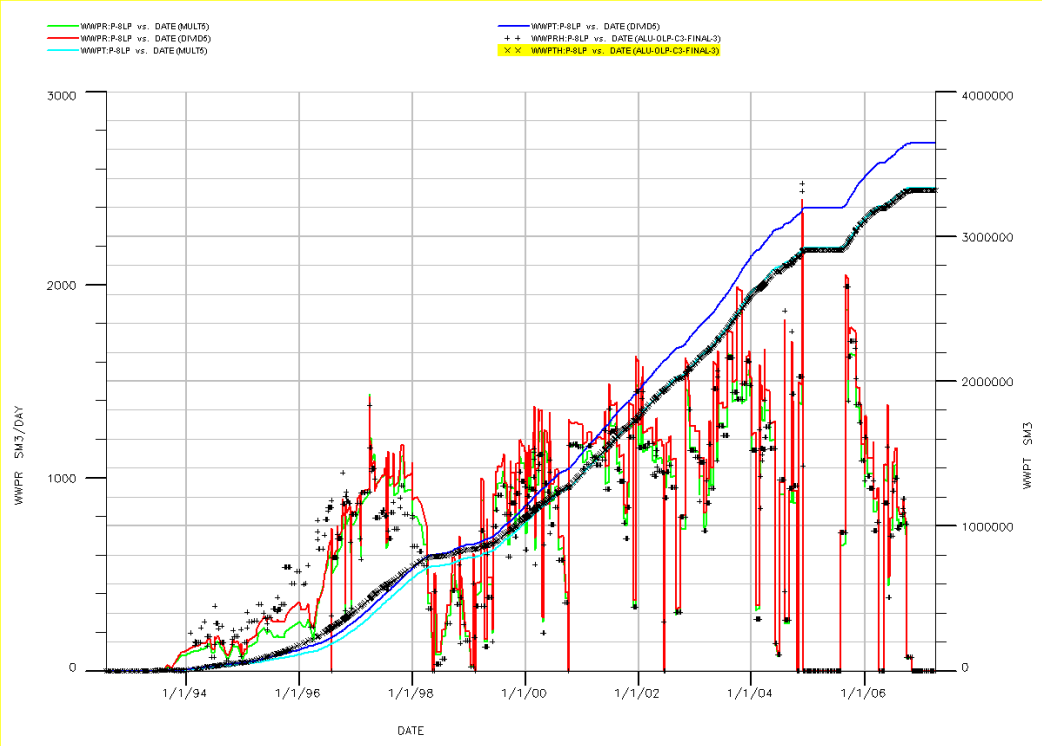

Figure 8-9 Comparison of MULT5 and DIVID5 with historical water production data

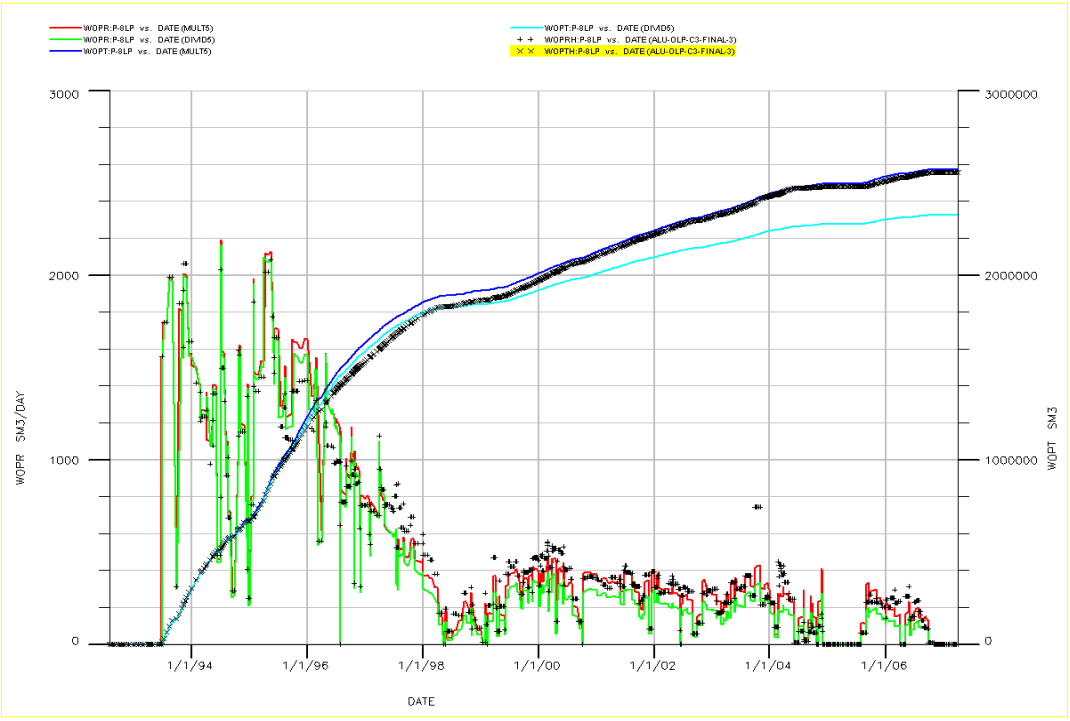

Figure 8-10 Comparison of MULT5 and DIVID5 with historical oil production data

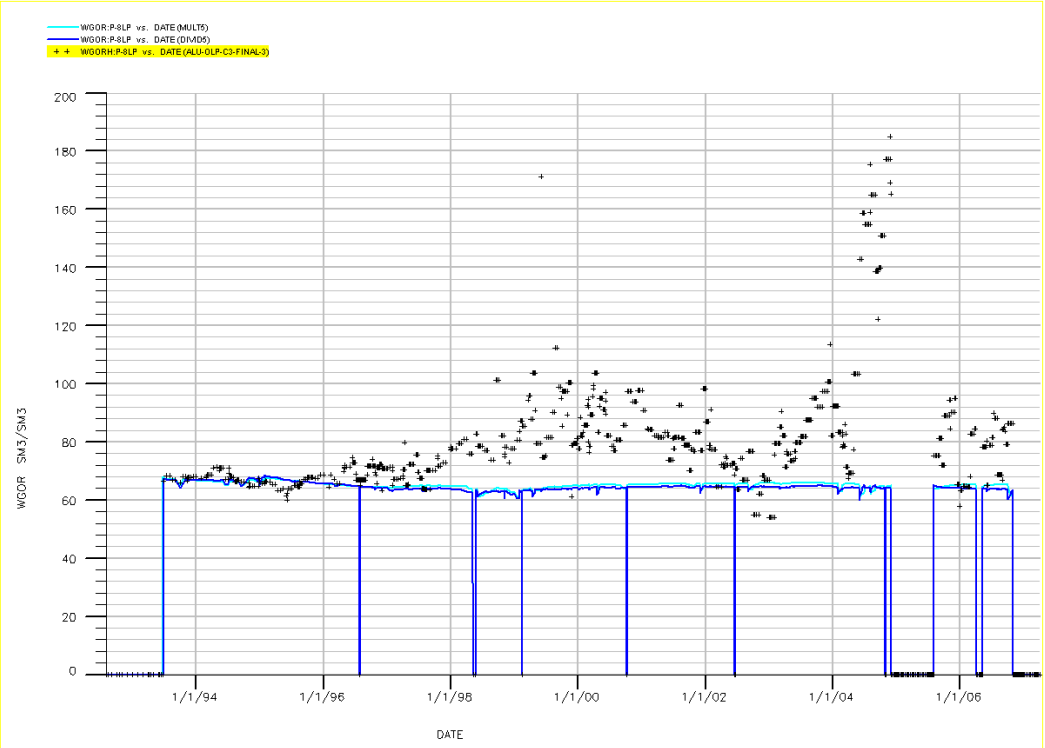

Figure 8-11 Comparison of MULT5 and DIVID5 with historical gas production data

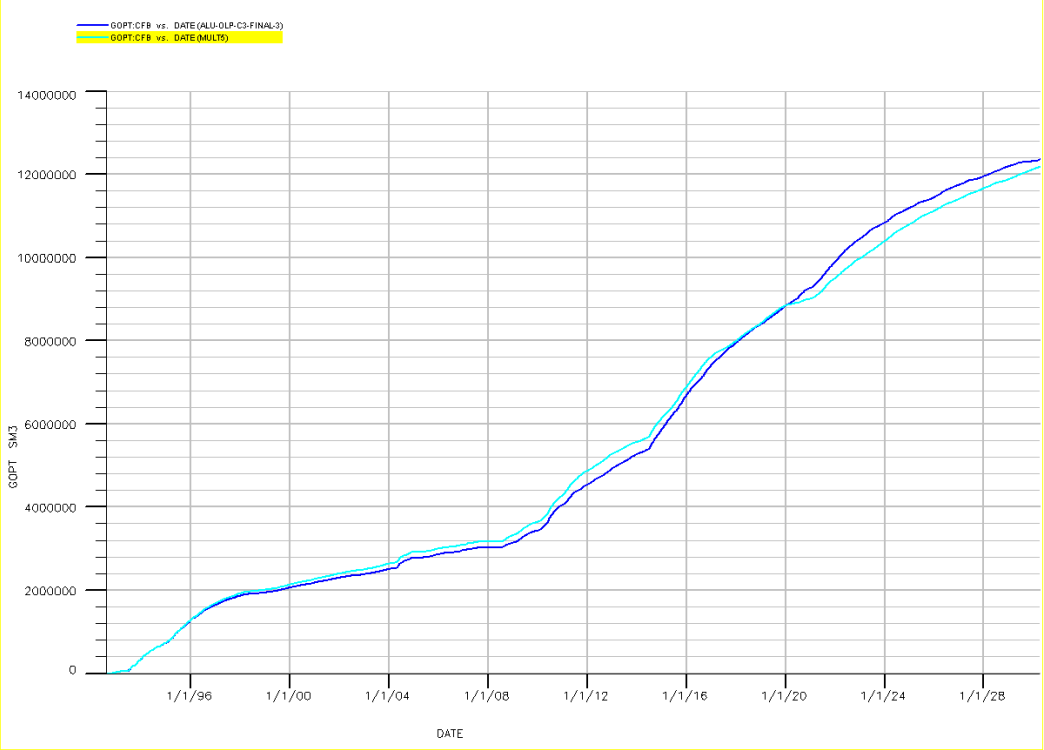

Figure 8-12 Predicted oil production for A-Lu and MULT5

8.2.2.3 ECFB

The ECFB is a very challenging fault block to model, since the block is split between A-Lu and B-Lu models. Well contribution to each model, from wells situated in both models, is difficult to estimate. Figure 8-13 represents the total oil production for MULT20 (red line), DIVID20 (blue line) and the A-Lu case (green line) compared with historical data from the East Central Fault Block. The figure reveals that the case where the fault transmissibility is reduced by a factor 20 matches the historical data the best. The MULT20 case gives far too high production compared with observed production, especially after 1. January 2002. The A-Lu case is also giving too high oil production from this fault block. This can indicate that the faults in this area are too open and different cases with adjusted fault transmissibility were tested against RFT pressures in well P-23P. The RFT from this well was taken in April 1997. The first well in the fault block, P-22, was drilled in October 1996.

Figure 8-14 and Figure 8-15 show the RFT pressure match for the different cases simulated. The RFT pressures from 2405 m TVDMSL and below are pressures taken in the area covered by the B-Lu model. In general, pressures from this well are very difficult to match because of the varying pressure regimes. In Figure 8-14 one can see that the different cases where the fault transmissibility is increased will give a poorer history match than the A-Lu case. Figure 8-15 shows that there is a satisfying pressure match for case DIVID5. It was decided to investigate the DIVID5 case regarding history match to water, oil and gas production for ECFB. The well P-23P was also used in this evaluation. The results from the expected case (A-Lu model) are included for comparison. Figure 8-16 through Figure 8-19 show the results of the study. In Figure 8-16 the water production in P-23P from case DIVID5 is presented. The total water production from the A-Lu case is also included in the figure. Both the A-Lu case (dark blue line) and the DIVID5 case (light blue line) give too late water breakthrough in the well compared with historical data. The green line in the figure shows the simulated water production rate from the DIVID5 case. The match to the historical rate is not good but the same trends are observed. The total water production from DIVID5 gives a much better overall match to historical data than the A-Lu case.

Figure 8-17 shows the oil production rates for the DIVID5 case (red line) and the A-Lu case (green line) case compared with historical rates. In addition, the total oil production from the two cases are included and compared with historical oil production. Total oil production from the DIVID5 case is represented by the dark blue line, while the A-Lu case is represented by the light blue line. The DIVID5 case gives an overall better match to the historical oil production from well P-23P compared with the A-Lu case, both when it comes to total production and production rates.

In Figure 8-18 the GOR values from the two cases are represented. Case DIVID5 is represented by the dark blue line and the A-Lu case by the light blue line. Both cases give approximately the same results, but the DIVID5 case seems to give the best overall match.

Figure 8-19 shows the predicted performance until 2030 of the ECFB for the two cases. The A-Lu case is represented by the dark blue line and the DIVID5 case by the light blue line. Oil production from the fault block stopped in 2005 and at that time the A-Lu case had produced

more oil than the DIVID5 case. Based on the results above it may seem like the oil production in ECFB is over predicted.

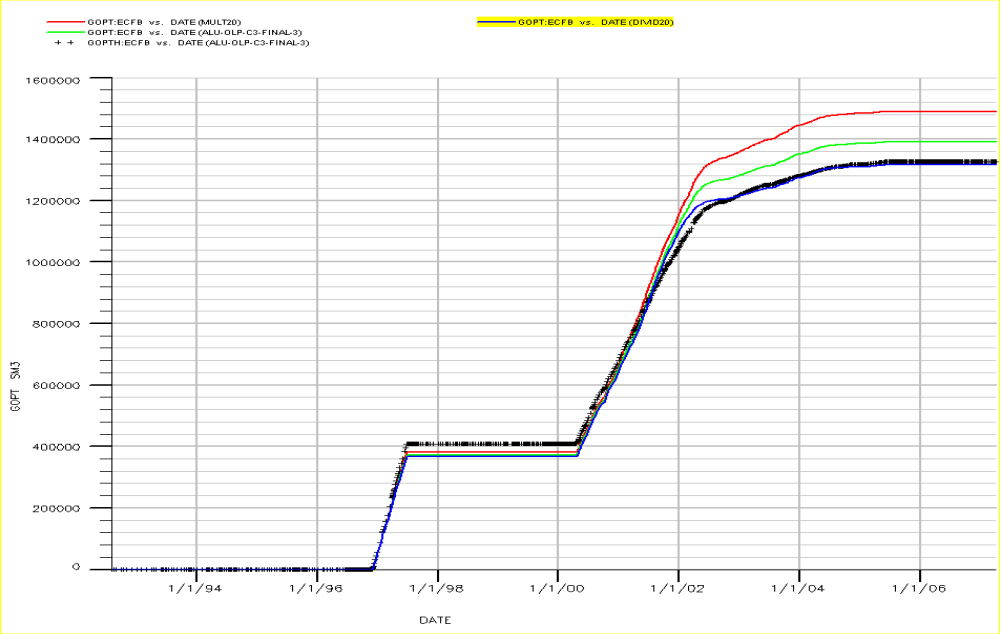

Figure 8-13 Total oil production for the different cases compared with historical oil production from ECFB

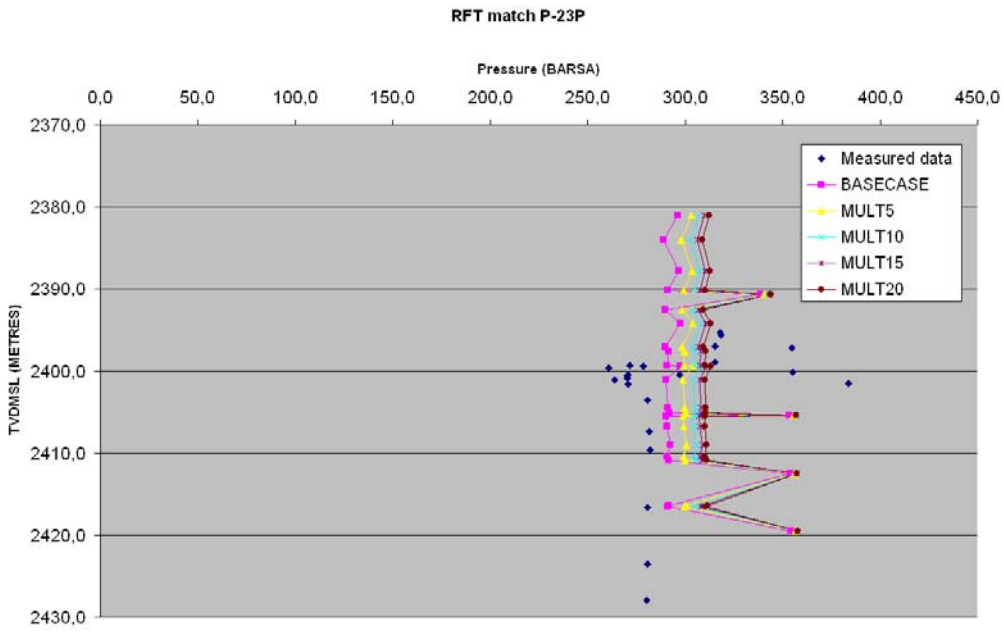

Figure 8-14 RFT match for the different cases where fault transmissibility is increased

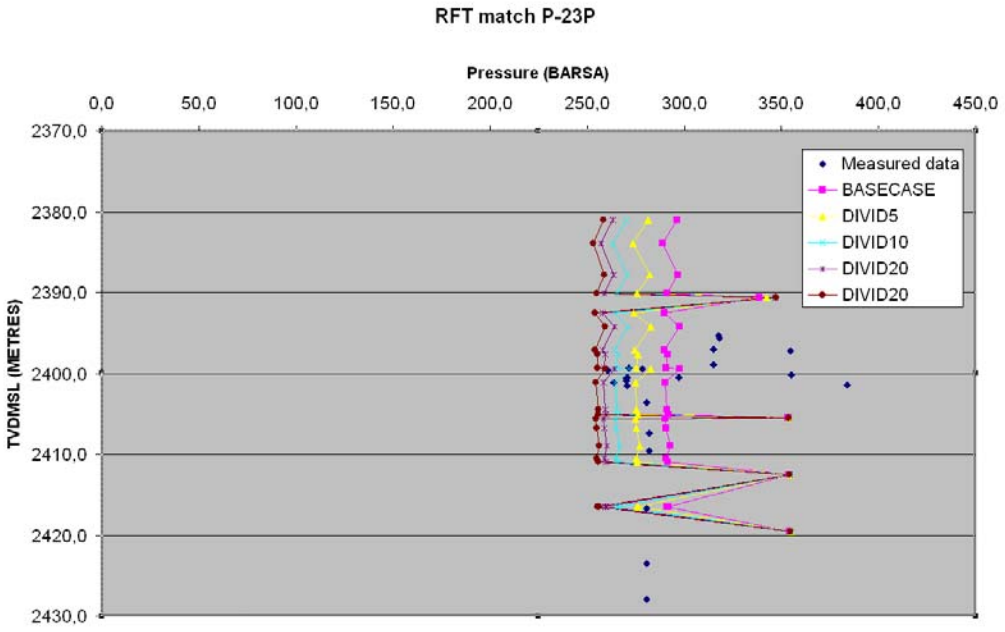

Figure 8-15 RFT match for the different cases where fault transmissibility is decreased

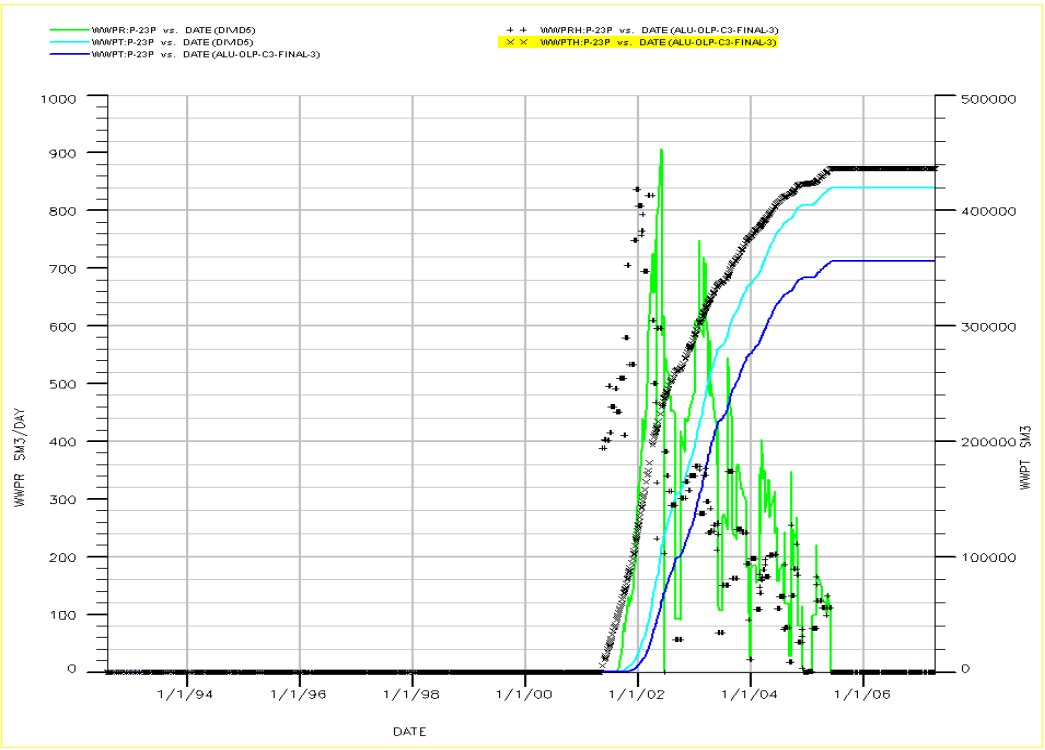

Figure 8-16 Comparison of DIVID5 and A-Lu with historical water production data

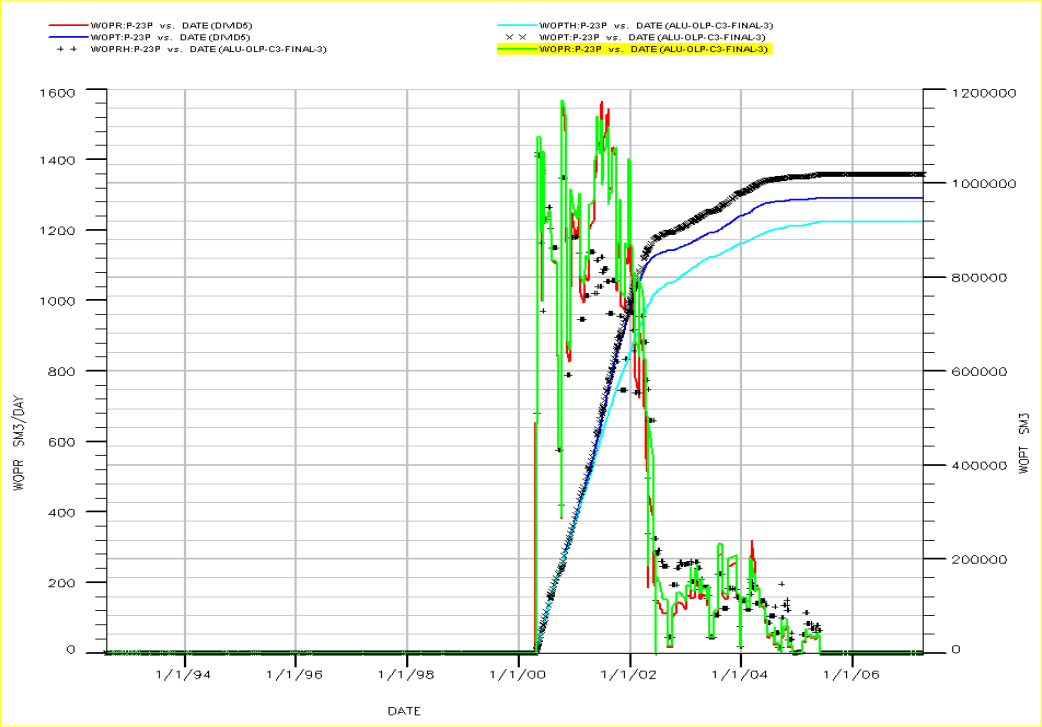

Figure 8-17 Comparison of DIVID5 and A-Lu with historical oil production data

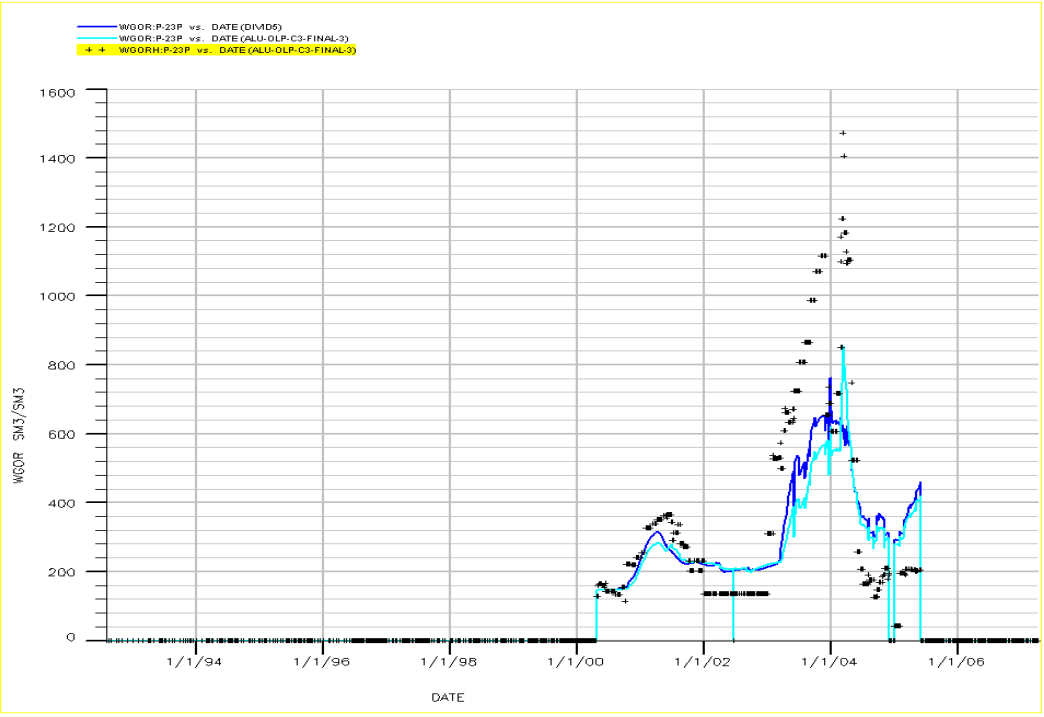

Figure 8-18 Comparison of DIVID5 and A-Lu with historical gas production data

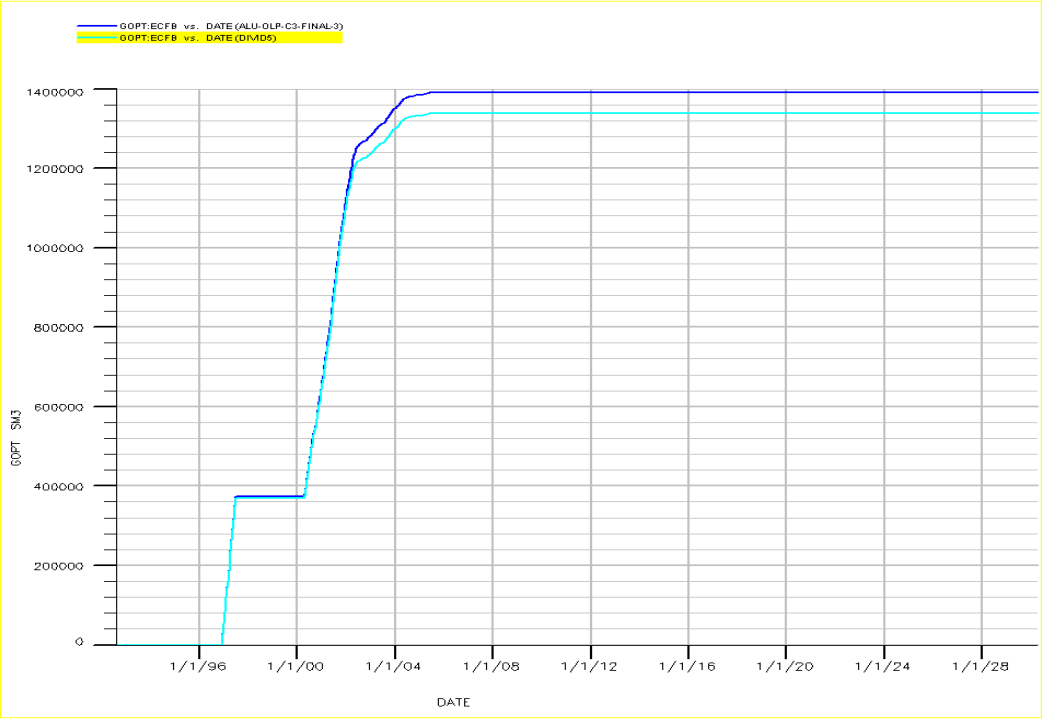

Figure 8-19 Predicted oil production for A-Lu and DIVID5

8.2.2.4 EFB

Figure 8-20 shows the total oil production from the East Fault Block for case MULT20 (dark blue line), DIVID20 (light blue line) and the A-Lu case (red line) compared with historical oil production. The figure illustrates that all cases give a too low oil production compared with historical data. The difference is largest for the DIVID20 case, indicating that the fault transmissibility may be too low for this case.

RFT data from well P-36A was used to see the impact in the different cases. The RFT pressures in P-36A were measured in February 1999, more than four years after the first producers were drilled in the fault block. Figure 8-21 shows the RFT match in the well when the fault transmissibility is increased. One can observe from the RFT plot that pressures are varying with depth and difficult to match with the model. This is probably caused by several isolated sands having their own pressure regimes. The cases differ from the BASECASE (A-Lu case), but case MULT5 still gives a match to the measured RFT pressures in the well. In Figure 8-22 the RFT match for the cases with reduced fault transmissibility are illustrated. These cases give a poor match with measured pressures. Comparing the simulated pressures from the different cases and RFT pressures from well P-36A indicates that the area around the well may be too tight regarding communication across faults, as the MULT5 case gives a match with the pressures. The performance of well P-9LP, located in the same area as P-36A, was tested against historical data for the MULT5 case.

In Figure 8-23 through Figure 8-26 the results from the study are presented. Figure 8-23 shows the water production from well P-9LP for the MULT5 case and the A-Lu case. Water production rate from the MULT5 case (green line) gives too high values between 1998 and 2001 and too low values between 2001 and 2004, compared with historical data. In the last years of the historical period there is a relatively good match. The total water production from the MULT5 (light blue line) case gives a better overall match to historical water production compared with the A-Lu case (dark blue line).

Figure 8-24 shows the oil production from the MULT5 case (dark blue line), A-Lu case (light blue line) and historical data. The MULT5 case oil rates (green line) give a relatively good match with the historical rates. The A-Lu case gives the best match with total oil production from the fault block, although the difference between the cases is small.

Figure 8-25 shows the GOR values from well P-9LP in the different cases compared with measured values. The MULT5 case is represented with the light blue line and the A-Lu case with the dark blue line. The two cases give similar results, but the A-Lu case matches the GOR values between 1998 and 2001 best.

In Figure 8-26 the predicted oil production until 2030 for the two cases is illustrated. The figure reveals that there is little difference in the predicted performance of EFB for the two cases. Since both cases give a relatively good history match with the parameters tested above it seems like multiplying the fault transmissibility with factor 5 has little impact for EFB.

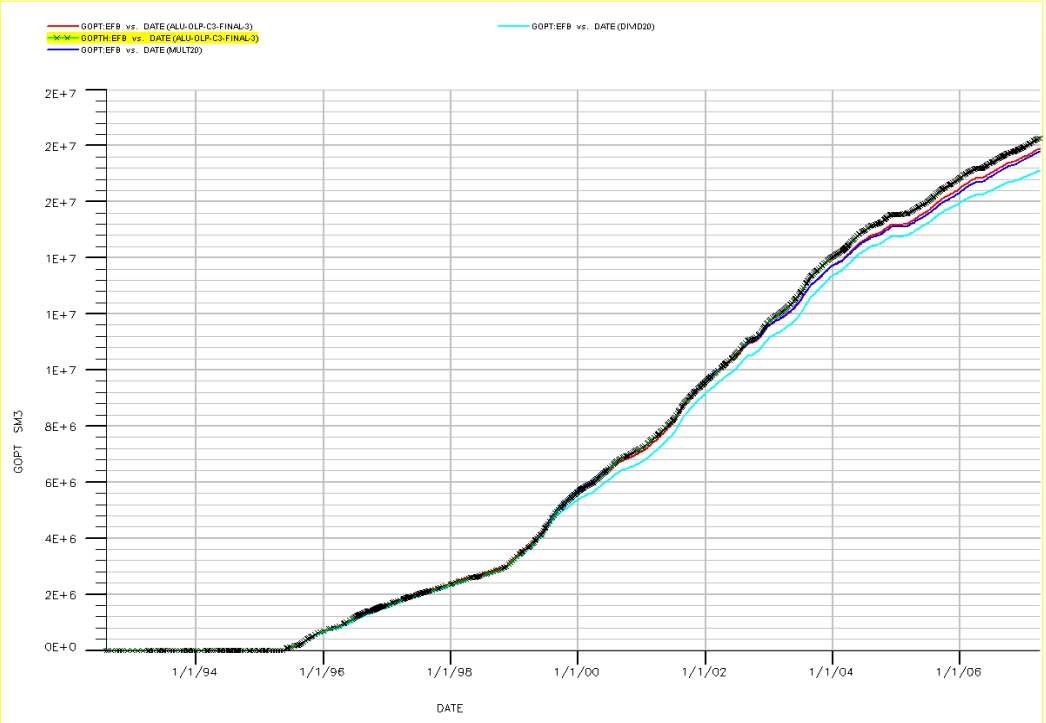

Figure 8-20 Total oil production for the different cases compared with historical oil production from EFB

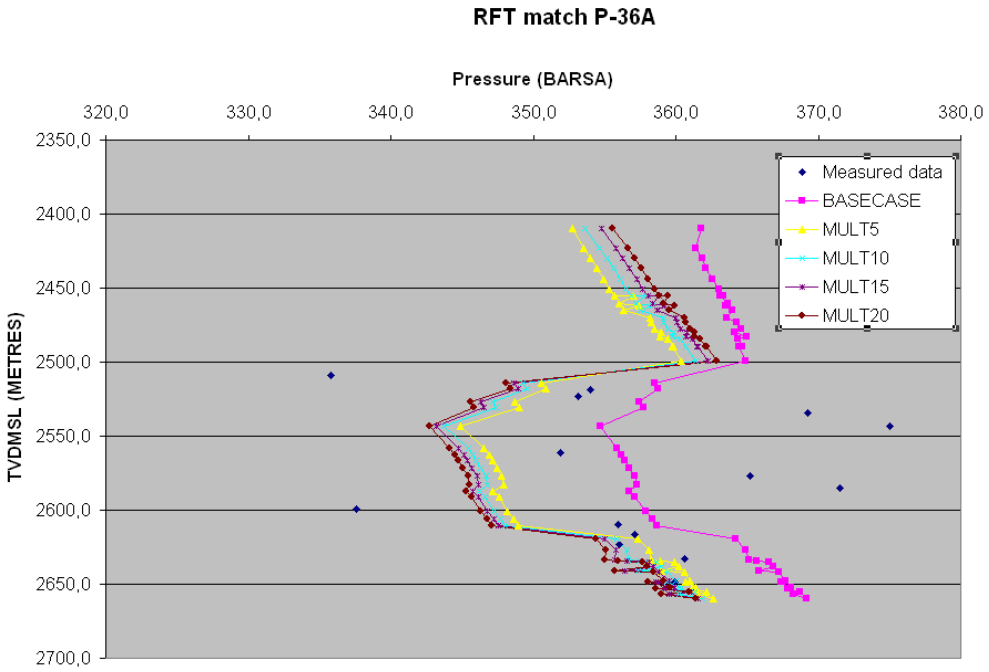

Figure 8-21 RFT match for the different cases where fault transmissibility is increased

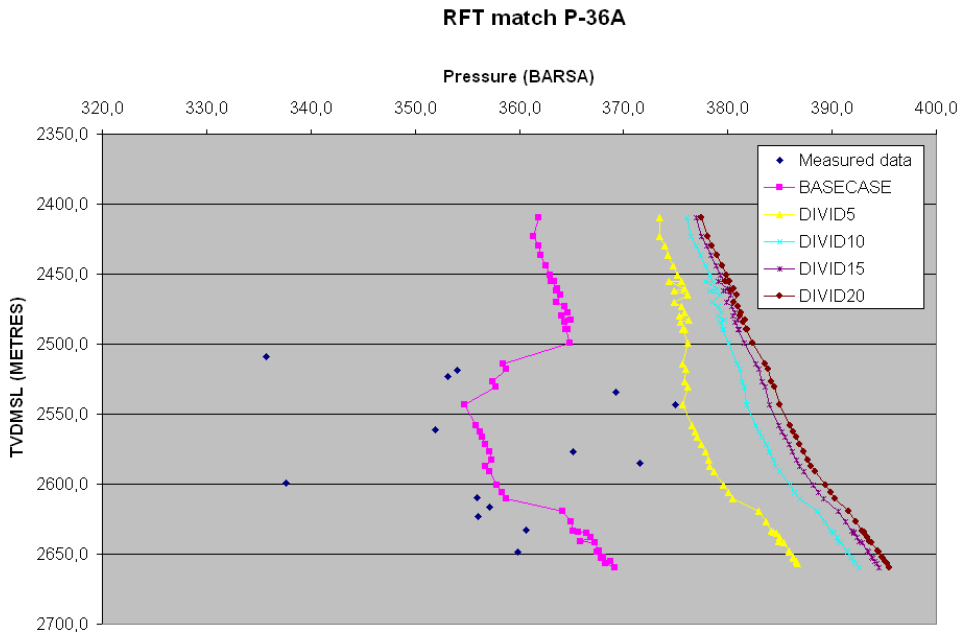

Figure 8-22 RFT match for the different cases where fault transmissibility is decreased

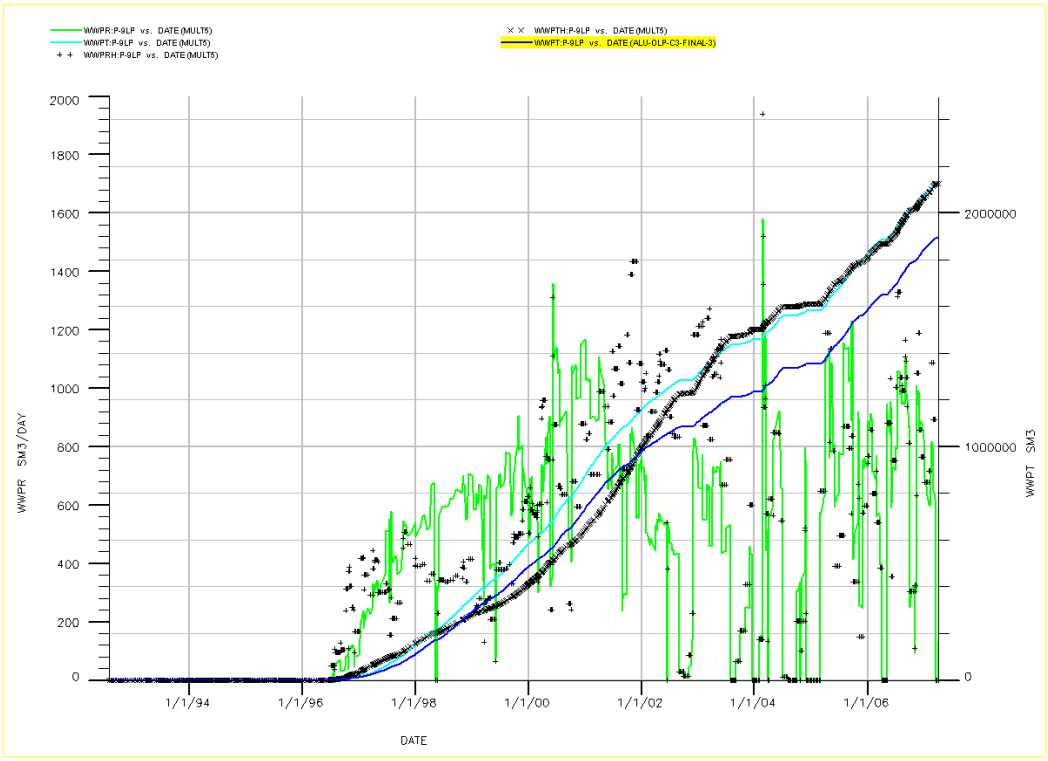

Figure 8-23 Comparison of MULT5 and A-Lu with historical water production data

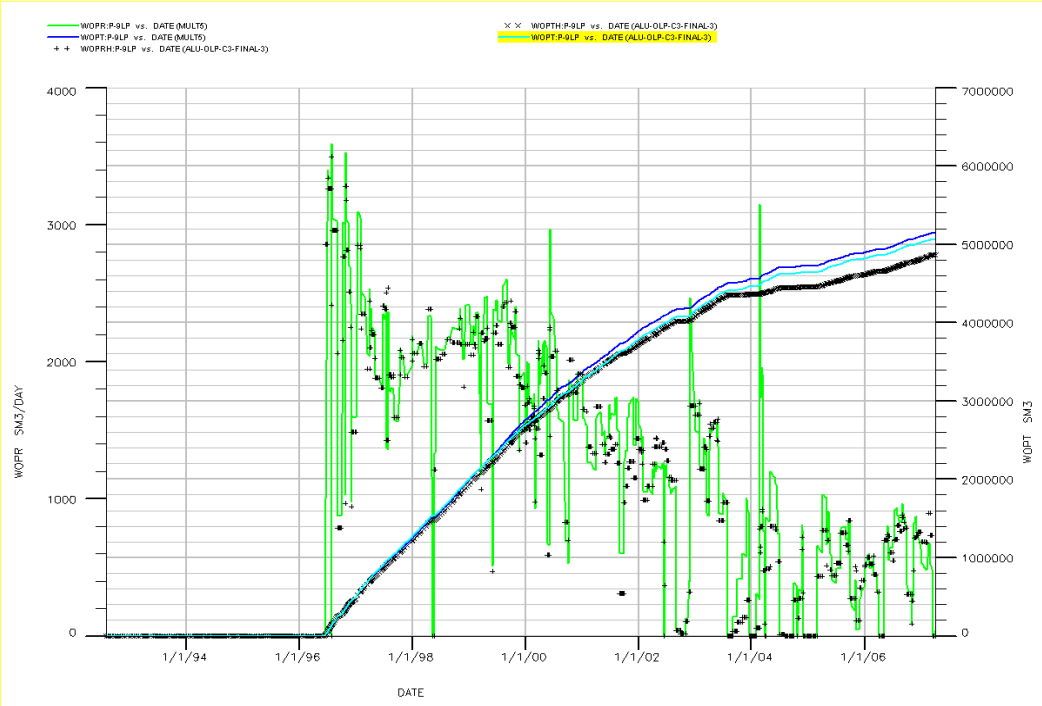

Figure 8-24 Comparison of MULT5 and A-Lu with historical oil production data

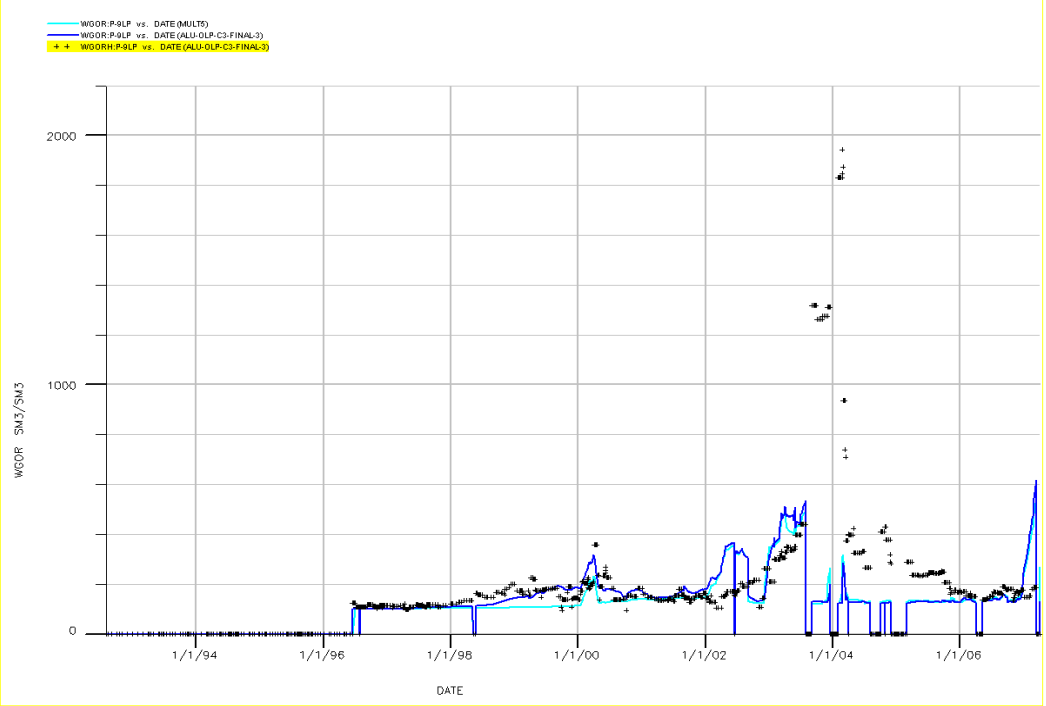

Figure 8-25 Comparison of MULT5 and A-Lu with historical gas production data

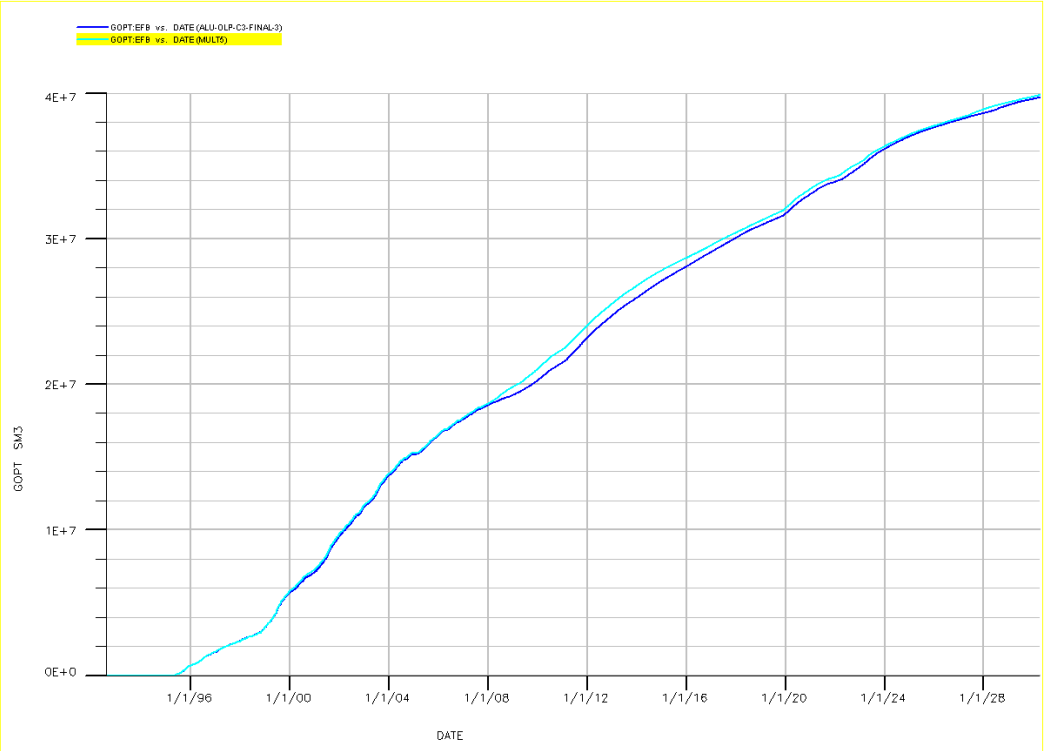

Figure 8-26 Predicted oil production from EFB for A-Lu and MULT5

8.2.2.5 NCFB

Figure 8-27 shows the total oil production from the North Central Fault Block for cases MULT20 (dark blue line), DIVID20 (light blue line) and the A-Lu case (red line) compared with historical oil production. From this study it does not seem like changing the fault transmissibility multiplier by a factor 20, have any effect on the oil production from NCFB. The different cases were checked against measured pressures in the well.

RFT pressures from well D-2H were tested against simulated pressures from the different cases. The RFT pressures from D-2H were taken in September 2004. The RFT measurements indicate that the well is drilled through homogeneous sands, since the same pressure regimes are occurring in the well. At about 2570 m TVDMSL there is a barrier between subzones SN8.1 and SN8.2. The results from the RFT match are illustrated in Figure 8-28 and Figure 8-29. In Figure 8-28 the simulated pressure from the cases with increased fault transmissibility is tested against measured RFT pressures from D-2H. In addition to the BASECASE (A-Lu), the MULT10 case also gives match with the RFT measurements. But the MULT10 case does not reproduce the pressures in SN8.1. From Figure 8-29 one can observe that reducing the fault transmissibility will give very poor match with the RFT pressures.

Well D-2AH has been the active producer in NCFB for the history matched period and the performance of this well in the MULT10 case was compared with historical data. The results from the evaluation are presented in Figure 8-30 through Figure 8-33. In Figure 8-30 the water production from D-2AH in case MULT10 (light blue line) and the A-Lu case (dark blue line) are compared with historical data. The historical water production indicates that there is no water breakthrough in the well for the historical period. For the A-Lu case there seems to be a massive water breakthrough in the end of the historical period. There is also a water breakthrough in the MULT10 case, but this is nearly negligible.

Figure 8-31 shows the total oil production from the MULT10 case (dark blue line) and the A-Lu case (light blue line) compared with historical oil production data. In addition, oil production rate for the MULT10 case is included (green line). The oil production rate from the MULT10 case gives a good match to measured rate. When it comes to total oil production both cases give a satisfying match.

Figure 8-32 illustrates the GOR for the two cases compared with measured data. Both cases give the same results and there is a relatively good match to historical data.

Based on the discussion and results above it is possible that multiplying the faults in the NCFB area by factor 10 will give a satisfying match with historical data in terms of RFT pressure and production of oil, water and gas.

Figure 8-33 shows the prediction runs for the two cases until 2030. There is a significant difference in total oil production for the two cases, indicating that the use of fault transmissibility multipliers have large influence in this part of the model. The D-2AH well is drilled in an area containing many faults reducing the transmissibility in the east-west direction

(Figure 7-4). Increasing the transmissibility across these faults is most likely the main contribution to the improved oil recovery.

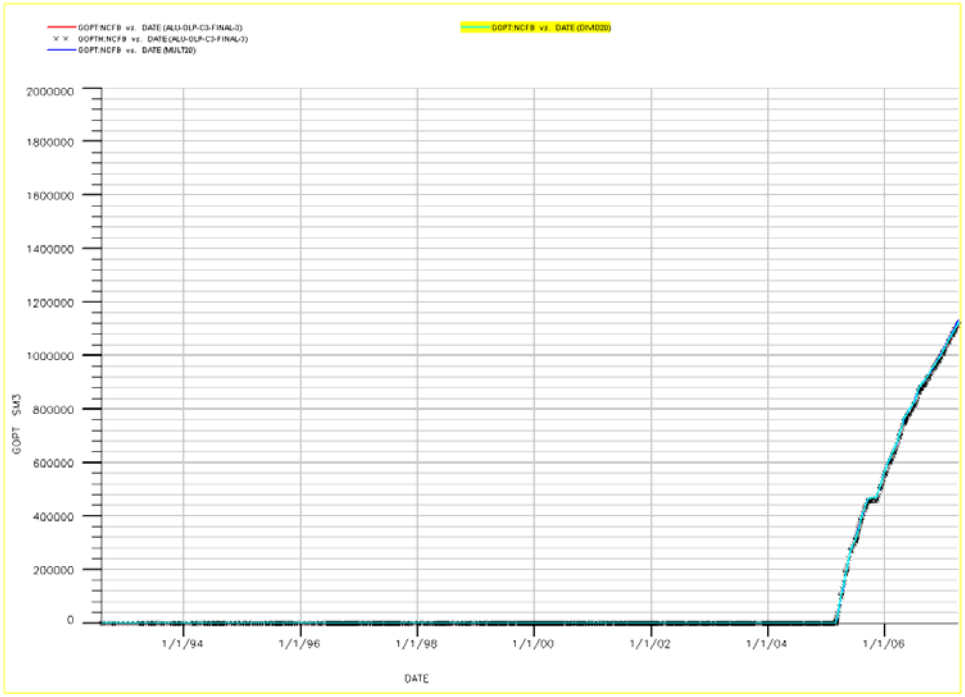

Figure 8-27 Total oil production for the different cases compared with historical oil production from NCFB

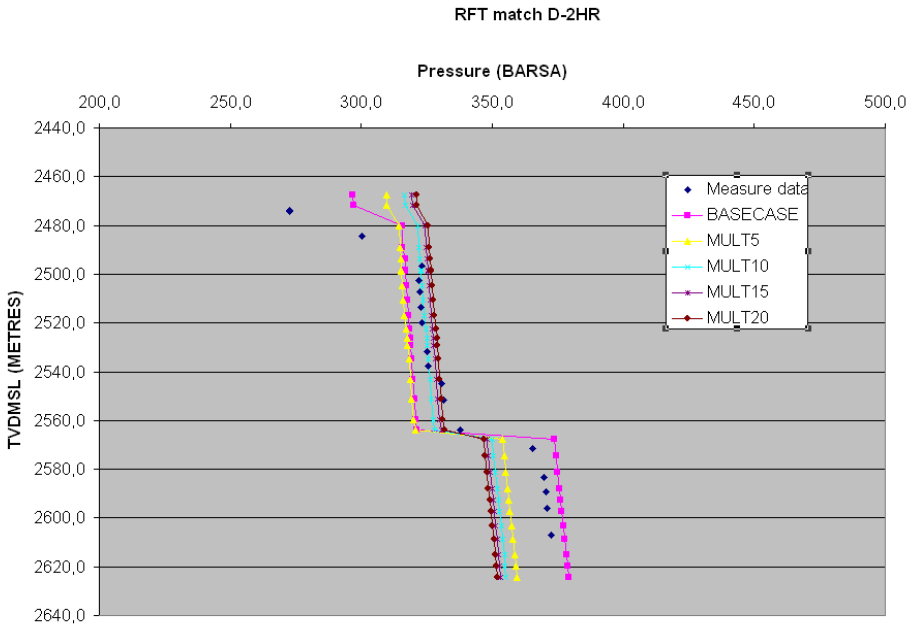

Figure 8-28 RFT match for the different cases where fault transmissibility is increased

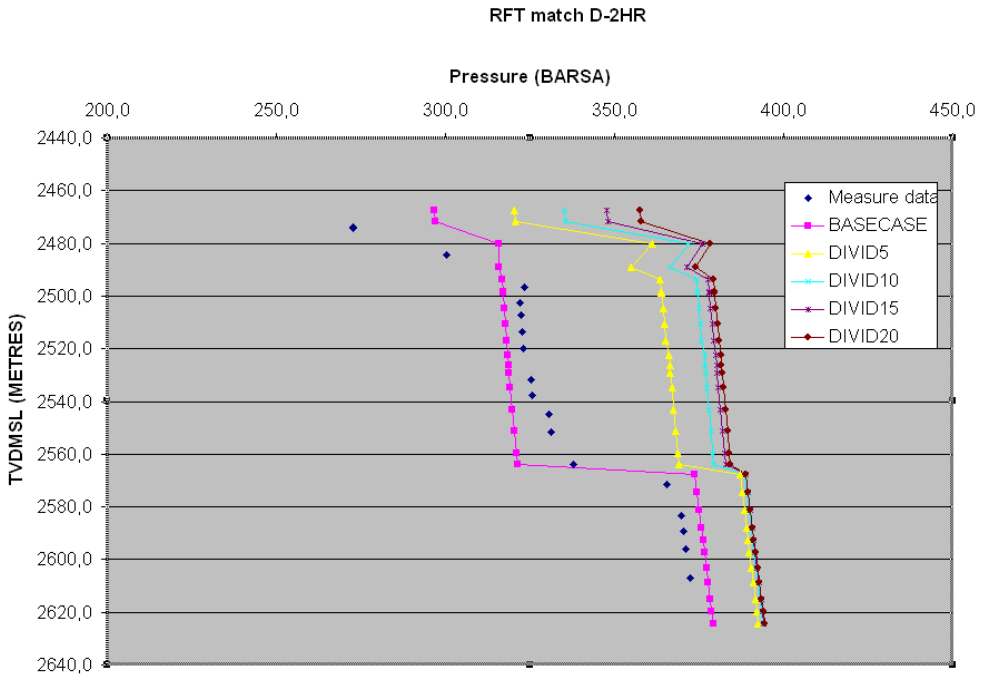

Figure 8-29 RFT match for the different cases where fault transmissibility is decreased

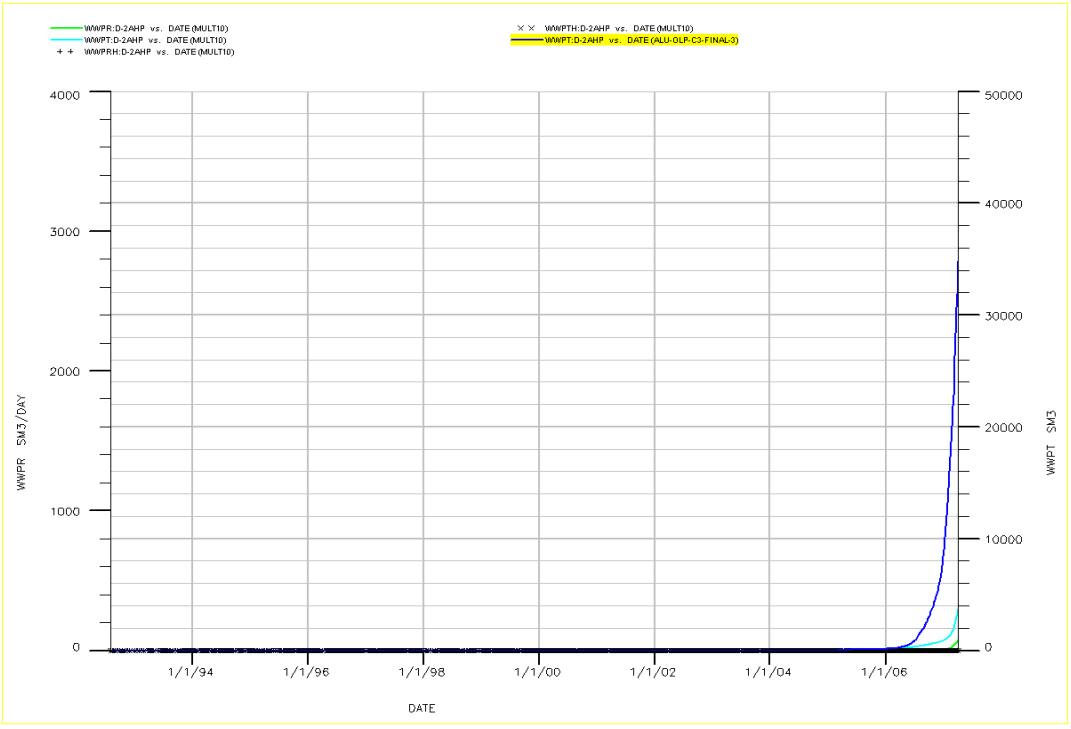

Figure 8-30 Comparison of MULT10 and A-Lu with historical water production data

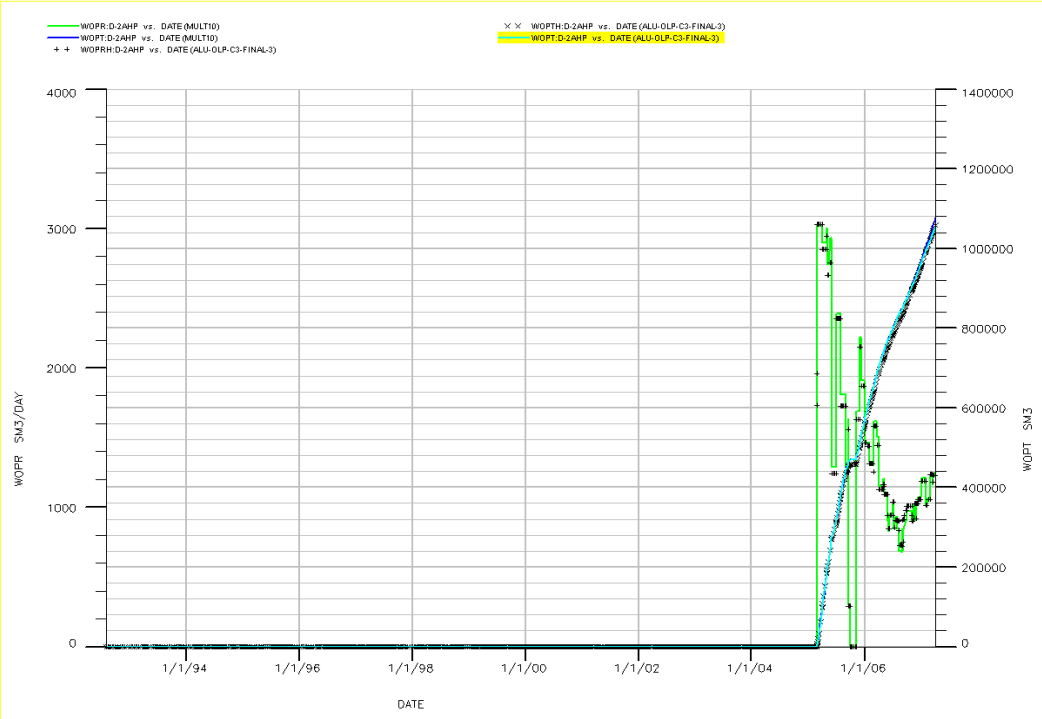

Figure 8-31 Comparison of MULT10 and A-Lu with historical oil production data

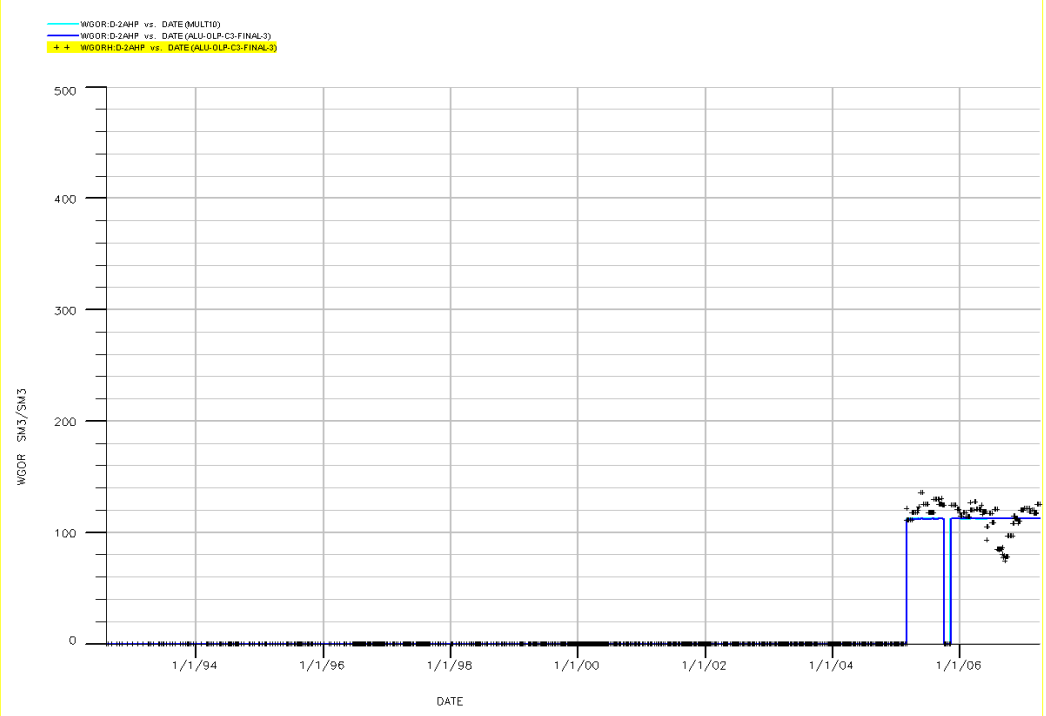

Figure 8-32 Comparison of MULT10 and A-Lu with historical gas production data

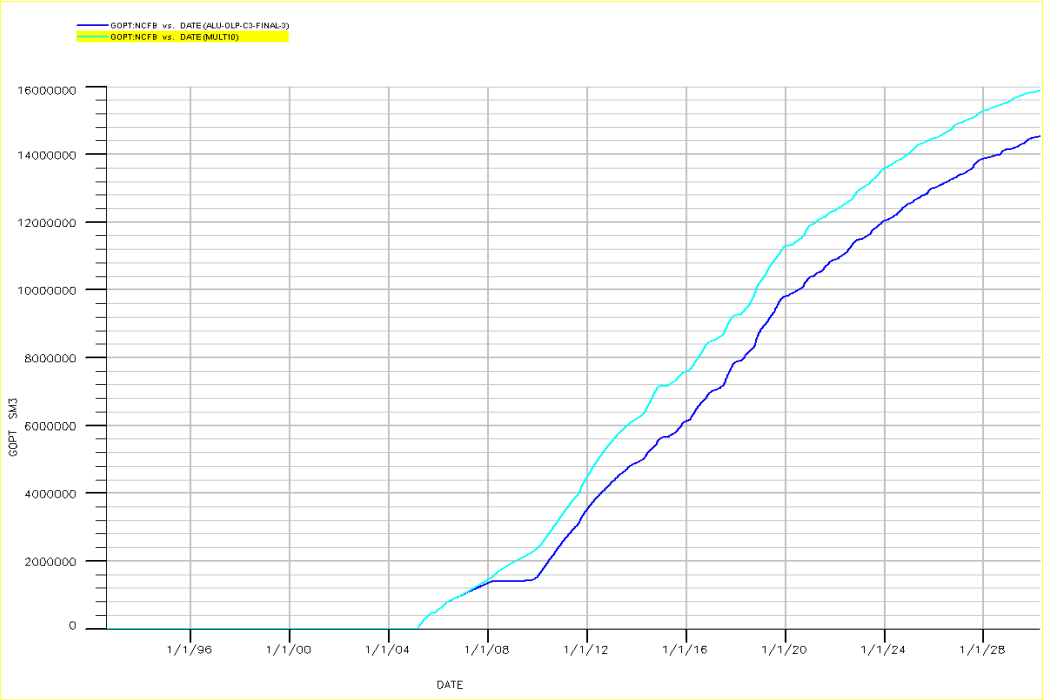

Figure 8-33 Predicted oil production from NCFB for A-Lu and MULT10

8.2.2.6 WFB

Figure 8-34 shows the total oil production from the Western Fault Block for the MULT20 case (dark blue line), DIVID20 case (light blue line) and the A-Lu case (red line) together with the historical production. All cases yield good match with the historical oil production, with the MULT20 case having a more or less perfect match.

Simulated pressure for the cases where the fault transmissibility was modified was tested against RFT pressures in well P-44. P-44 was the first producer in WFB and RFTs from well showed pressure depletion in the area. The results are illustrated in Figure 8-35 and Figure 8-36. It is obvious that the cases with increased fault transmissibility give better match to the RFT pressures than the cases with reduced fault transmissibility. The MULT5 case has the best match with the measured RFT pressures. Neither the A-Lu case nor the cases with modified transmissibility manage to represent the barrier between the upper and lower measurements.

Production data from well P-44 in the MULT5 case were tested against historical performance of the well. Figure 8-37 through Figure 8-40 shows the results of this evaluation. Figure 8-37 shows the water production from the two cases, where the MULT5 case is represented by the light blue line and the A-Lu case by the dark blue line. Both cases give approximately the same result for total water production, but differ some from the historical data. The MULT 5 case gives the best match. The water production rate from this case (green line) is in general too high compared with the historical rate.

Figure 8-38 shows the total oil production for the two cases compared with historical production. As for water production, the oil production is approximately the same for the two cases. Both cases have good match with the historical production. The green line in the figure shows the oil production rate from the MULT5 case and has very good match with measured data.

Figure 8-39 shows the GOR match for the two cases. Both cases give the same GOR values for the entire period and have a relatively good match with measured data.

The prediction run until 2030 in Figure 8-40 show that the multiplying of the fault transmissibility by a factor of 5 will have impact on the total oil production. Both cases (MULT5 and A-Lu) give a satisfying history match, indicating that there is large uncertainty in the prediction runs.

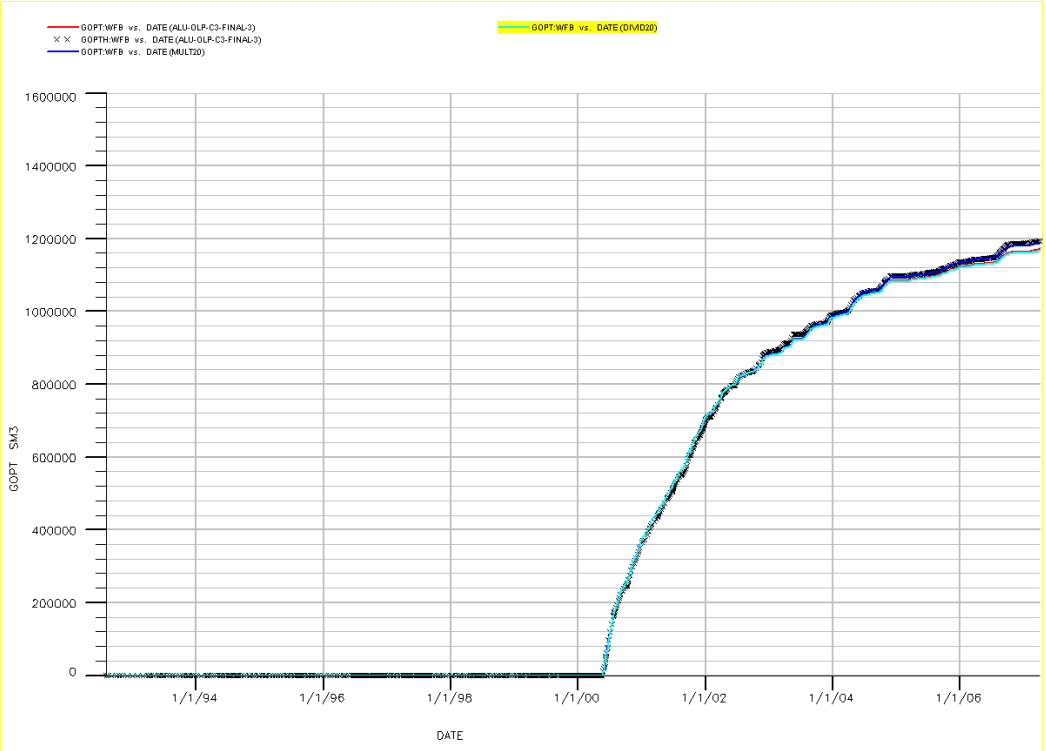

Figure 8-34 Total oil production for the different cases compared with historical oil production from WFB

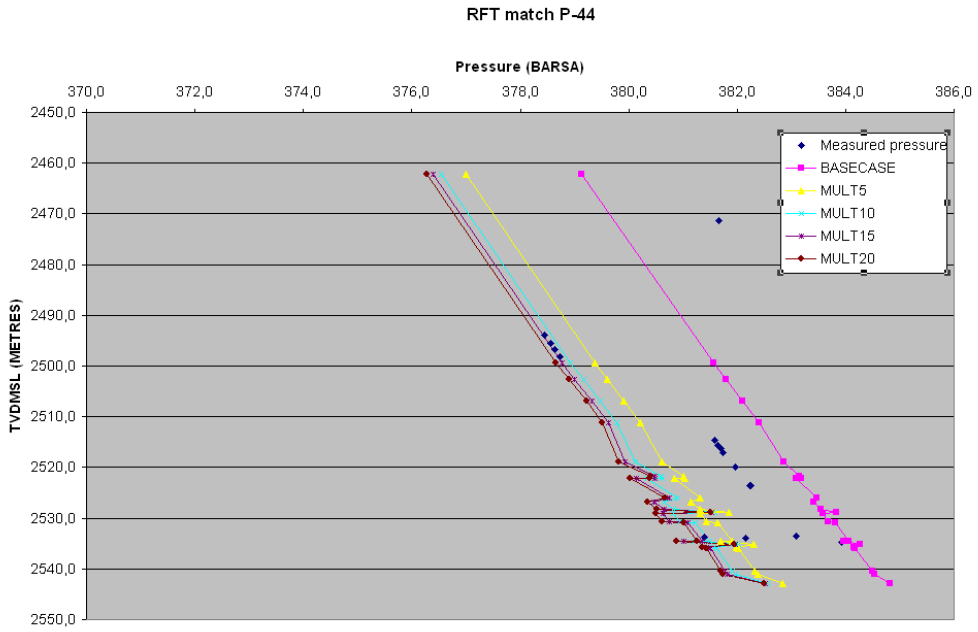

Figure 8-35 RFT match for the different cases where fault transmissibility is increased

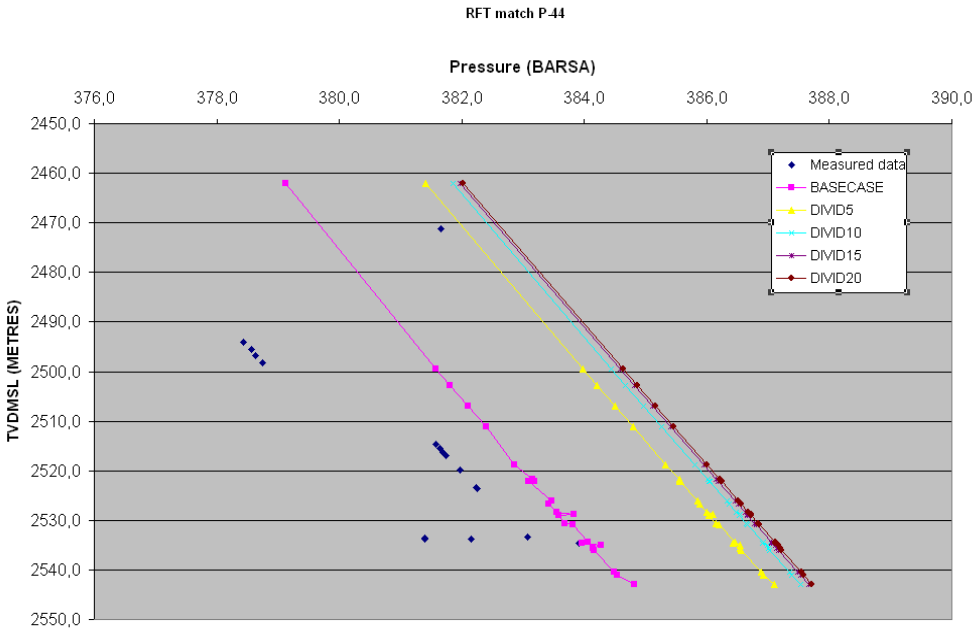

Figure 8-36 RFT match for the different cases where fault transmissibility is decreased

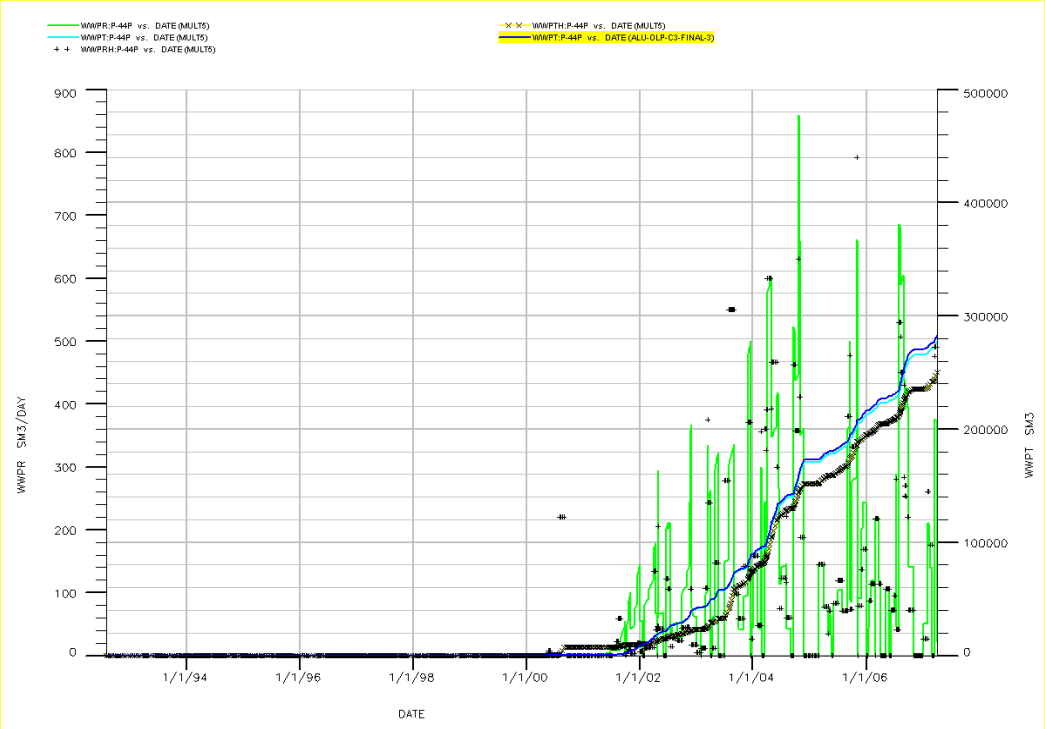

Figure 8-37 Comparison of MULT5 and A-Lu with historical water production data

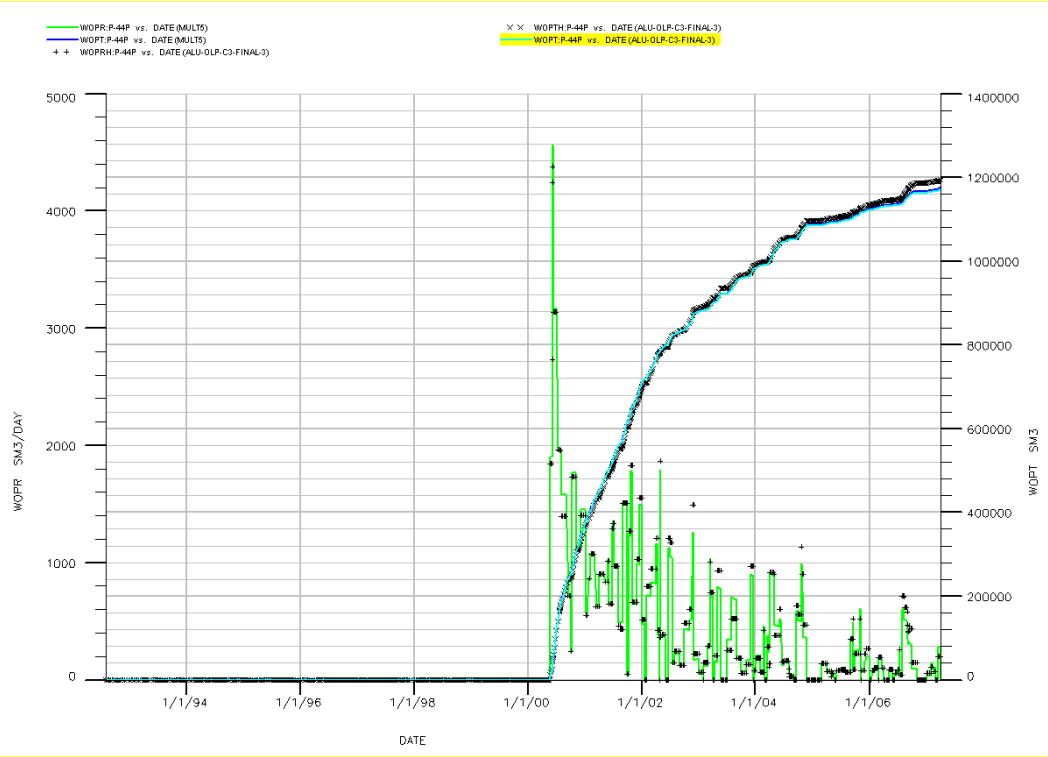

Figure 8-38 Comparison of MULT5 and A-Lu with historical oil production data

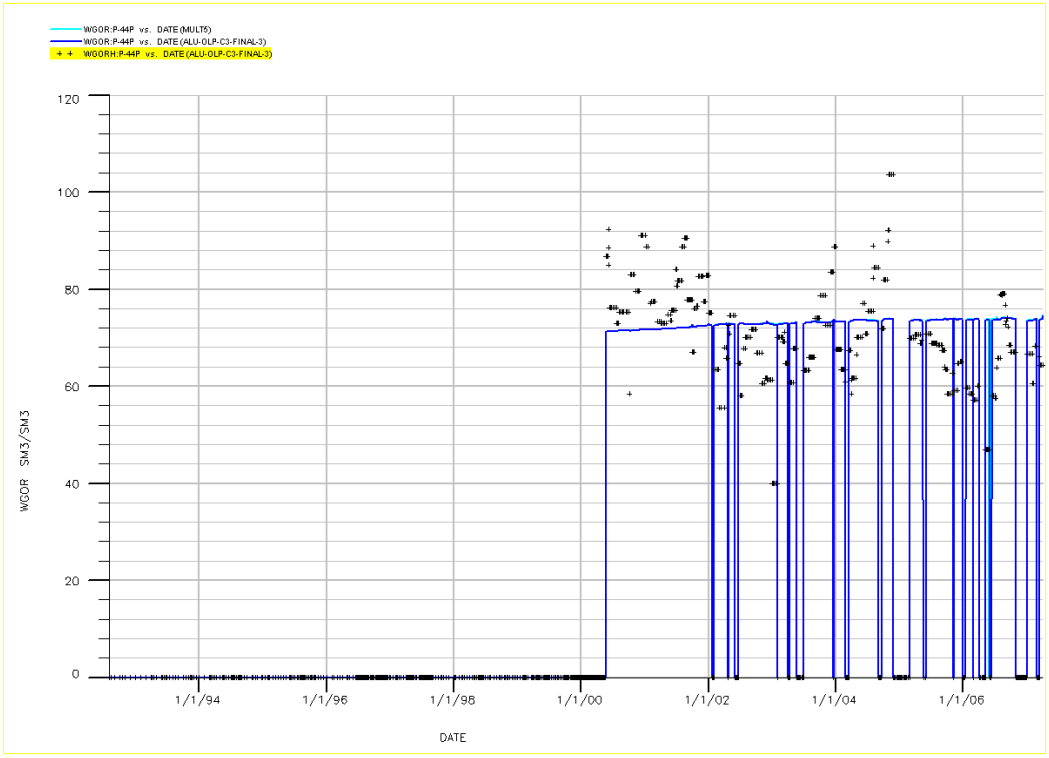

Figure 8-39 Comparison of MULT5 and A-Lu with historical gas production data

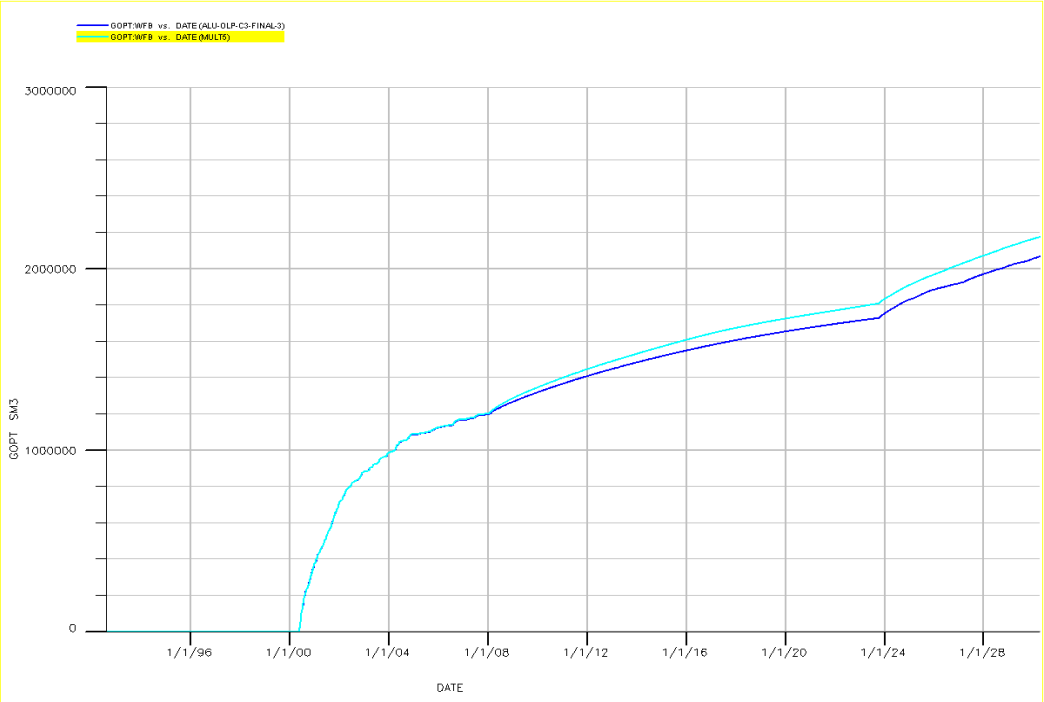

Figure 8-40 Predicted oil production from WFB for A-Lu and MULT5

8.3 Summary of Results

Figure 8-41 gives a summary of predicted total oil production and water injected in the model in 2030. The trend is that the oil production increases with better communication across the faults. Total volume of water injected differs in the cases and it is hard to see any trend.

The RFT pressures in the wells included in the A-Lu are difficult to match. Net to gross (NTG) is low in the A-Lu model and the pressures measured can vary much in the vertical direction. RFT measurements indicate varying pressure regimes in the vertical direction. The reason for this is that there are many isolated sands in the reservoir that have no communication with other part of the reservoir and these can be at initial pressure. When there are different pressures within small intervals the model is not sensitive enough to follow these local pressure trends. It is therefore very difficult to obtain a good match with RFT-pressures in such areas.

Figure 8-42 shows the predicted Snorre performance when modifications are performed regarding fault transmissibility in the different fault blocks. The alternative case is established based on the best alternatives (the cases presented in the study above) and compared with the expected case (A-Lu model) for each fault block. The total oil production for the expected case (A-Lu) is presented for the same fault blocks. Total oil production from the fault blocks modified is approximately 1.4 million Sm^3 higher than in the expected case.

The difference in oil production was highest for NCFB, where the fault transmissibilities were multiplied by 10. The improvement in oil production is most likely caused by opening faults influencing the flow in east-west direction. In EFB there is a relatively small difference in the oil production when changing the fault transmissibility. This can indicate that many of the faults are so tight or open that changing the fault transmissibility by a factor 5 has very little effect. Another explanation can be that fluid is simply flowing around the faults in areas where the fault has limited extent. If this is the case, adjustment of the fault transmissibility will have small effect.

In the study performed above the modifications of fault transmissibility are only matched with one RFT well in each fault block. Based on this match it is assumed that the same trend is present in the entire fault block. This can be a too simple approach because there is a very complex structure regarding faults within each fault block. Ideally more wells in each fault block should have been matched against RFT pressures to verify if the trend is the same for the entire grid block. Due to limited time during the work of this thesis this was not performed.

The A-Lu model is history matched against RFT pressures and shut in pressures of wells. Some of the new wells have down hole pressure gauges that measure the flowing bottom hole pressure in the well. Many of the Lunde wells are included both in the A-Lu model and B-Lu model and the production is split between the models. It is therefore difficult to get representative pressure measurements for each model. The pressure gauge is placed at the top of the perforation interval and it is difficult to find separate flowing well bore pressure for each model. Ideally all wells on the field should have been matched against flowing wellbore

pressure, because changing fault transmissibility will give high response in simulated bottom hole pressures in the wells.

This simulation study has only tested the sensitivity of the fault transmissibility on the field. The communication across faults is one of the main parameters adjusted to obtain a satisfying history match of the A-Lu model. It is possible that the same effects, as in the study performed above, could have been achieved by adjusting other parameters. The A-Lu model has in general very low net to gross ratio, and the vertical communication is an uncertain parameter. In addition, the pressure support from water zones is uncertain. Numerical aquifers have been applied in the history match of the model to increase the pressure in some areas. Applying numerical aquifers could have given some of the same effects as changing fault transmissibility.

The choice of geological realization is also a parameter that is very uncertain and that will have large impact on the field performance. The realization used in the A-Lu model is based on the geological concept that channel direction goes from east to west. This is assumed to be a regional effect and all channels in the model are modelled in this direction. The choice of channel direction has been subject to discussions between geologists. Channel direction in the other fields in the area is modelled with channel direction from north to south and since this is a regional parameter it is possible that Snorre has the same channel direction. It has to be mentioned that the channel direction is very uncertain and production data can be used to argue for both alternatives.

A very high number of faults (129) have been incorporated into the Snorre reservoir model. It is possible that in some areas of the model an average permeability value could have been used instead of incorporating the faults into the model. This can be done within compartments where smaller faults are present. Since there is such high uncertainty associated with the modelling of faults, averaging the permeability may give a similar result within the same limits of uncertainty.

The predicted performance for the Snorre reservoir is extremely important when planning further strategies and investments for the area. The results from the reservoir simulation model will be used as a basis for these decisions. It is therefore vital to have a model that gives the best possible representation of the dynamic behaviour of the reservoir. Fault modelling is one of the parameters having largest impact on the predicted oil production. Different cases have been established, where both tight and more open faults are applied, to investigate the uncertainties in predicted field performance. If it is possible to achieve history match for cases outside these limits of uncertainty, the predicted performance of the Snorre Field will be even more difficult to estimate.

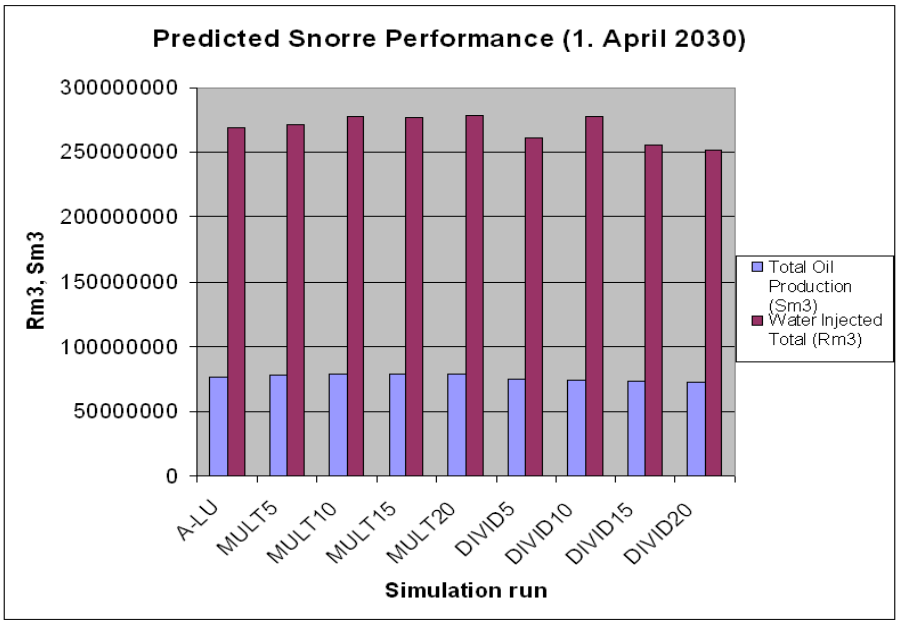

Figure 8-41 Field oil production and water injection when using different fault transmissibilities

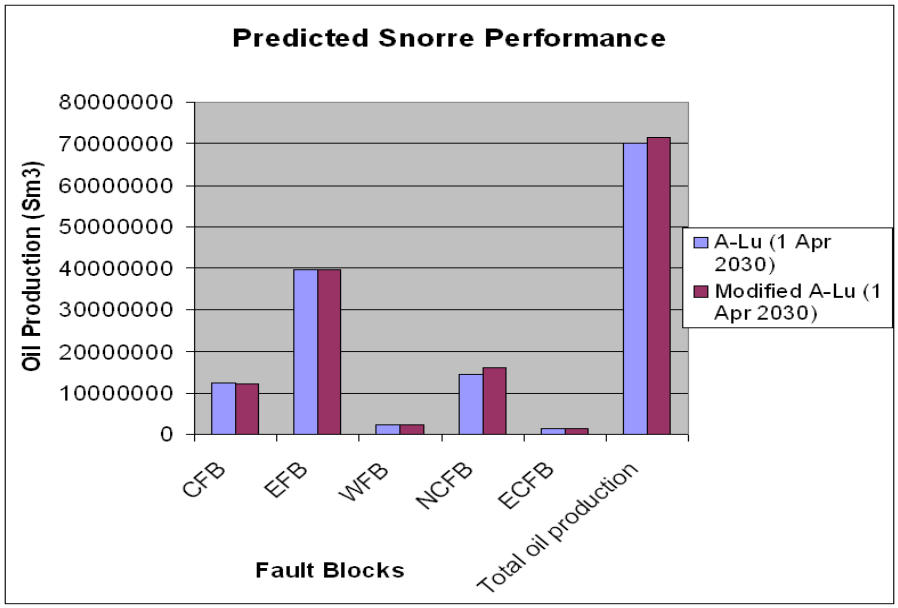

Figure 8-42 Comparison between predicted oil production from the A-Lu model and the modified A-Lu model for the fault blocks modified

8.4 Effect of Changing Fault Seal Parameters in the A – Lu model

8.4.1 Procedure

A small segment was taken out of the A-Lu model in order to investigate the sealing properties of a fault when changing different parameters affecting the fault seal. The segment, located in the Central Fault Block (CFB), includes one oil producer (P-8LP) and one water injector (P-12LW) (Figure 8-43). The injector and producer were separated by a fault, *C230*, (Figure 8-44) which intersects the whole vertical thickness of the segment.

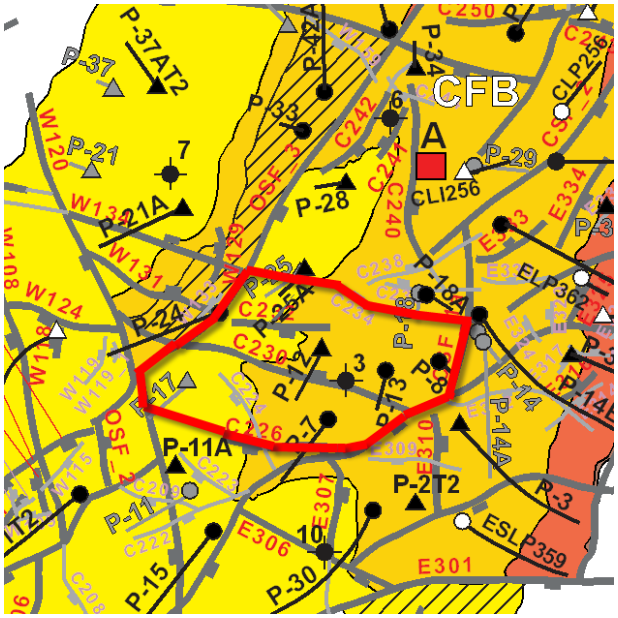

Figure 8-43 Red curvature indicates approximately the area of the segment

The segment was cut out from the Snorre geological model by using the Irap RMS 3D modelling software. The grid and upscaled petrophysical properties were exported from RMS into the reservoir simulation model in Eclipse. A reference case, referred to as *BASECASE_3*, was established to be used for comparison. The reference case was intended to have the same properties as the segment had when it was part of the A-Lu model. The fault C230 has been elongated and divided into smaller parts vertically in the A – Lu model, in order to get a better history match. As described in section 7.4.11.2, fault C230 was elongated to fault CSF_1 and given different transmissibility in the vertical direction during the history matching. There is not performed any fault seal analysis in RMSfaultseal for this elongation. The flow in this part of the fault is only restricted by applying fault transmissibility multipliers in Eclipse. The elongation of the fault is divided into four parts vertically: C230_1, C230_1B, C230_2 and C230_3. C230_1 goes from layer 1 to 4, C230_1B from layer 5 to 11, C230_2 from layer 12 to

15 and C230_3 goes from layer 16 to the bottom of the model (layer 71). C230_1 is given a multiplier value of 0.05, C230_1B a value of 0.003, C230_2 a value of 1 and C230_3 a value of 0.01. This elongated part of the fault will have much better transmissibility than the rest part of C230, especially in part C230_2 where there is no restrictions to flow (multiplier of one). The main part of the fluid flow from the injector to the producer side of C230 is assumed to occur in the eastern part. The same elongation and division as described above of fault C230 was used in the segment. In addition the same modifications of the fault transmissibility as in the A-Lu model were performed.

The segment has the dimensions 26 x 23 x 71 (Figure 8-45) and the simulations were run from production start of the field in 1993 until April 2015. The Eclipse keywords MINPV and MULTPV applied in the A-Lu model, are excluded in the segment to avoid problems with limited drainage volume. The MINPV keyword is used to inactivate cells with pore volume lower than a certain value and has no importance in the OOIP, while the MULTPV keyword has been used to match the A-Lu model to the official 2D geologic model HCPV. During the generation of the Schedule file (described later) these keywords were active in order to get the same perforation intervals as in the A-Lu model.

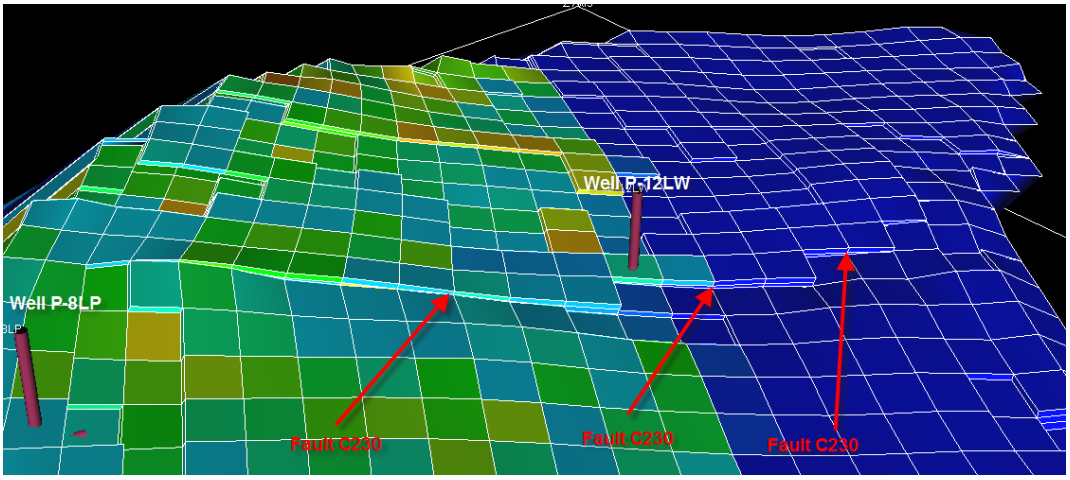

Figure 8-44 Simulation grid where fault C230 is pointed out

The two wells (P-8LP and P-12LW) were incorporated in the segment using their exact well paths and perforation intervals. The *Schedule* module in the Eclipse reservoir simulation software was used to generate new schedule files. Prior to the generation of the schedule file, the segment was initialized. The same schedule file was used in all cases where grid dimensions and grid properties were the same. Separate schedule files were generated for the cases where alternative geological realizations were tested because of the changes in reservoir properties. Based on reservoir properties, perforation lengths and wellbore diameter the Schedule module calculated connection factors for the wells. The schedule files were based on the same input data as in the A-Lu model (production rates, control mode of wells,

perforation intervals etc.) but wells were given new coordinates according to the new grid. Based on this new connection factors were calculated for the wells.

Well P-12 had leakage in a straddle from October 1997 to February 1999 and the well was shut in for about one year. A cross-flow well (P-12XLW) was created in the A-Lu model to compensate for flow from Lunde to Statfjord in this period [26]. The same cross flow well was included in the segment.

In the history matching period the control mode of well P-8LP is the observed reservoir fluid rate, which means oil and water flow into the well (no free gas present). The reservoir volume production rate is used as input in model and the model will try to reproduce this rate. The well will produce the liquid available in the reservoir to match this rate, which means that if there is limited oil available the well will produce more water instead, if available. Historical production rates are included from production start of the well in June 1993 until November 2006. The water injector P-12LW is controlled by the surface flow rate and injects at the same rate for all cases in the historical period. Historical injection rates are included from Aptil 1994 until March 2006.

In the predicted period well P-8LP is controlled by the tubing head pressure and the well will produce as long as there is high enough pressure available.

The production well P-8LP has an effective perforation interval of 73 m in the grid while the injector P-12LW has a effective perforation interval of 115 m. P-8LP has production start 24. June 1993 and P-12LW starts to inject 9. April 1994, indicating a production period of pure volume depletion.

RMSfaultseal was used to calculate fault transmissibility multipliers for the fault in the different cases. In the calculation of fault transmissibility multipliers for the reference case fault seal parameters from the history matched A-Lu model (P70) was used. The fault transmissibility multipliers were imported from RMS into Eclipse using the keywords TRANX, TRANY and EDITNNC.

In order to quality check the segment the performance of well P-8LP in the segment was compared with well P-8LP in the history matched A-Lu model. The comparison revealed some differences due to difficulties maintaining exact fluxes when a segment is cut out from a large grid. Figure 8-48 through Figure 8-50 show the match regarding oil, water and gas production. In addition, historical data is included in the graphs for comparison. The figures show that there is a satisfying match between production performance of well P-8LP in the segment and in the A-Lu model.

The bottom hole pressures in wells P-8LP and P-12LW in the segment are compared to the same pressures in the A-Lu model (Figure 8-51). Pressure drop from the injector to producer is approximately the same for the two cases. The bottom hole pressures for the wells in the A-Lu model is higher (around 40 bars) than the in the segment. This indicates that there is more energy in the A-Lu model for this area, probably caused by pressure support from a part of the field not included in the segment. The segment is cut out from the A-Lu model with no

boundary conditions included and the segment will produce as a separate reservoir. A numerical aquifer or a pseudo well (injector) could have been applied to increase the pressure in the segment and given a better match with the A-Lu model. The intention of this study was primarily to look at the dynamic behaviour of the segment when varying different parameters affecting the fault seal, rather than obtain a perfect match with the behaviour of the A-Lu model.

Figure 8-52 shows the pressure drop from injector to producer and across the fault for the reference case. The pressure drop from injector to producer is assumed to be the difference between the bottom hole pressure for the two wells. The model was programmed to calculate the bottom hole pressure in each well at the bottom of the last perforation interval. In addition, the model were set to report pressure from two grid blocks located on each side of the fault. These grid blocks were situated at the middle of the fault and at the same depth as the bottom hole pressures are calculated. The difference in pressure between the two grid blocks was assumed to be the pressure drop caused by the fault. This will indicate what impact the fault has on the pressure drop in the different cases. The pressure drop across the fault was evaluated at two different time steps to verify that the block pressure is not affected by local effects.

A high pressure drop across the fault indicates that the fault transmissibility is the limiting factor between the injector and the producer. In such cases the introduction of new injectors on the injection side of the fault will have no effect on the recovery of the field, since the transmissibility across the fault will control the flow. When the pressure drop across the fault is small, it is the pressure drop from the wells to the faults that will mainly affect the fluid flow. Drilling of new injectors on the injector side of the fault will in such cases most likely contribute to a higher recovery [38].

The dynamic behaviour of the segment was studied in detail in the Eclips module *FloViz*. Because of barriers to vertical flow (Figure 8-46) there are different pressure regimes in the vertical direction. In this study it was decided to investigate the pressure in the lowest pressure regime (below the blue coloured grid blocks) (Figure 8-47), since the largest perforation interval of the well was located at this depth. For each parameter tested the pressure drop from injector to producer was registered from two of the cases at two different dates (1. Jan 1997 and 1. Jan 2002). The pressure values were taken in periods with relatively stabile production from the well.

One region was defined on each side of the fault to monitor the oil and water flow from one side of the fault to another. Oil and water flow from injector to producer side of fault, water injection total and production of oil and water was checked at two different time steps (1. Jan 1998 and 1. Feb 2006). This was done to investigate the dynamic behaviour of the segment at two discrete time steps.

After the preparation of the segment was finished a qualitative fault sensitivity study was done for different parameters affecting the sealing properties of the fault. Different fault seal parameters were changed one at a time, and new fault transmissibility multipliers were calculated in the RMSfaultseal module. In addition, the effect of alternative geological

realizations, the use of different algorithms for predicting fault zone permeability and the application of fault transmissibility multipliers (MULTFLT keyword in Eclipse) were tested. The results were compared to the reference case (BASECASE_3).

App B shows all of the different cases tested in this reservoir simulation study. All blocks with a light blue colour have the same values as the BASECASE_3. All cases with same colour in the left column of the table belong to the same group. All cases within one group are simulated with different sensitivities of the same parameter. In the cases where fault seal parameters are changed, four sensitivities are run for each case. All results are compared with BASECASE_3 which gives the approximately same results as the history matched A-Lu model. The initial volumes in place in BASECASE_3 can be found in table Table 8-1.

In the first cases the SGR-curve used in the A-Lu model was changed by shifting the fault zone permeability by different factors. Simulations were run for the four cases and were compared to the reference case.

Simulations run in CASE5_3 to CASE8_3 are performed with a grid where the fault throw is increased. Due to some problems with changing the throw in the RMS software, the fault throws were manually increased by using the keyword *ADDZCORN* in Eclipse. No fault transmissibility multipliers were calculated in RMS for these cases, but the same *MULTFLT* modifications as in the A-Lu model were applied. Ideally fault transmissibility multipliers should have been calculated for these cases as well, for being comparable with the reference case. Although, the effects of changing the fault throw were clearly observable in the simulations.

Sensitivities were also tested on fault seal parameters like displacement-thickness ratio, cementation factor, shale smear factor limit, brittle factor and oblique slip angle. In CASE21_3 and CASE22_3 the effect of changing geological realization was tested. In CASE21_3 geological realization #5 was used. In CASE22_3 the geological realization #10, where an alternative channel direction was applied, was tested. Table 8-2 and Table 8-3 show the initial volumes in place for the two cases with alternative geological realizations.

Two cases where different algorithms for predicting fault zone permeability (Manzocchi and Sperrevik) was applied, were tested in CASE23_3 and CASE24_3.

In CASE33_3 through CASE36_3 different fault transmissibility multipliers were used at the fault. Both C230 and the elongation of the fault were multiplied with different factors. In the last case, CASE37_3, the performance of the segment was tested when no fault seal or fault transmissibility multipliers were applied.

.

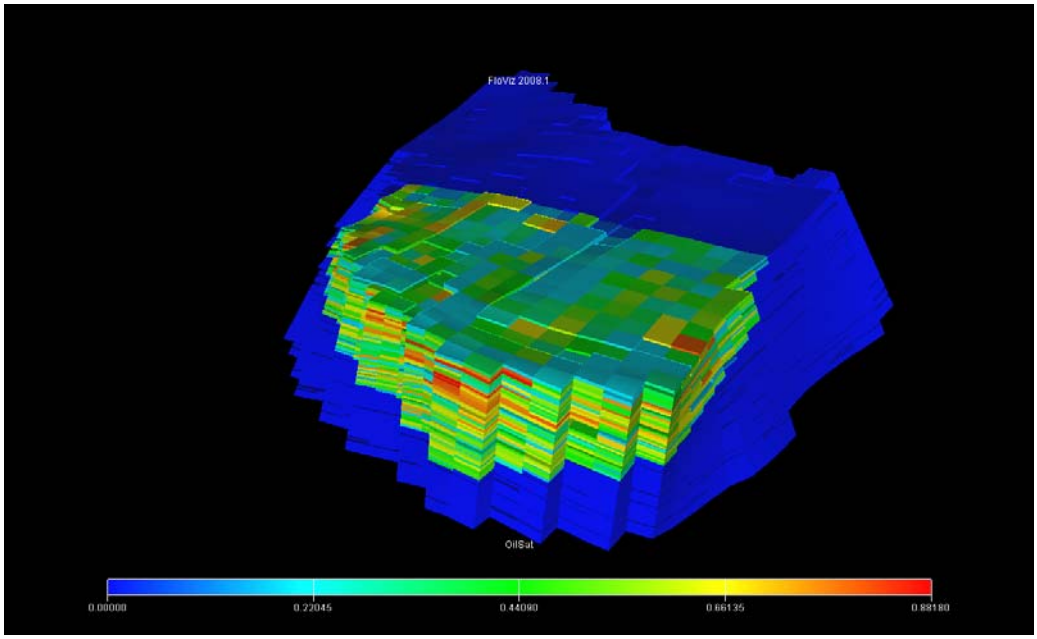

Figure 8-45 Segment with initial oil saturation

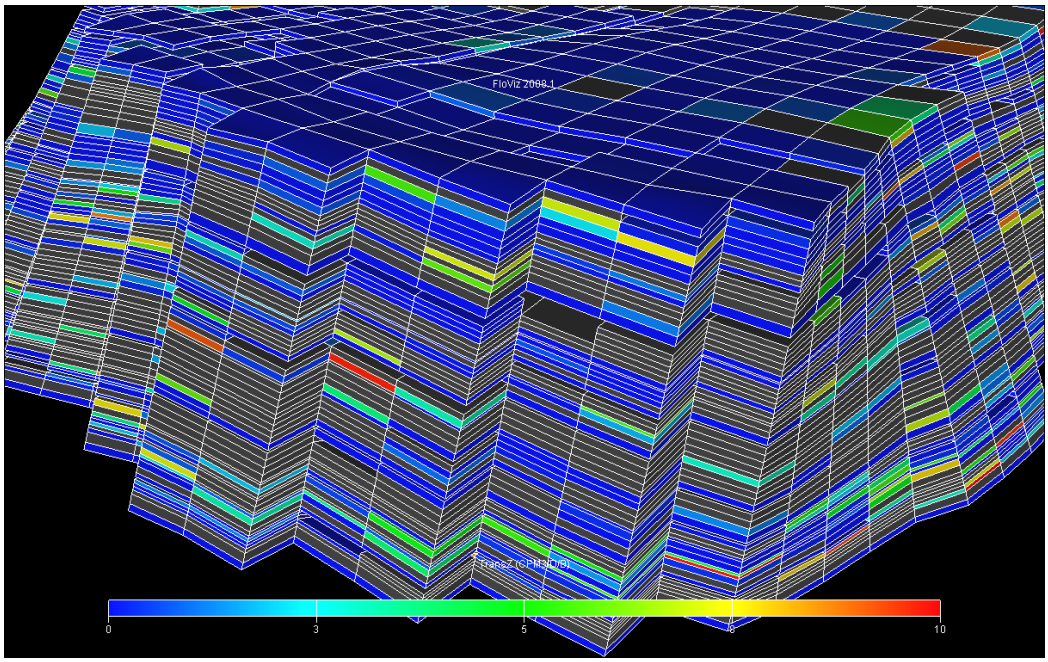

Figure 8-46 Barriers to vertical flow present in the segment (grid blocks with blue colour)

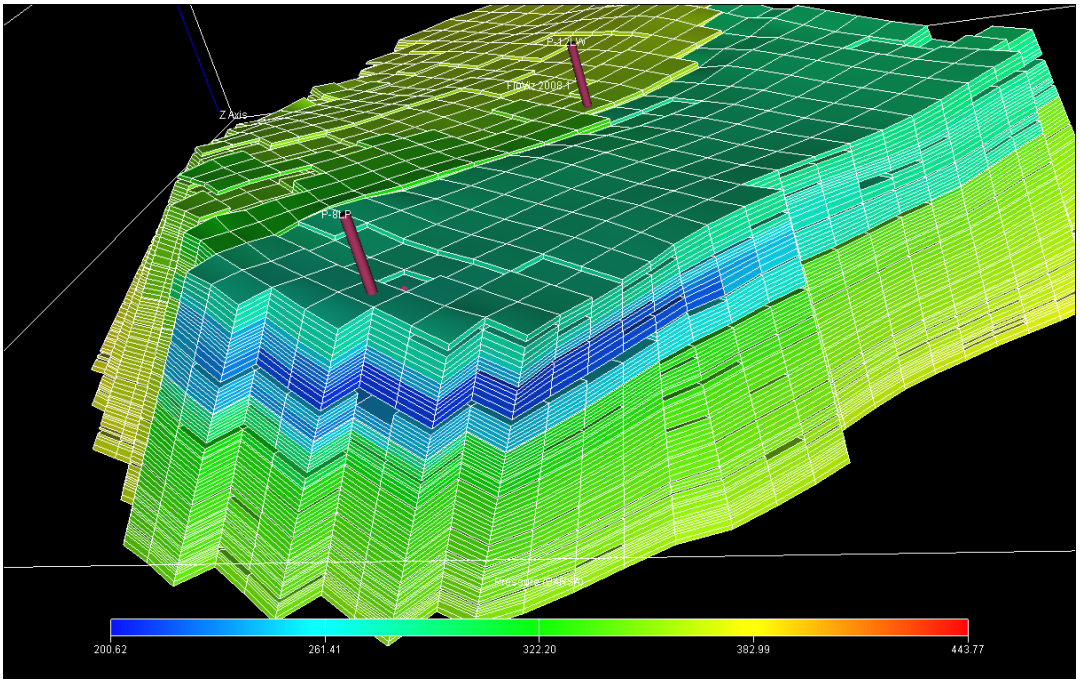

Figure 8-47 Illustration of the different pressure regimes in the vertical direction

	BASECASE_3				
	POREVOLUME (Rm3)	OOIP (Sm3)	Water volume (Sm3)	Dissolved gas (Sm3)	Average pressure (BARSA)
Injector side	83466835	3464070	77337631	218014740	386.06
Producer side	54652921	4205272	48230132	269743858	385.46
Field	138119755	7669342	125567763	487758598	385.73

Table 8-1 Initial reserves in place in the segment when using geological realization #3

	CASE21_3				
	POREVOLUME (Rm3)	OOIP (Sm3)	Water volume (Sm3)	Dissolved gas (Sm3)	Average pressure (BARSA)
Injector side	86602507	3024175	80945687	189108690	386.26
Producer side	51180872	3840033	45300292	243211119	385.85
Field	137783379	6864208	126245979	432319809	386.03

Table 8-2 Initial reserves in place in the segment when using geological realization #5

	CASE22_3				
	POREVOLUME (Rm3)	OOIP (Sm3)	Water volume (Sm3)	Dissolved gas (Sm3)	Average pressure (BARSA)
Injector side	86655471	3510654	80397298	220930382	386.06
Producer side	47476524	4064543	41379002	266466854	384.76
Field	134131995	7575197	121776300	487397236	385.36

Table 8-3 Initial reserves in place in the segment when using geological realization #10

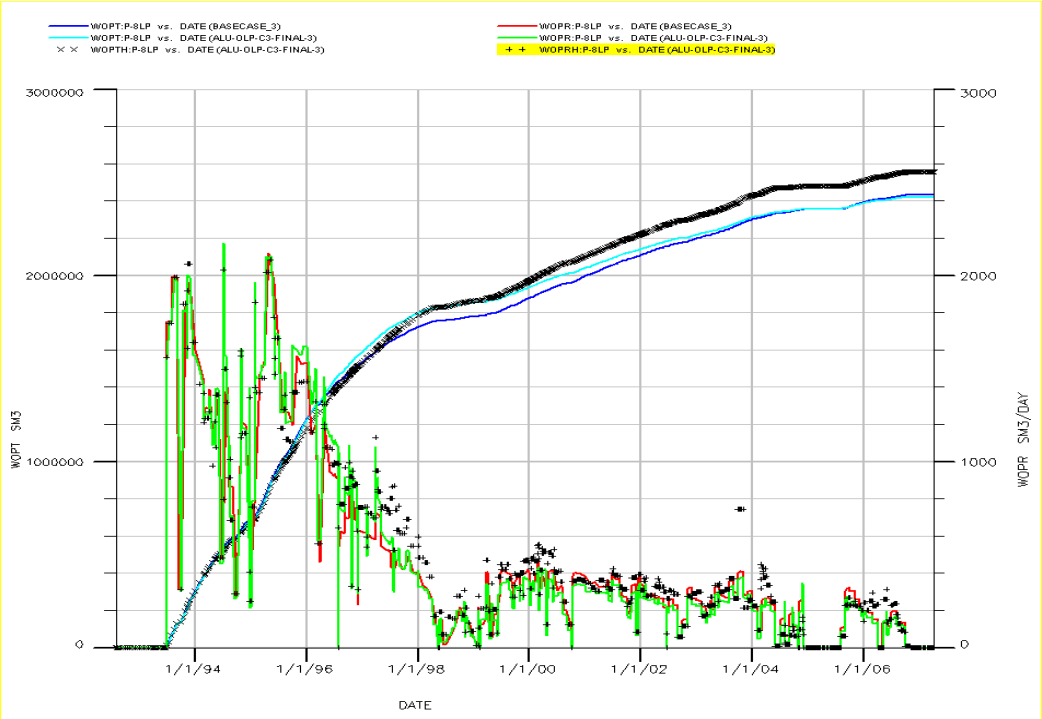

Figure 8-48 Oil production from the segment compared with historical data and the A-Lu model

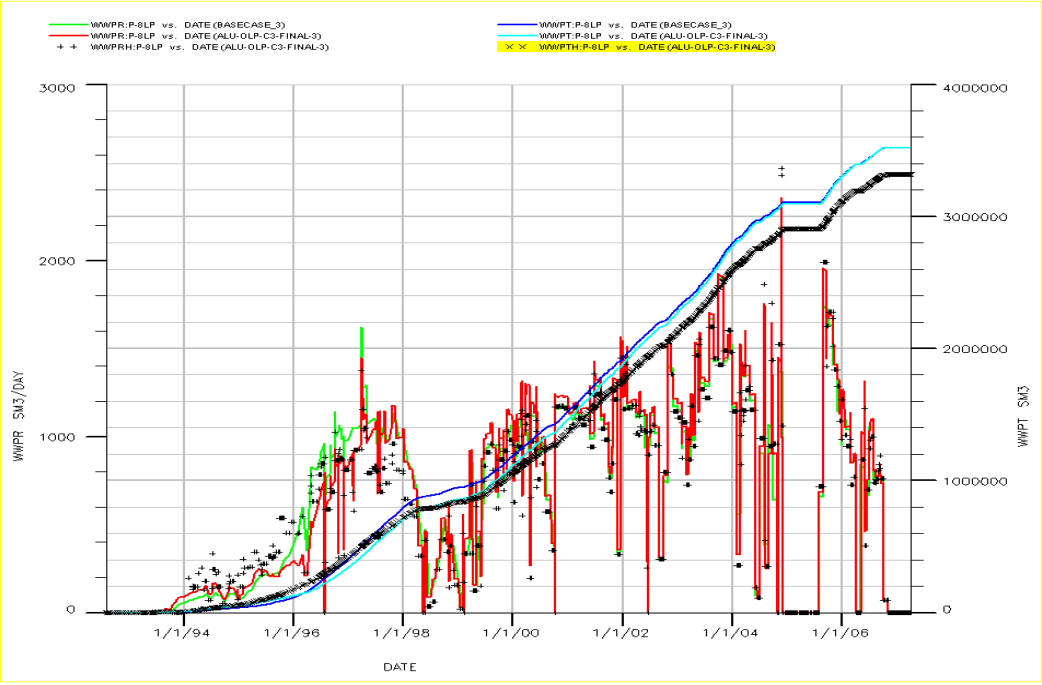

Figure 8-49 Water production from the segment compared with historical data and the A-Lu model

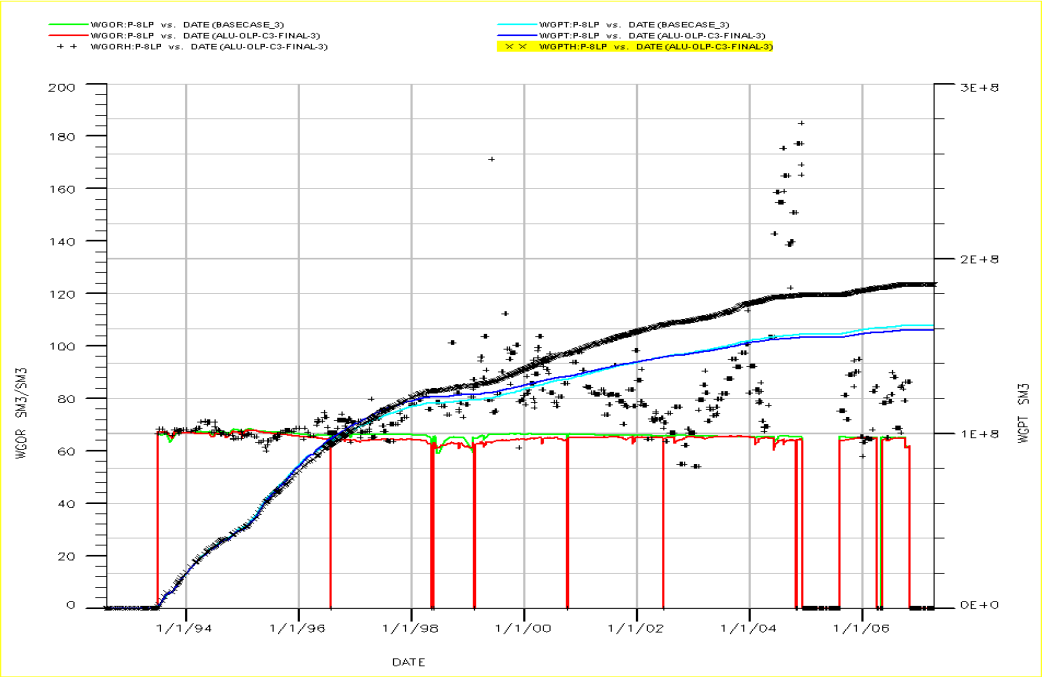

Figure 8-50 Gas production and GOR from the segment compared with historical data and the A-Lu model

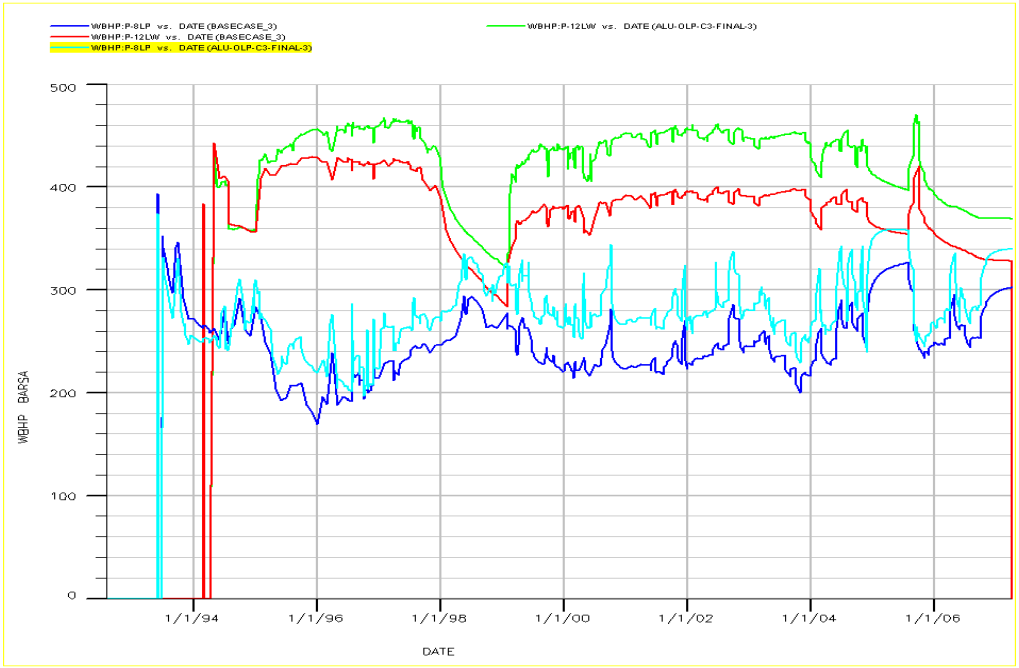

Figure 8-51 Comparison between injector bottom hole pressure and producer bottom hole pressure for the A-Lu model and the segment

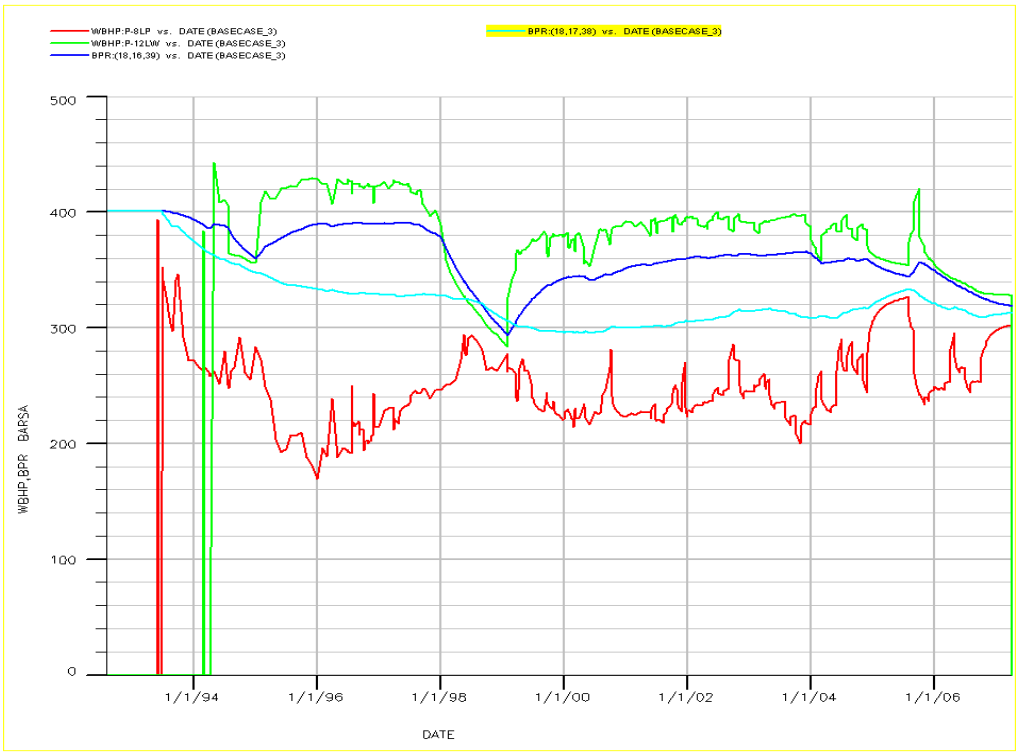

Figure 8-52 The graphs are illustrating pressure drop from injector to producer and across the fault for BASECASE_3 (reference case)

8.4.2 Results and Discussion

8.4.2.1 SGR – curve

The impact of using different SGR-curves in the calculation of fault transmissibility multipliers was tested. The SGR – curves used in the history matched A-Lu model was shifted by multiplying the fault permeability by different factors. The original SGR-curves on the Snorre Field were shifted with 15 % in order to achieve a satisfying result in the models. The table in App D shows the values used to create the SGR – curves (Snorre properties). The fault permeability in the reference case is based on the SGR curve (P-70) used in the history matched A-Lu model.

Figure 8-53 through Figure 8-56 show the results from the simulations. Changing the SGR – curves will have impact on the oil production from the cases both in the historical period until April 2007 and in the predicted interval until 2015. For the case where the fault zone permeability is divided by 10 (CASE4_3) (pink line) well P-8LP can not produce enough oil to match the reference case, neither in the historical period nor in the predicted period. The three other cases have only small differences in the oil production in the period where historical data is included. In the predicted interval the cases with the highest fault zone permeability will have the largest oil production. Water production from CASE4_3 is slightly higher than the other cases in the historical period (Figure 8-54). The reason for this is that to compensate for limited oil production the well produces more water (as long as there is water available) to match the reservoir volume rate given as input to the model. The other cases match the oil volume in the reference case and the water production will be approximately the same in these cases.

Figure 8-55 shows the status for the segment at two different times in the production period. CASE4_3 has more oil flowing from the injector to the producer side than CASE2_3 at the two different times. At the same time steps more water has flowed across the fault in CASE2_3 than in both CASE4_3 and in the reference case. This is due to the fact that more of the injected water is flowing across the fault in CASE2_3 building up the pressure on the producer side of the fault. In CASE4_3 the pressure is built up on the injector side of fault and there is less pressure maintenance on the producer side. More oil will therefore flow across the fault in CASE4_3, mainly in the fault elongation, to compensate for the pressure depletion. There will be a more effective displacement of oil in CASE2_3 since water is flowing across the fault and acting as a piston to the water on the producer side of the fault. When looking at the predicted oil production until 2015 it is clearly that CASE2_3 has the potential of producing more oil because there is much more pressure available on the producer side of the fault.

Figure 8-56 shows the pressure drop from injector to producer for the two cases at two different time steps. BASECASE_3 is also included for comparison. The blue part of the columns is illustrating the pressure drop across the fault, while the purple part of the column illustrates the pressure drop when fluid flow to and from the fault. The main part of this pressure drop is occurring at the producer side of the fault because the transmissibility was reduced here in the history matching of the model. When multiplying the fault permeability by

a factor of 10 the pressure drop from the injector to the producer is reduced compared with the reference case. It is also observable that the pressure drop of fluid flow through and from the fault is higher than in the reference case at this time. This is because there is higher flow rate of liquid (oil + water) from the injector side of fault to the producer side of fault for CASE2_3 at this time. In January 2002 the flow rate across the fault is more equal for BASECASE_3 and CASE2_3 (equal pressure drop to and from fault) and one can observe that the pressure drop across the fault is reduced by approximately 35 bar for CASE2_3 compared with the reference case. CASE 4_3 has, as expected, a larger pressure drop from the injector to the producer compared with the reference case because of lower transmissibility across the fault.

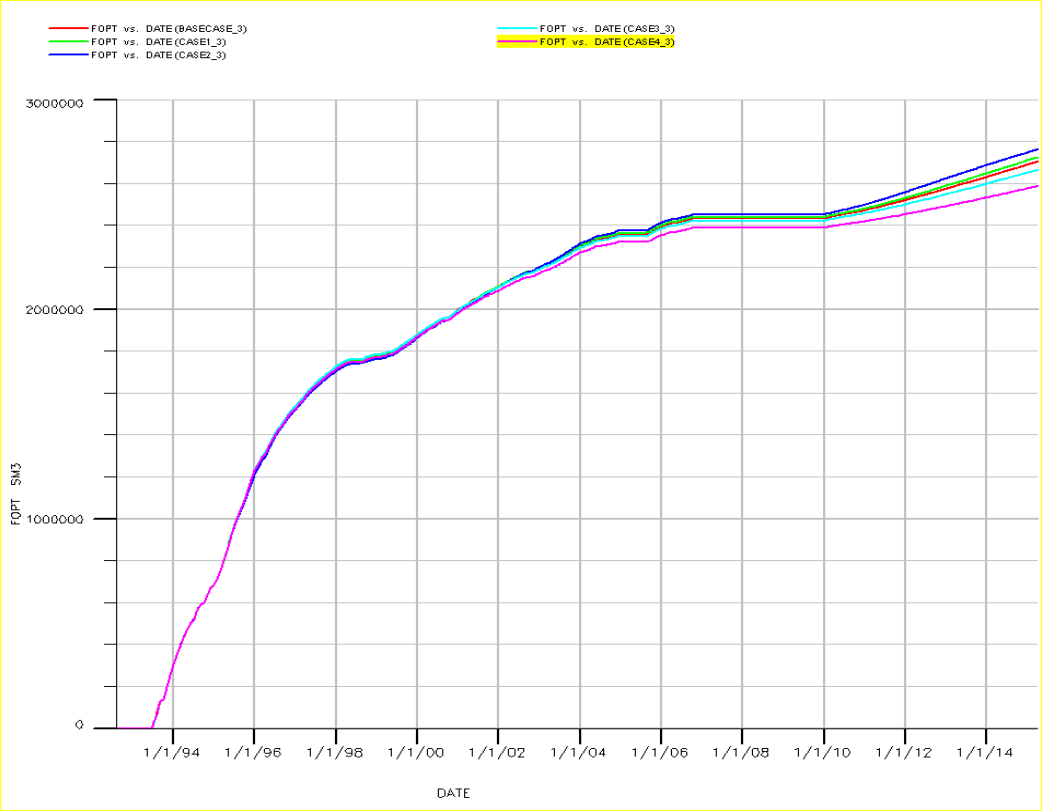

Figure 8-53 Comparison of the total oil production for the different cases

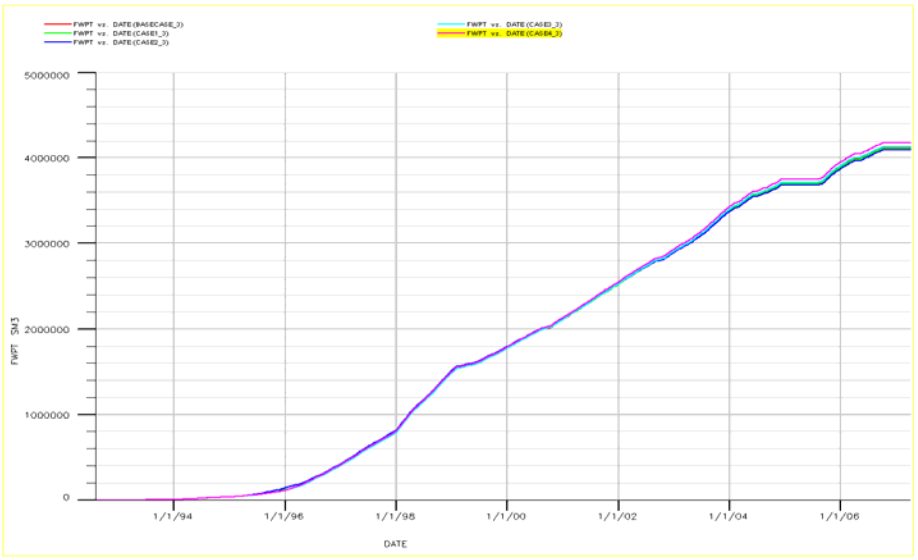

Figure 8-54 Comparison of the total water production for the different cases

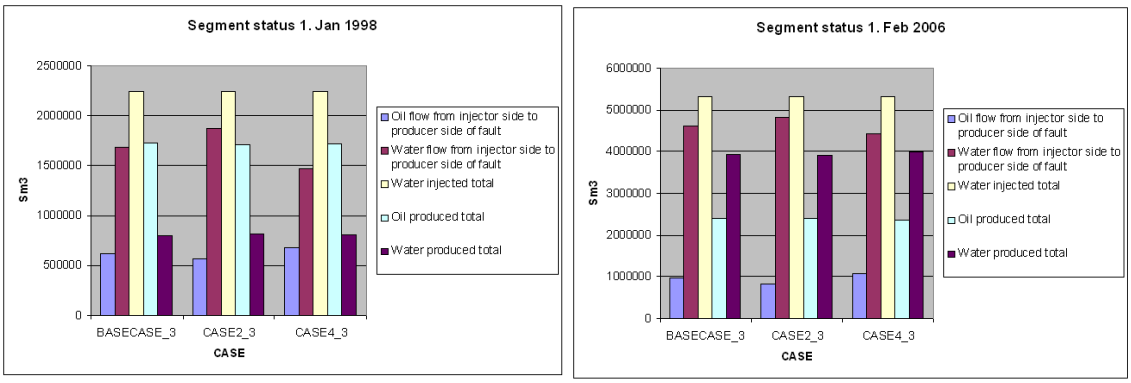

Figure 8-55 Segment status at two different times (1. Jan 1998 and 1. Feb 2006)

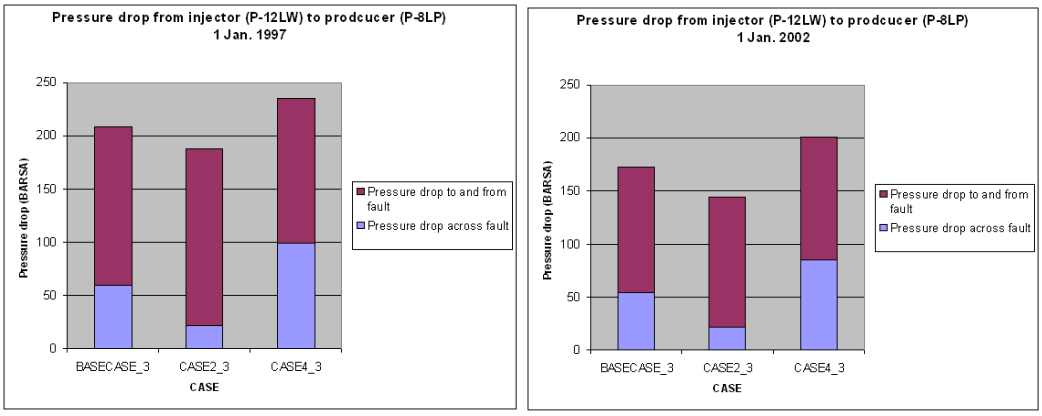

Figure 8-56 Pressure drop from injector to producer at different times (1. Jan 1997 and 1 of Jan. 2002)

8.4.2.2 Fault Throw

To investigate the impact of changing the fault throw four cases were established. In the four cases the fault throw was increased by 25, 50, 75 and 100 m respectively. No fault seal was performed in these cases and the same model as in the reference case was used, excluded fault transmissibility multipliers from RMSfaultseal (TRANX, TRANY and EDITNNC). The same MULTFLT adjustments as in the reference case were used for the fault, but the fault will have significant higher transmissibility for this case than if a fault seal analysis had been performed on the fault. The aim of this sensitivity study was to investigate the effect on recovery when the throw is increased. A significant amount of the oil in place at the injector side of the fault will become unavailable when the fault throw is increased.

Figure 8-57 and Figure 8-58 show that the effect of increasing fault throw on oil and water production is significant. For the most extreme case (CASE8_3) there is very low oil production, but the water production is significant higher than in the reference case. There is limited volume of oil available for the well in this case, but still there is enough water to match the reservoir volume rate used as input in the model. The same trend, with low oil production and high water production, is also occurring in the other cases where the fault throw is increased.

Figure 8-59 shows the status for the segment at two different times in the historical period of the well. In CASE5_3 where the fault throw is increased with 25 metres there is some lower oil flow across the fault than in the reference case. The water flow from the injector to the producer side of the fault for this case is larger than in the reference and the model produces more reservoir volume than the reference case. In CASE8_3 there is approximately no oil flow across the fault, but significant amount of water will flow across the fault. In this case the reservoir volume rate will be very high and mostly water will be produced. It seems like injected water is just pumped through the model and produced through the well. There will be relatively high transmissibility across the fault in this sensitivity study because no fault transmissibility multipliers from the RMSfaultseal have been calculated. This means that fluid (oil + water) that is available on the injector side of the fault will flow without any considerable pressure drop across the fault.

Figure 8-60 shows the pressure drop from the injector to the producer for the two cases. As already motioned there is nearly no pressure drop across the fault for the two cases. CASE8_3 has a few bars higher pressure drop across the most likely caused by juxtaposition of some low quality reservoir units against reservoir units.

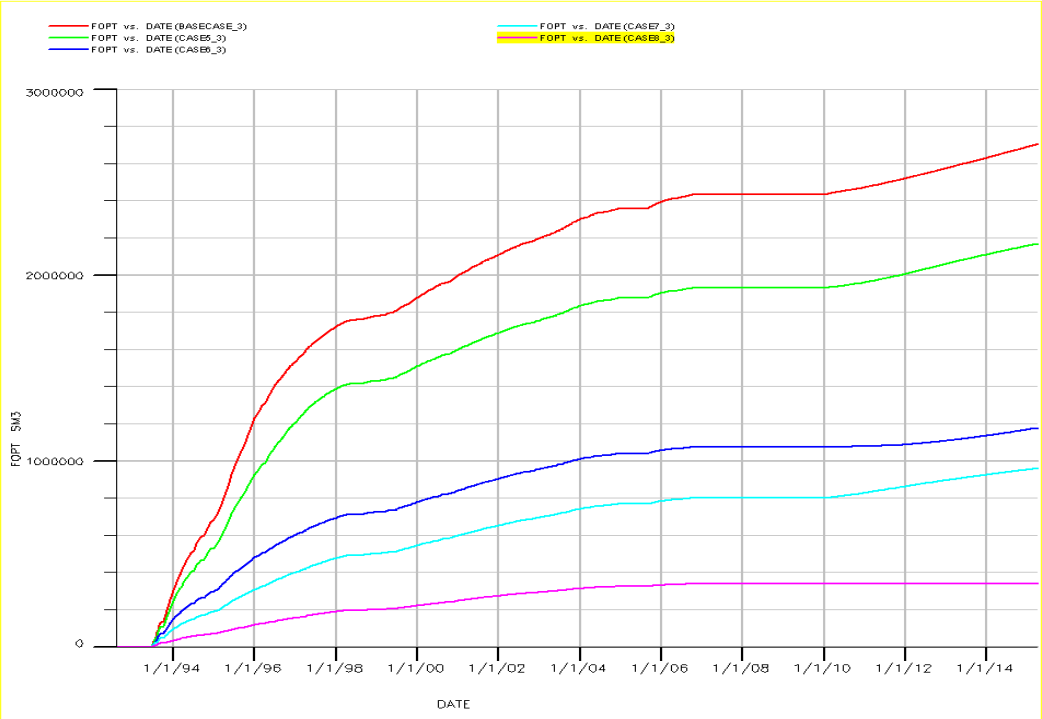

Figure 8-57 Comparison of the total oil production for the different cases

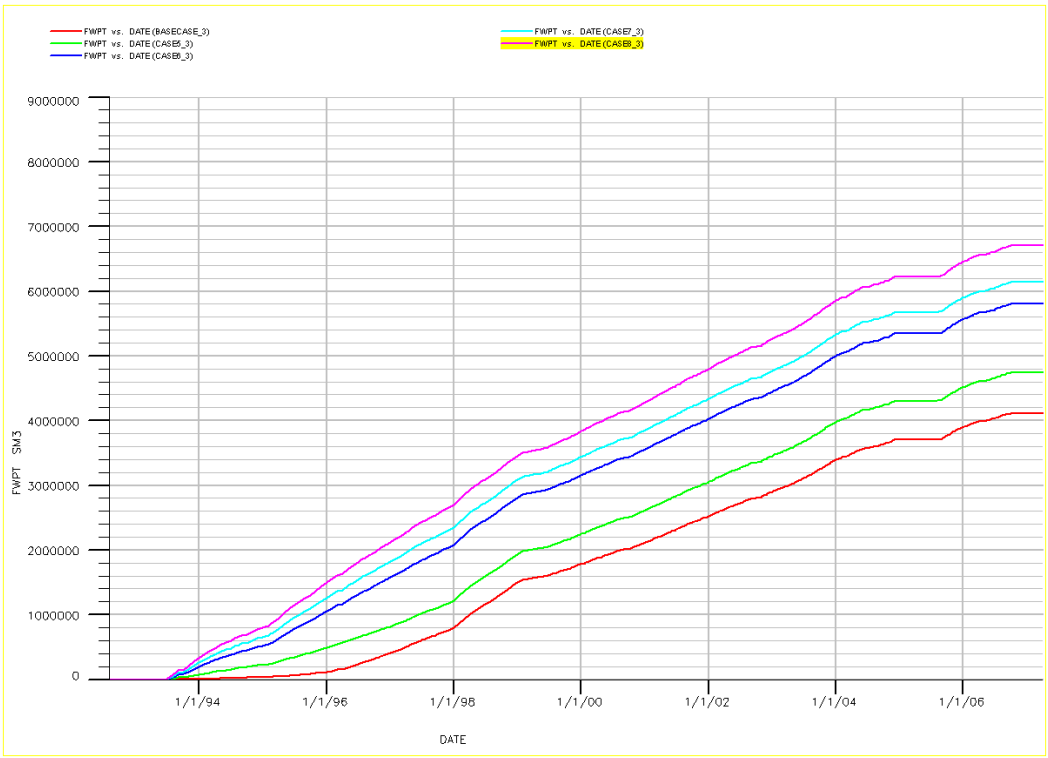

Figure 8-58 Comparison of the total water production for the different cases

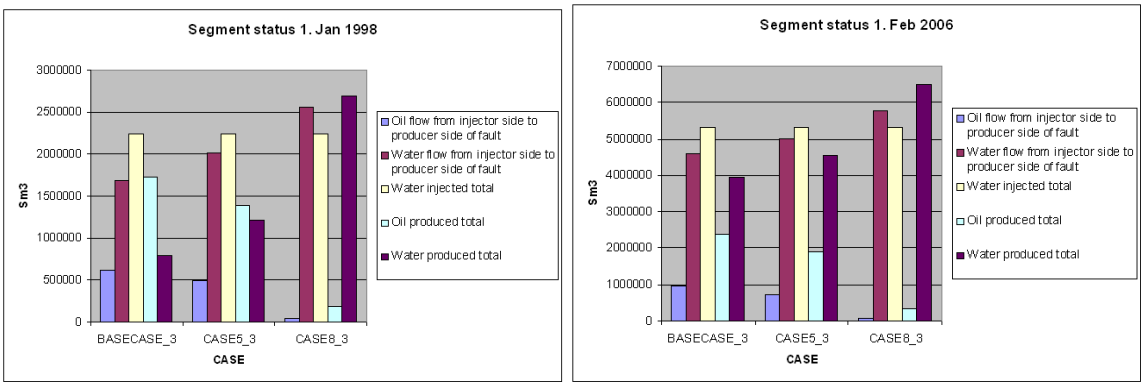

Figure 8-59 Segment status at two different times(1. Jan 1998 and 1. Feb 2006)

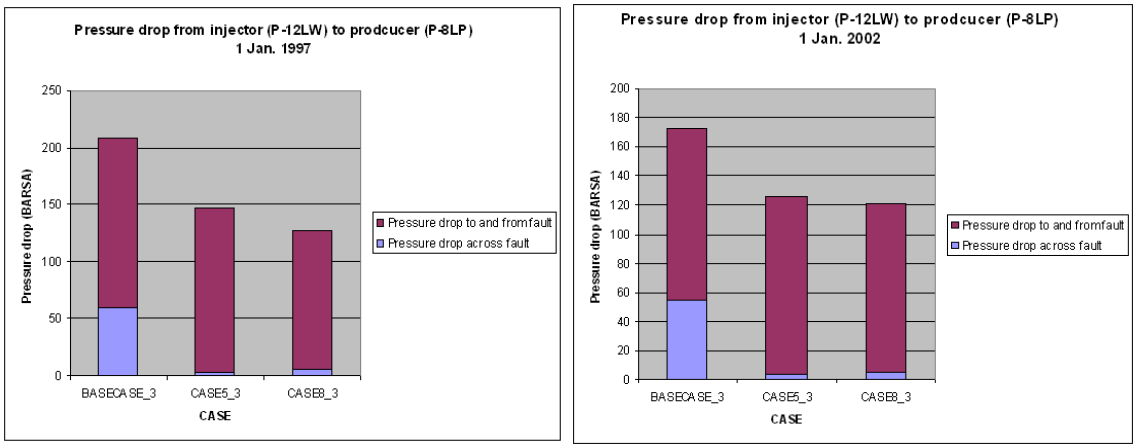

Figure 8-60 Pressure drop from injector to producer at different times (1. Jan 1997 and 1. Jan 2002)

8.4.2.3 Displacement/thickness ratio

Different values of the displacement-thickness ratio were tested in order to reveal the impact of this parameter. Studies that have been performed on the relationship between displacement and thickness show that the ratio varies from 50 to 200 for normal faults [24]. In the history matched A-Lu case there is used a value of 50 for this parameter. Values of 200, 100, 25 and 1 were tested in this sensitivity study. A displacement-thickness of 1 is geological unrealistic, but was tested (CASE12_3) to look at the influence of such an extreme value.

Figure 8-61 through Figure 8-64 show the results from the simulations. When looking at oil production for the different cases CASE12_3 does not manage to deliver enough oil compared with the reference case. To compensate for this CASE12_3 produce a larger a volume of water in the historical period than the other cases. The three other cases produce about the same amount of oil and water as the reference case. The trend in the prediction run is that a higher displacement-thickness ratio gives higher oil production. For a given fault displacement a higher value of the displacement-thickness ratio means that the fault thickness is smaller and there will be better communication across the fault.

Figure 8-63 shows the status for CASE9_3 and CASE12_3 at two different times. One can observe that the oil flow from injector side of the fault to the producer side of the fault is largest for CASE12_3 at both times. In the same case the water flow across the fault is lower than the two other cases. Using a displacement-thickness ratio of 1 will reduce the transmissibility across the fault and the effect of the water injection is not so good in this case. The explanation to the trends in CASE9_3 and CASE12_3 regarding water and oil flow across the fault is the same as in the SGR-case.

Figure 8-64 shows the pressure drop from injector to producer for the two cases together with the reference case. CASE9_3 gives a smaller pressure drop from the injector to the producer than the reference case. In January 1997 one can observe that CASE9_3 has a larger pressure drop to and from the fault than the reference case. This is because there is a higher rate of oil and water flowing across the fault for this case at the given time. The graph shows that changing the displacement-thickness ratio from 50 to 200 will reduce the pressure drop across the fault with about 30 bars. In CASE12_3 the pressure drop is larger than reference case because of the large fault zone thickness. The pressure drop across the fault is around 60 bars larger than the reference case indicating that the fault will have large impact on the predicted oil recovery (Figure 8-61).

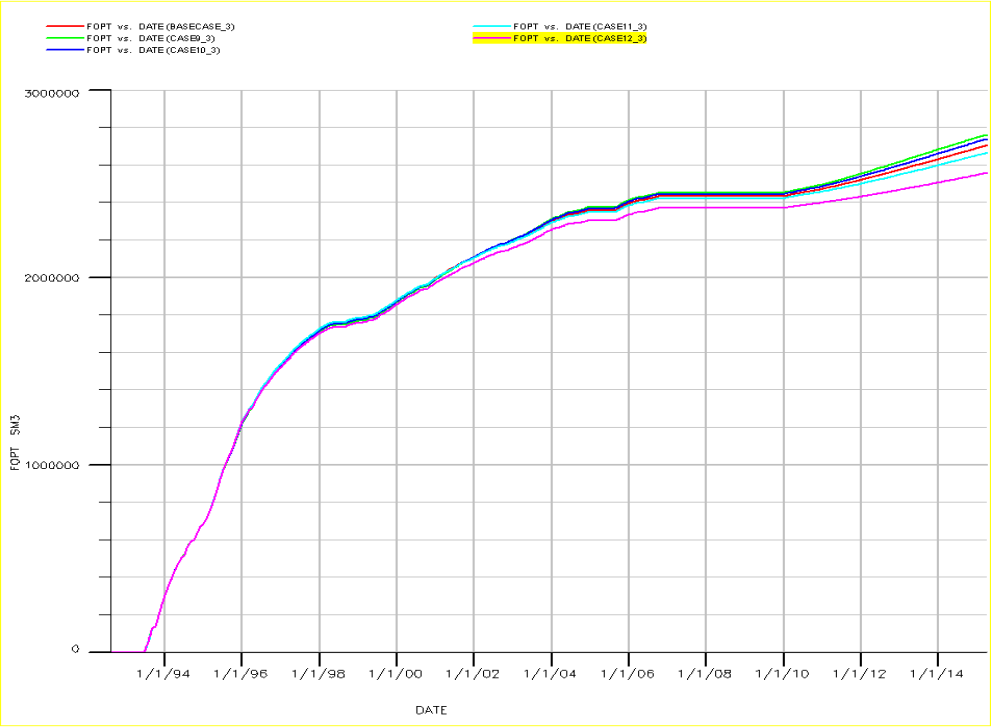

Figure 8-61 Comparison of the total oil production for the different cases

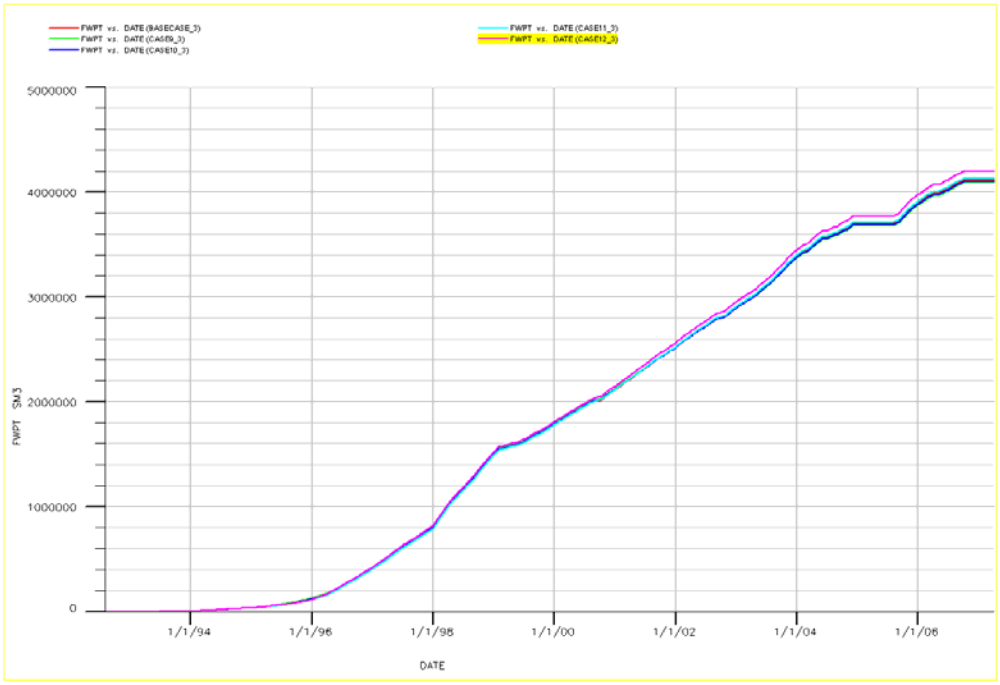

Figure 8-62 Comparison of the total water production for the different cases

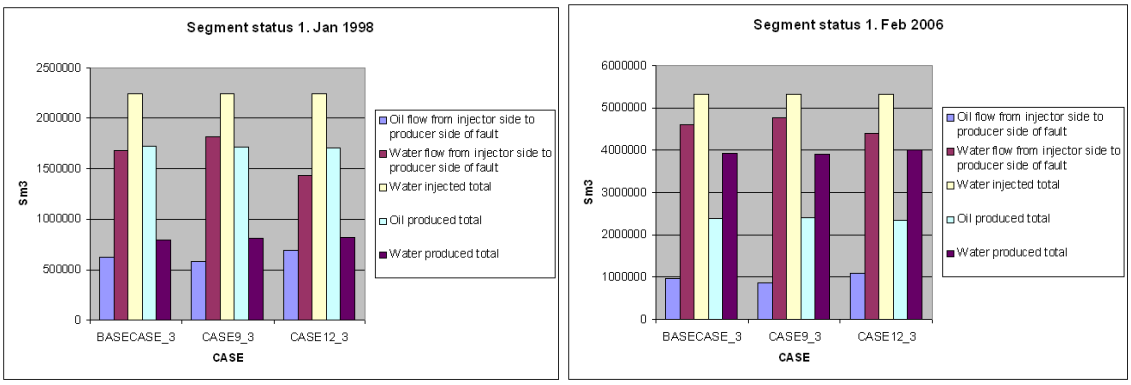

Figure 8-63 Segment status at two different times (1. Jan 1998 and 1. Feb 2006)

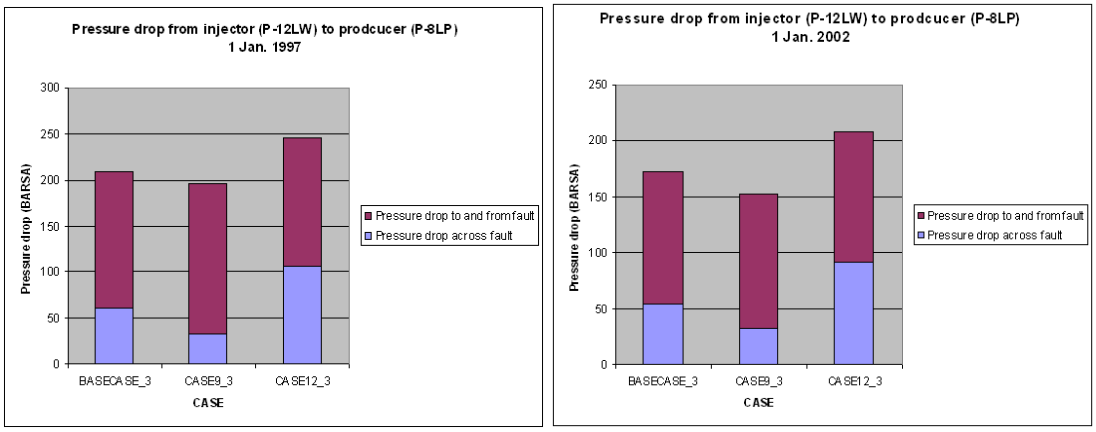

Figure 8-64 Pressure drop from injector to producer at different times (1. Jan 1997 and 1. Jan 2002)

8.4.2.4 Cementation factor

Cementation is a mechanism that tends to close the fault. In RMSfaultseal it is possible to vary the cementation factor between 1 (default) and 0, where the latter makes the fault sealing (chapter 6.5.2.3). In the A-Lu case there is utilized a cementation factor of 1, which indicates no influence from this parameter. Cementation factors of 0, 0.25, 0.5 and 0.75 were tested in this study.

Figure 8-65 through Figure 8-68 show the results from the simulations when changing the cementation factor. The results of total oil production from the segment presented in Figure 8-65 shows that the case with a sealing fault (CASE13_3) gives the highest oil production from the segment, both in the historical period and in the predicted period until 2015. This is not as expected because there in CASE13_3 has been applied a cementation factor of 0 which makes the fault sealing. The other cases produce approximately the same amount of oil in the historical period. In the predicted period a higher cementation factor will result in higher predicted oil production, which means that the cementation factor gives the expected response for these cases. Figure 8-66 shows the water production for the different cases until April 2007. CASE13_3 has a lower total water production than the other cases. This is due to the fact that CASE13_3 has a higher oil production and water production will be less in this case to match the reservoir fluid rate given as input to the model. In the other cases there are only small differences in the water production compared with the reference case.

Figure 8-67 shows the status of the segment at two different times (1. Jan 1998 and 1. Feb 2006). BASECASE_3 and CASE16_3 give approximately equal results at both times. In January 1998 CASE13_3 gives approximately the same oil flow across the fault as in the two other cases, but the water flow is some higher. In February 2006, there has flowed less oil across the fault than in the other cases. Still there has been more water flowing across the fault. CASE13_3 had been expected to have lower fault transmissibility across the fault and same trend as in the other cases with reduced fault communication, regarding oil and water flow across the fault. No good explanation can be given to this physical behaviour.

Figure 8-68 shows the pressure drop from injector to fault for the different cases. An interesting observation is that the pressure drop from injector to producer is lower for CASE13_3 than in the reference case. In addition, the pressure drop across the fault is significantly lower. This is not the expected behaviour since the fault is supposed to have lower fault transmissibility than the reference case. To verify if some mistakes were done during the establishment of this case, the procedure was repeated. The simulations gave exactly the same results for CASE13_3 and no good explanation can be given to this behaviour. The pressure response in CASE16_3 is as expected. The pressure drop from the injector to the producer is some larger than the reference case since some cementation is applied to the fault in this case. This extra pressure drop is caused by cementing making the fault more sealing.

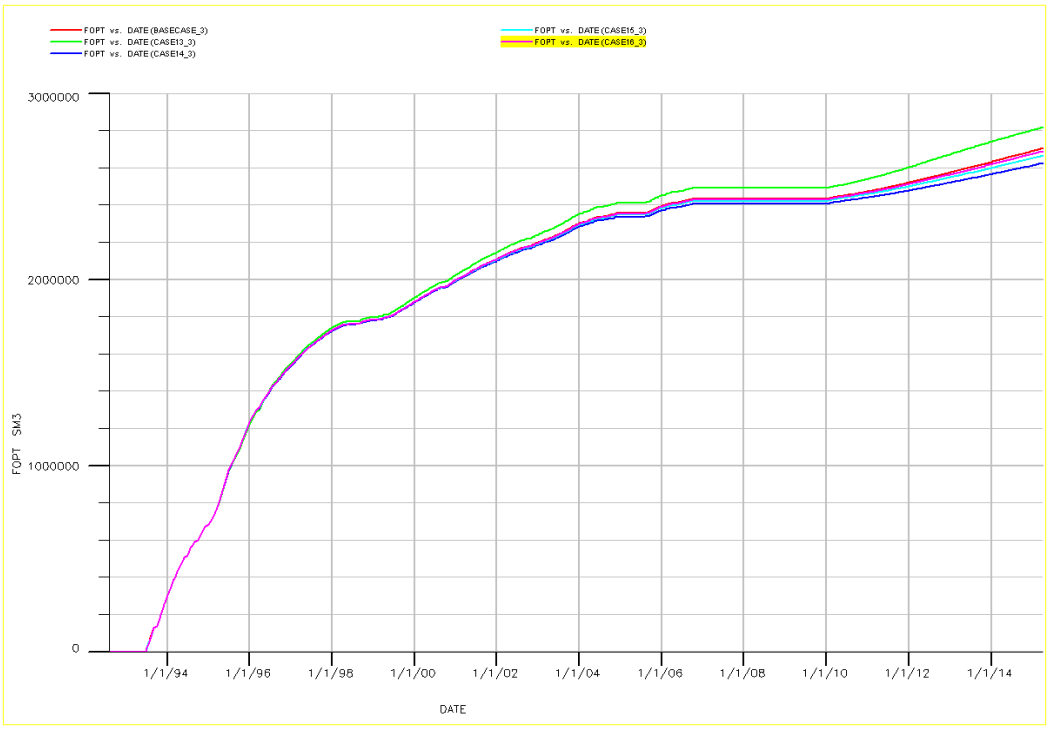

Figure 8-65 Comparison of the total oil production for the different cases

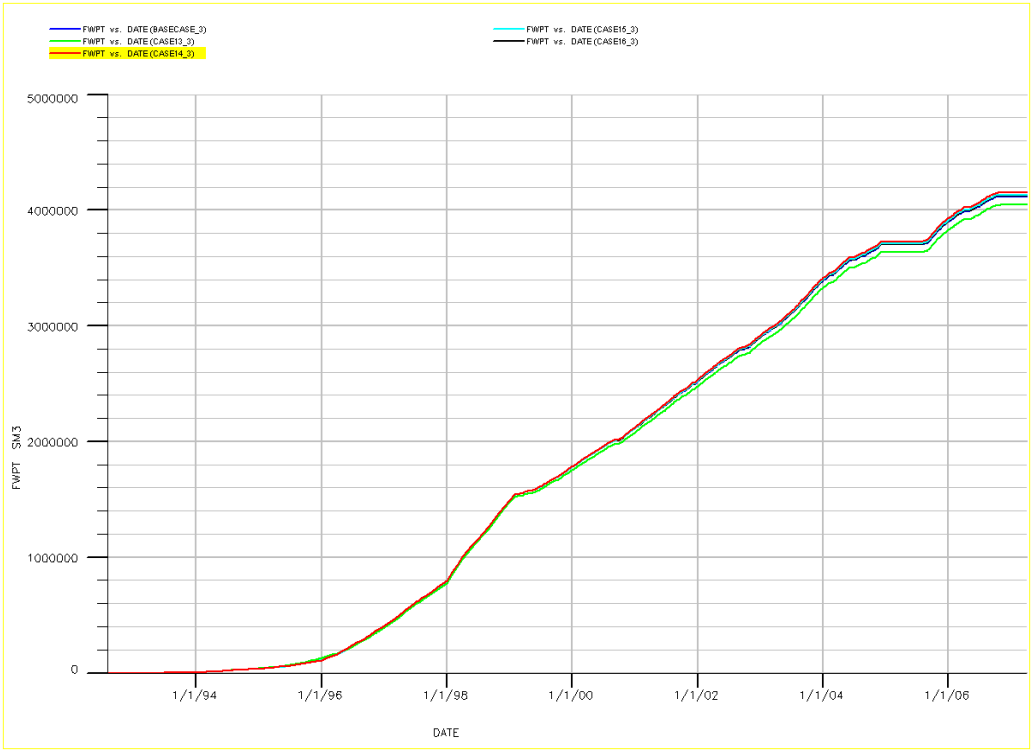

Figure 8-66 Comparison of the total water production for the different cases

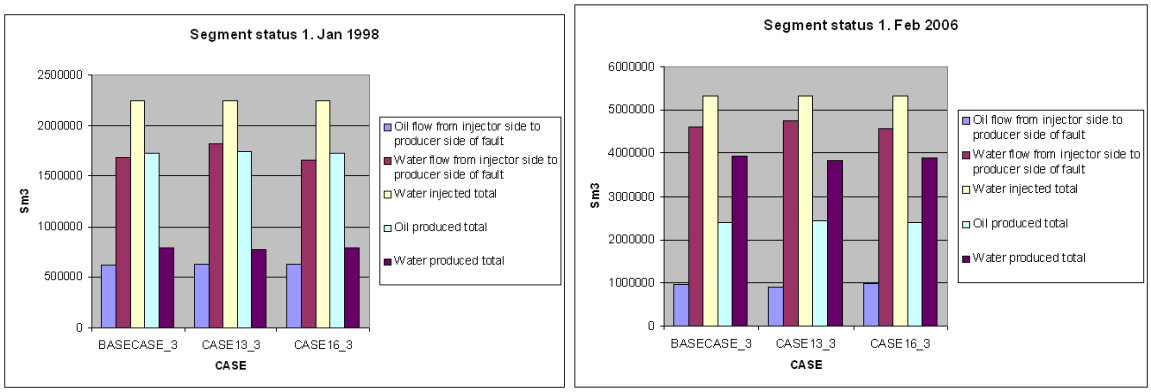

Figure 8-67 Segment status at two different times (1. Jan 1998 and 1. Feb 2006)

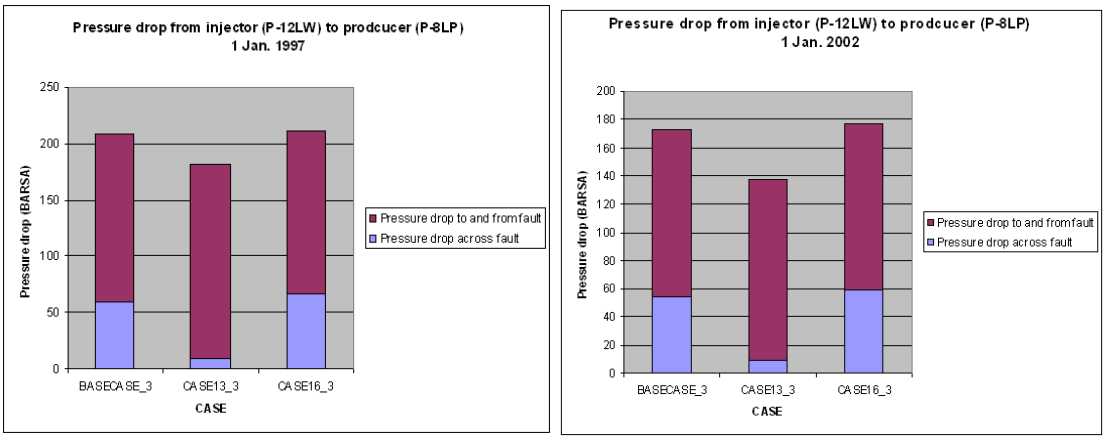

Figure 8-68 Pressure drop from injector to producer at different times (1. Jan 1997 and 1. Jan 2002)

8.4.2.5 *Shale Smear Factor Limit*

The shale smear factor (SSF) limit is a parameter that determines when the clay smear is continuous (chapter 6.4.2.2). If a calculated SSF value is below the limit defined, the clay smear is assumed to be continuous and the fault is sealing. In the reference case there was used a SSF-limit of 6. Values of 0, 3, 7 and 10 were tested in this sensitivity study.

The results from the simulations are presented in Figure 8-69 through Figure 8-72 and show that changing this factor has more or less no impact on the performance of the segment. The different cases have nearly exactly the same oil and water production, fluid flow across the fault and pressure drop from injector to producer. Some differences had been expected for CASE17_3 (SSF = 0) because there here will be a transmissibility value larger than zero for the entire fault. A sealing fault will in this case have extremely small transmissibility along the entire fault plane. The total sum of all these small transmissibility values had been expected to give some lower pressure drop across the fault. CASE20_3 was expected to have the opposite effect and increase the pressure drop across the fault, because larger part of the fault will be fully sealing when a high SSF-limit is applied. The fault has probably high SSF values along the fault surface, and the changes done to the SSF limit have small effect. Most values are likely to be higher than 10 since there is no effect of the values tested.

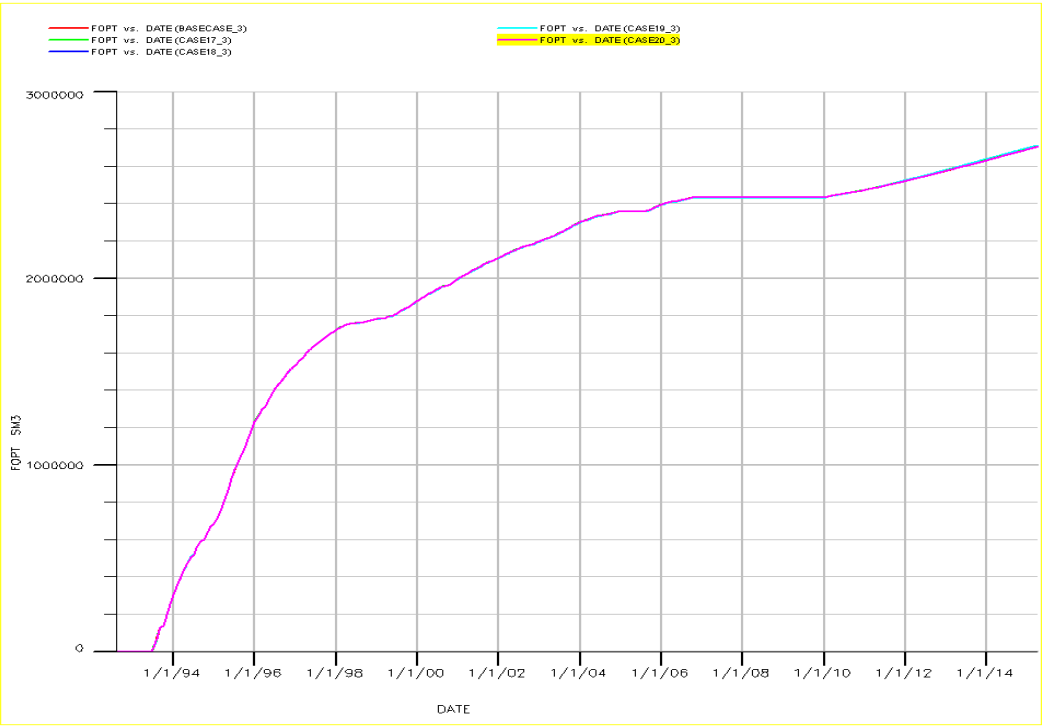

Figure 8-69 Comparison of the total oil production for the different cases

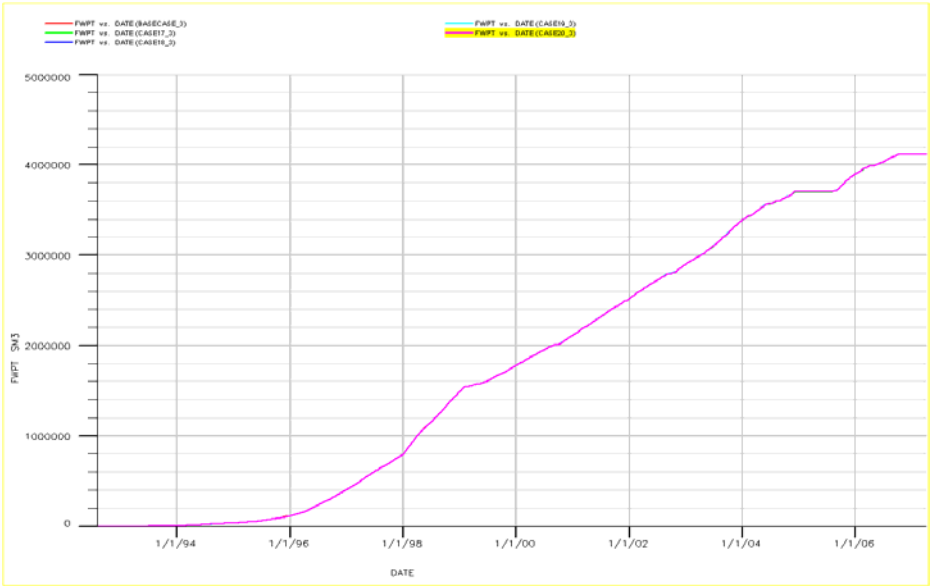

Figure 8-70 Comparison of the total water production for the different cases

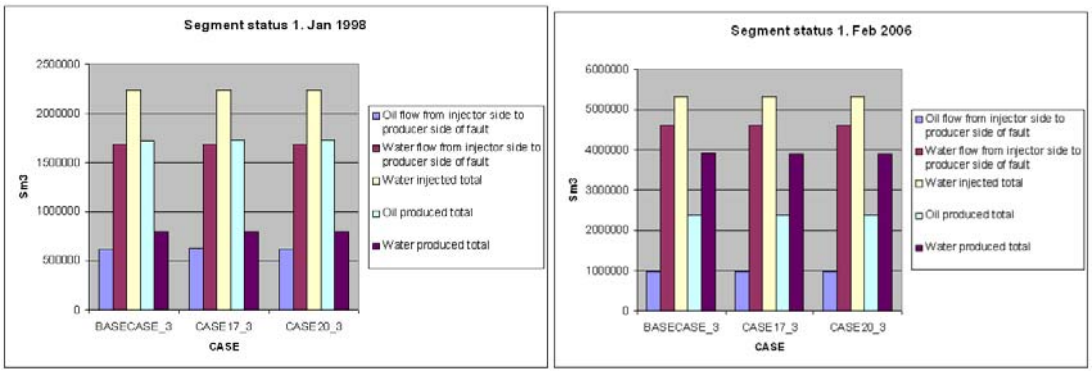

Figure 8-71 Segment status at two different times (1. Jan 1998 and 1. Feb 2006)

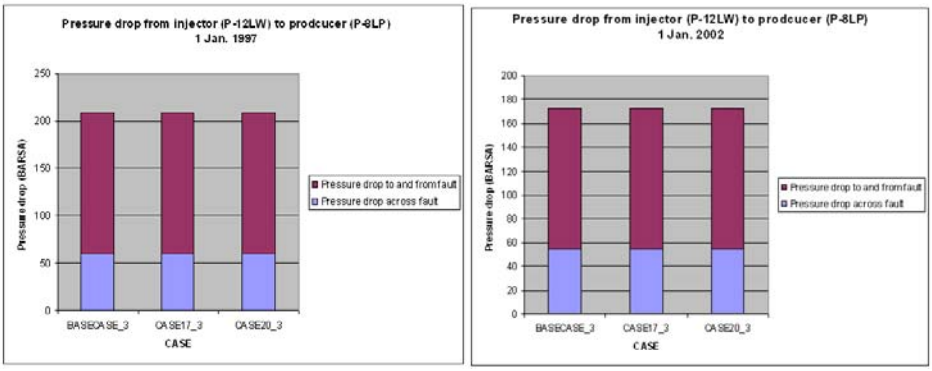

Figure 8-72 Pressure drop from injector to producer at different times (1. Jan1997 and 1. Jan 2002)

8.4.2.6 Brittle Factor

The fault zone permeability can also be modified by the brittle factor (chapter 6.5.2.2). The brittle factor can be used in the fault seal calculations by using values between 1 and 100. Brittle factor value of 1 (default) means no change, while 100 means a second order of magnitude higher fault permeability. In the reference case there is used a default value of brittle factor assuming no influence from this parameter. The brittle factor is supposed to work on the whole fault surface and is multiplied by the calculated fault permeability [24].

The results presented in Figure 8-73 and Figure 8-74 show that changing the brittle factor will have small impact on the total oil production and of water production in the historical period for the cases. For all cases there is enough oil available and the oil production will be approximately the same for all the cases. In the prediction run until 2015 the cases with higher brittle factor will give some higher oil production. These responses were expected since the brittle factor is increased. Applying a value of the brittle factor will increase the transmissibility across the fault and therefore the model in all cases manages to reproduce the oil and water production in the historical period.

Figure 8-75 shows the status of the segment at two different time steps. CASE25_3 and CASE28_3 give more or less the same results regarding oil and water flow from injector to producer side of the fault at both times. Both cases have less oil and more water flowing across the fault than the reference case. The reason for this is the same as for the other cases where the fault transmissibility is increased. Better communication across the fault will result in more water flowing across the fault. This results in better pressure maintenance on the producer side of the fault. Less oil will therefore flow across the fault because of the high pressure on the producer side of the fault. There will be higher recovery of oil located on the producer side of the fault for CASE25_3 and CASE28_3.

Figure 8-76 shows the pressure drop from the injector to the producer for the two cases. The pressure drop for both cases are reduced compared with the reference case. The pressure drop across the fault is, as expected, less in CASE28_3 where a higher brittle factor is utilized. The results show that by applying a maximum value of the brittle factor the pressure drop across the fault can be reduced by 40 bars compared with the reference case. At both times there is some larger pressure drop to and from the fault for CASE25_3 and CASE28_3 than in the reference case. This is because there is higher liquid rate across the fault for these cases and this will cause a higher pressure drop to and from the fault.

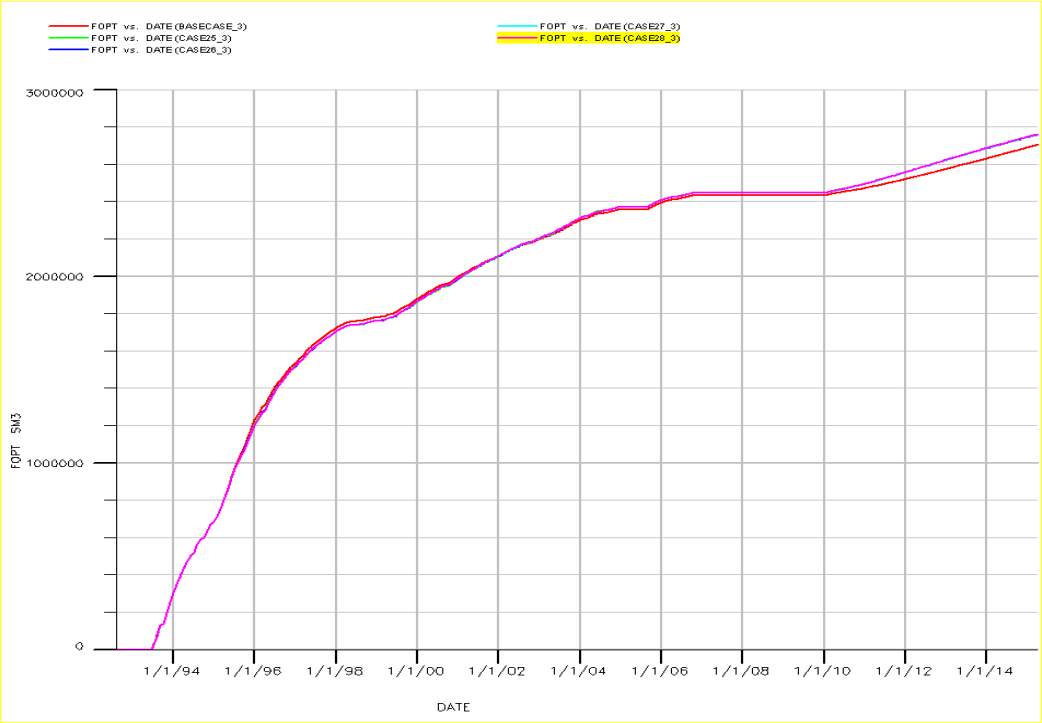

Figure 8-73 Comparison of the total oil production for the different cases

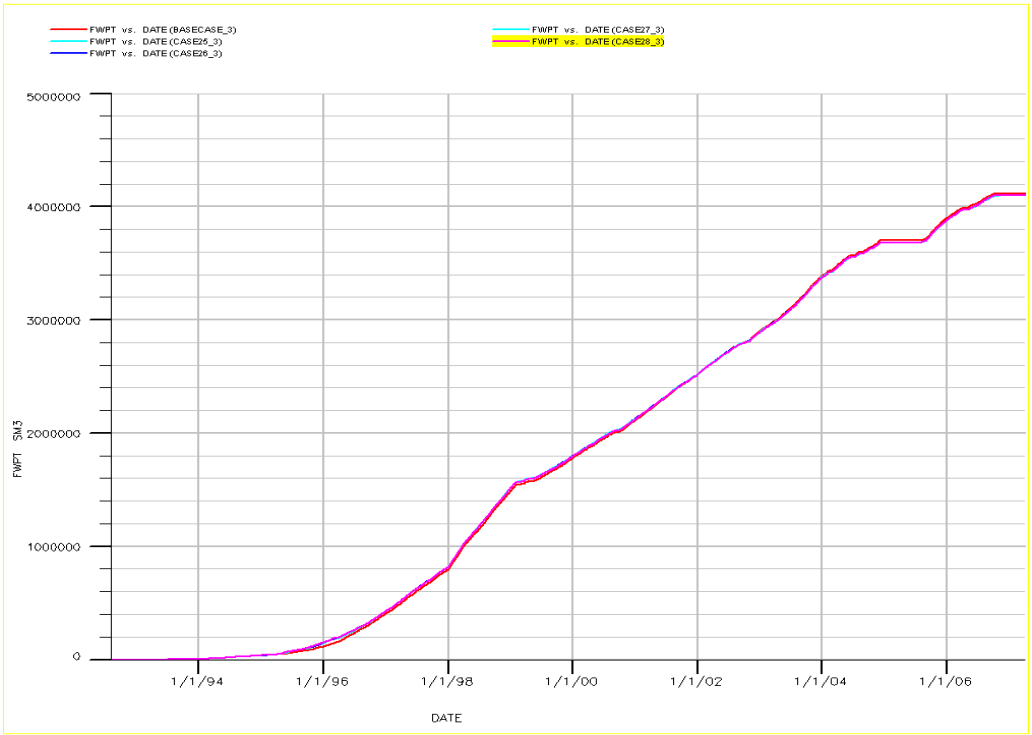

Figure 8-74 Comparison of the total water production for the different cases

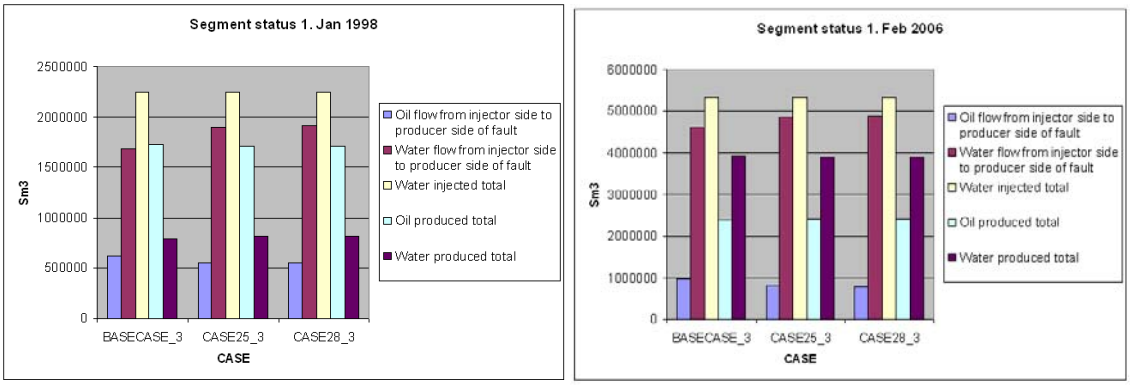

Figure 8-75 Segment status at two different times (1. Jan 1998 and 1. Feb 2006)

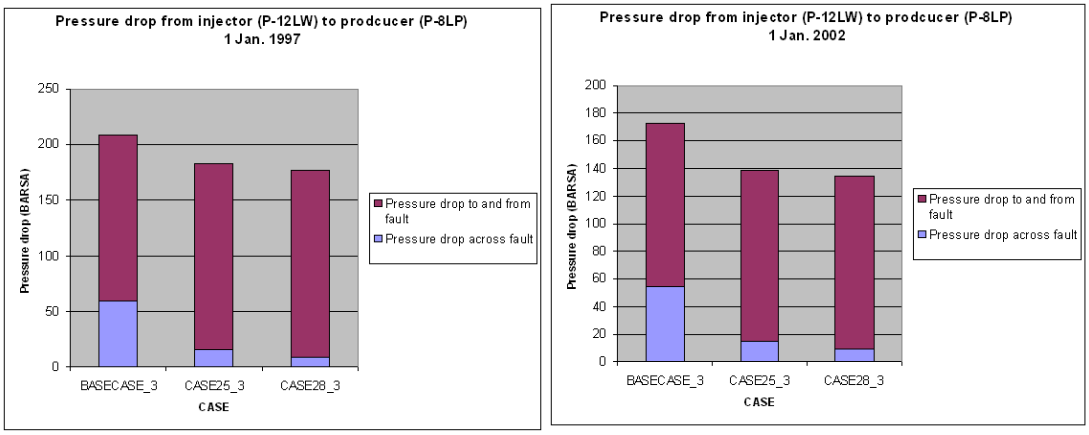

Figure 8-76 Pressure drop from injector to producer at different times (1. Jan 1997 and 1. Jan 2002)

8.4.2.7 Oblique Slip Angle

The oblique slip angle can be used in the RMSfaultseal to give a more exact description of the fault displacement (chapter 6.5.2.1). The displacement will affect the calculation of the fault zone thickness in a sense that a larger value of the displacement will give a thicker fault zone. Different oblique slip angle values were used in the four cases and it was revealed that this parameter had no affect compared with the reference case. This is due to the fact that the fault throw of C230 is relatively small and changing the oblique slip angle will have no effect in such cases. If the throw had been higher more differences in the simulations had been expected.

The largest displacement of the fault C230 is about 14 m (from visual inspection in FloViz). The impact of oblique slip angle was studied in more detail (Table 8-4). The calculations are based on equation 6-1. From Table 8-4 it can clearly be seen that the oblique slip angle will have no significant impact on fault zone thickness when the throw is 14 m. Even not for slip angles up to 50 degrees. To see the effect of the oblique slip angle on the fault zone thickness high values of the oblique slip angle and large fault displacement are needed. In the calculations summarized in the table a constant displacement-thickness ratio of 50 is used.

Figure 8-77 through Figure 8-80 show that there is no difference in the performance of the segment compared with the reference case.

		Fault displacement (m)		
	14	**20**	**50**	**100**
Oblique slip angle (degrees)				
5,2	14,1	20,1	50,2	100,4
9,8	14,2	20,3	50,7	101,5
20,2	14,9	21,3	53,3	106,5
30	16,2	23,1	57,7	115,5
50	21,8	31,1	77,7	155,5
		Fault zone thickness (m)		
Oblique slip angle (degrees)				
5,2	0,3	0,4	1,0	2,0
9,8	0,3	0,4	1,0	2,0
20,2	0,3	0,4	1,1	2,1
30	0,3	0,5	1,2	2,3
50	0,4	0,6	1,6	3,1

Table 8-4 Fault zone thickness calculated by using oblique slip angle

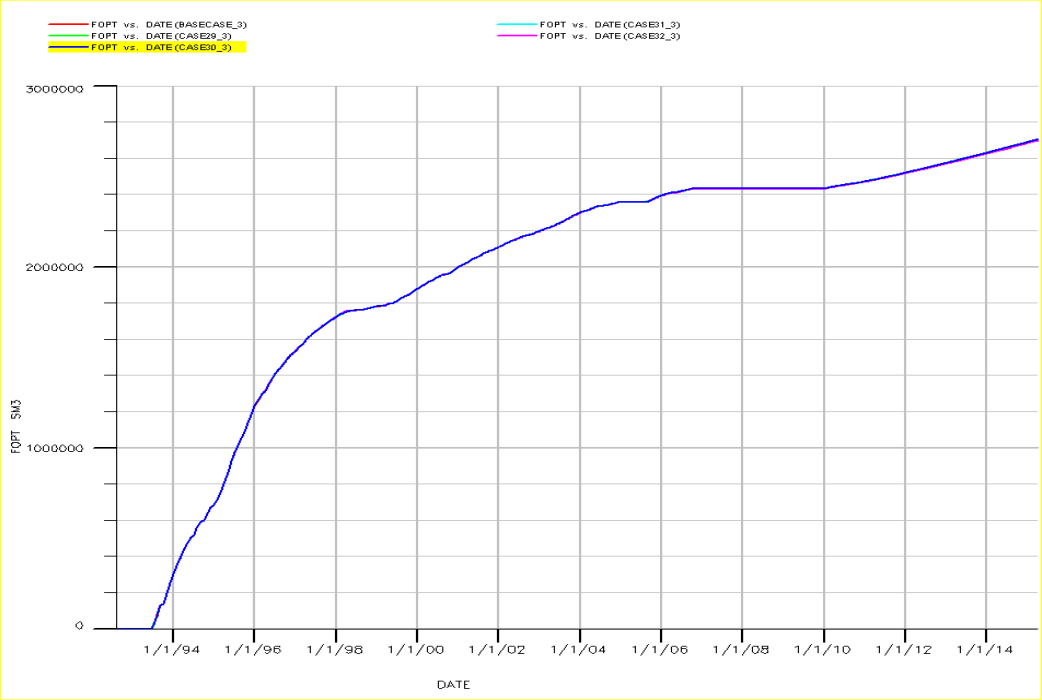

Figure 8-77 Comparison of the total oil production for the different cases

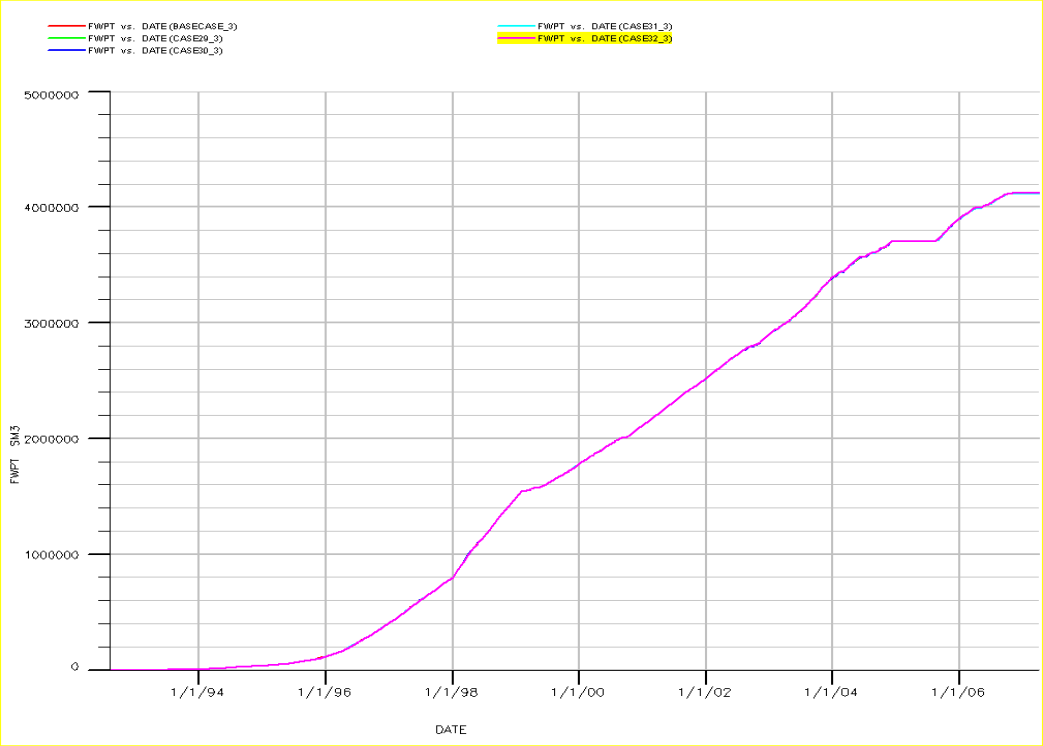

Figure 8-78 Comparison of the total water production for the different cases

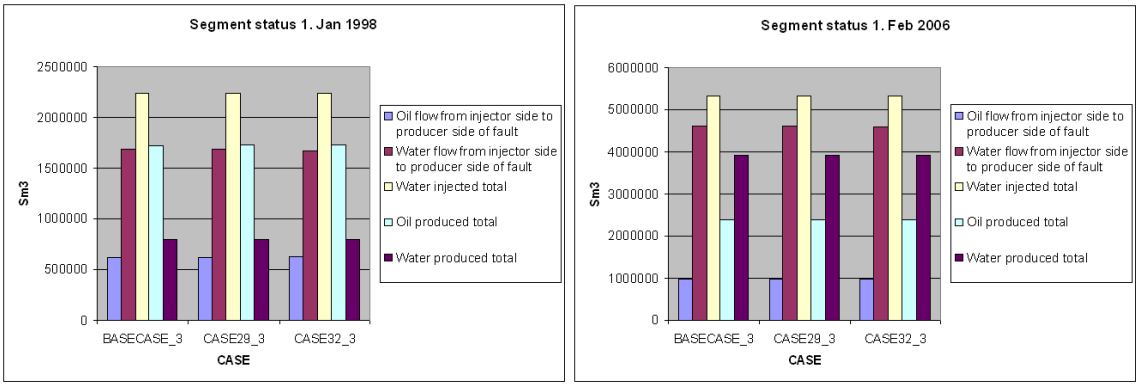

Figure 8-79 Segment status at two different times (1. Jan 1998 and 1. Feb 2006)

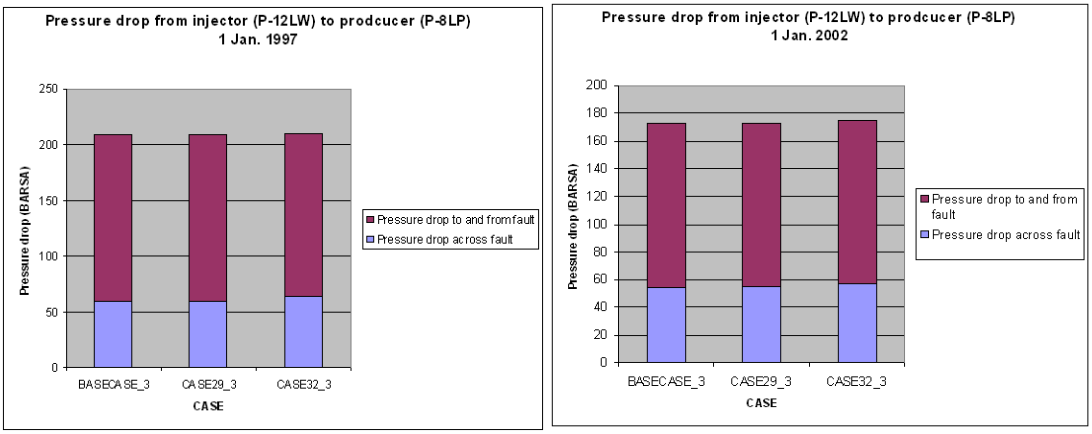

Figure 8-80 Pressure drop from injector to producer at different times (1. Jan 1997 and 1. Jan 2002)

8.4.2.8 Change in Geological Realization

Different geological realizations were generated in the development of the new reservoir models for the Snorre Field in 2006. Realization #3 is used in the official Snorre reservoir models at this time. Two alternative realizations, realization #5 and realization #10, were tested in this study (App E). Table 8-2 and Table 8-3 show the initial conditions for each case. CASE21_3 has less oil original in place on both the injector and the producer side of the fault. For CASE22_3 the original oil in place is some less than in the reference case, but higher than CASE21_3. Realization #5 represents an alternative sand distribution, while realization #10 represents an alternative channel direction (north to south). The direction of the sand channels has been subject to discussions between geologists for long time at Snorre.

The results from the simulations are represented in Figure 8-81 through Figure 8-84 and show that the choice of geological realization will have significant impact on the production of oil and water from the segment. Both CASE21_3 and CASE22_3 give a lower production of oil than the reference case, both in the historical and predicted period. There is nearly no oil production from the two CASE21_3 and CASE22_3 after the middle of 2006. This is most likely caused by limited bottom hole pressure in P-8LP because of poor communication between reservoir sands and the well. Water production is high in both cases and there is probably not enough bottom hole pressure to lift the liquid column in the well. The water production is high in both cases to compensate for the limited oil volume in communication with well P-8LP. As long as there is enough water available the well will produce water to match the observed reservoir volume rate used as input in the model.

Figure 8-83 shows the status of segment at two different times. CASE21_3 has less oil flowing from injector to producer side of the fault at both times, compared with the reference case and CASE22_3. At the same there is more water flowing from the injector to the producer side of the fault. This can indicate that there is good communication between sands located in the water zone of the segment. Injection water is most likely flowing through some high permeable sands connected between the injector and the producer. There are probably poor communication between the oil bearing sands and P-8LP resulting in limited oil production. CASE22_3 has more oil and less water flowing across the fault compared with the reference case in January 1998. In February 2006 the total oil and water flow across the fault is almost equal for CASE22_3 and the reference case. The total oil production from the cases is different though. This can mean that there is relatively good communication across the fault in CASE22_3, but that much of the oil located at the producer side of the fault is unavailable due to poor communication between the sands and well P-8LP. The high water production for CASE22_3 indicates that there is good communication between the producer and the sands in the water zone.

Figure 8-84 shows the pressure drop from injector to producer for the two cases, compared with the reference case. CASE22_3 has a very high pressure drop from the injector to the producer and a major part of it is caused be flow to and from the fault. This indicates that there is very low communication between the wells because of limited communication between the permeable sands. CASE21_3 has a lower pressure drop than CASE22_3, but in this case the pressure drop across the fault is higher indicating that there is lower fault transmissibility. It is

possible that some layers of good quality are connected with layers of lower reservoir quality on each side of the fault.

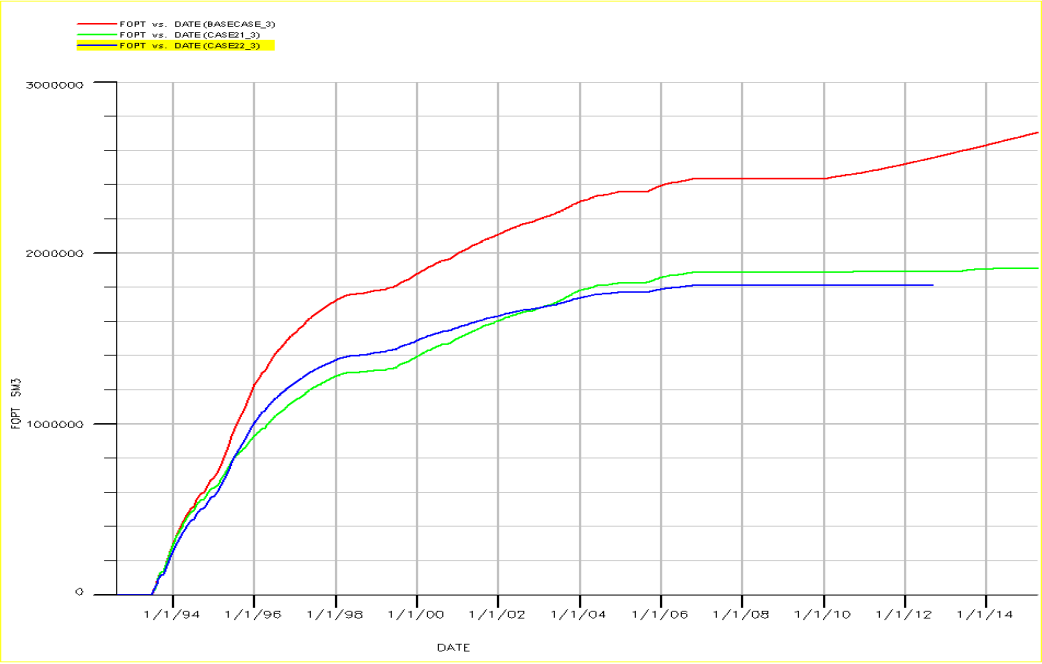

Figure 8-81 Comparison of the total oil production for the different cases

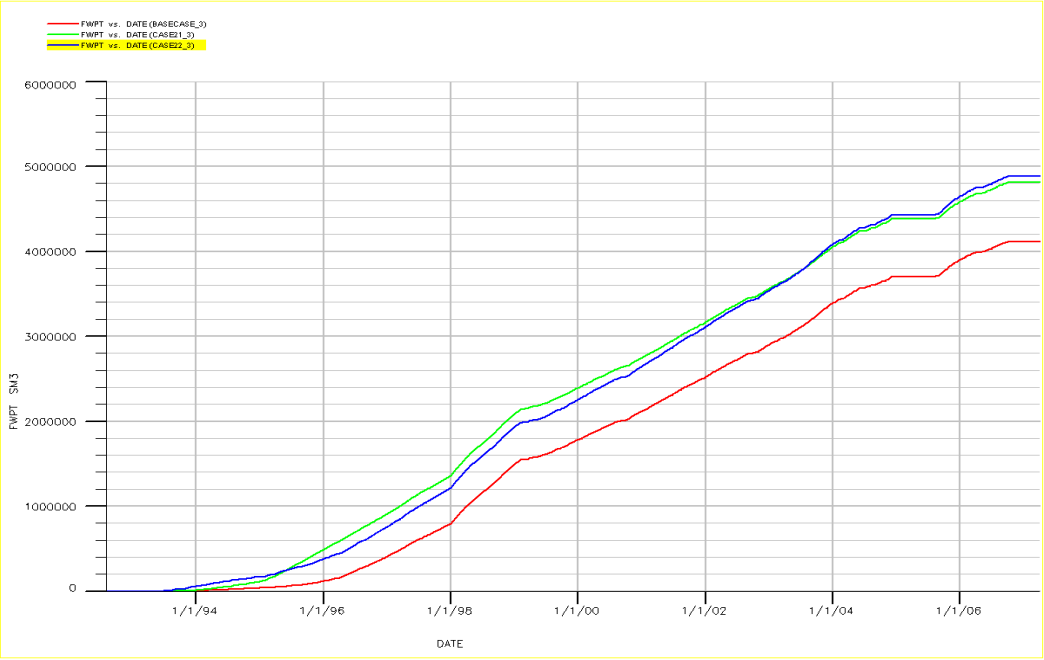

Figure 8-82 Comparison of the total water production for the different cases

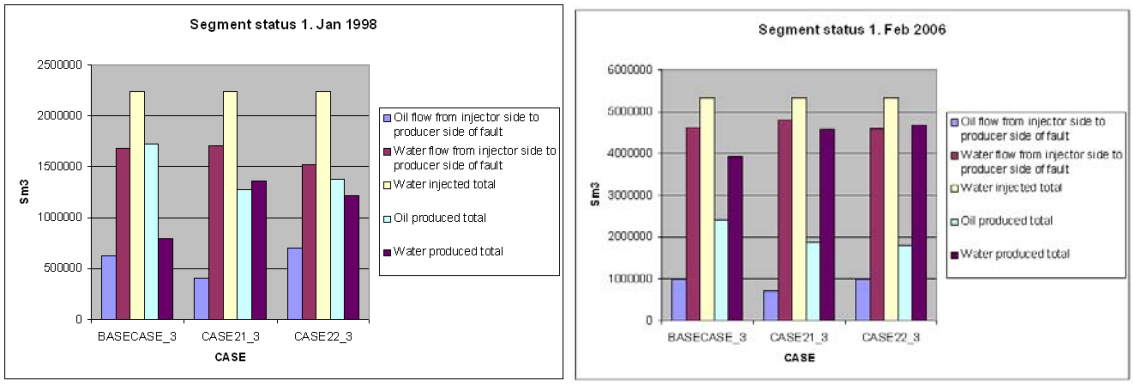

Figure 8-83 Segment status at two different tims (1. Jan 1998 and 1. Feb 2006)

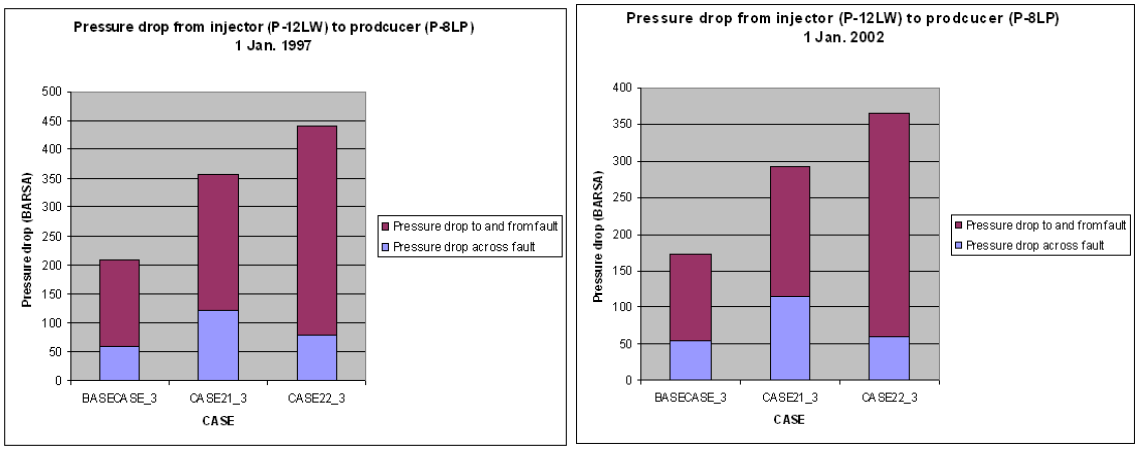

Figure 8-84 Pressure drop from injector to producer at different tims(1. Jan 1997 and 1. Feb 2002)

8.4.2.9 Algorithm for Calculating Fault Permeability

The Sperrevik and Manzocchi algorithms for calculation of fault permeability were tested. Comparison of the two algorithms has showed that the Manzocchi algorithm will give higher values for fault zone permeability if SGR values are larger than ca. 0.2. The Sperrevik algorithm is strongly dependant of on burial depth at time of deformation when SGR values are lower than ca. 0.4 [24]. App C shows the distribution of SGR-values along the fault for the P-70 case. Many of the SGR-values along the fault plane seems to be in the region between 0.2 and 0.4, so it difficult to predict which algorithm that is supposed to give the highest fault permeability. The burial depth at time of deformation, z_f, was set to 2000 meters in the Sperrevik algorithm.

Figure 8-85 shows the predicted oil production (until 2015) and Figure 8-86 represents water production for the two cases compared with BASECASE_3. The figures show that there is relatively good match between the cases regarding oil and water production in the historical period. The Sperrevik algorithm though, seems to give some higher oil production. In the predicted period the Sperrevik and Manzocchi algorithms give a higher oil production than the reference case and the Sperrevik method gives a slightly higher predicted oil production.

Figure 8-87 shows the segment status for the cases at two different times. Oil flow from injector to producer side of fault is lower both in CASE23_3 and CASE24_3 compared with the reference case at both times. There is also more water flowing from the injector to the producer side of the fault for these two cases (most in CASE 23_3). CASE23_3 seems to have some better communication across the fault than CASE24_3 regarding fluid flow. This may indicate that CASE23_3 has some higher fault permeability than CASE22_3. When looking at the predicted oil production from the segment (Figure 8-85) CASE24_3 gives slightly higher oil production than in CASE23_3. Though the difference is small it had been expected to be some higher oil production for CASE23_3 based on the information from Figure 8-87.

Figure 8-88 shows the pressure drop from injector to producer for the cases. The Sperrevik and Manzocchi algorithm give a lower pressure drop from the producer to the injector side of fault than the reference case, indicating that the fault permeability is higher for these cases. The Manzocchi algorithm gives the lowest pressure drop across the fault indicating that this method gives the highest fault zone permeability. It had been expected that the Manzocchi algorithm had given higher predicted oil recovery than the Sperrevik algorithm based on the evaluation made above. A possible explanation may be that the Manzocchi algorithm gives some lower transmissibility in the oil zone of the fault, compared with the Sperrevik algorithm.

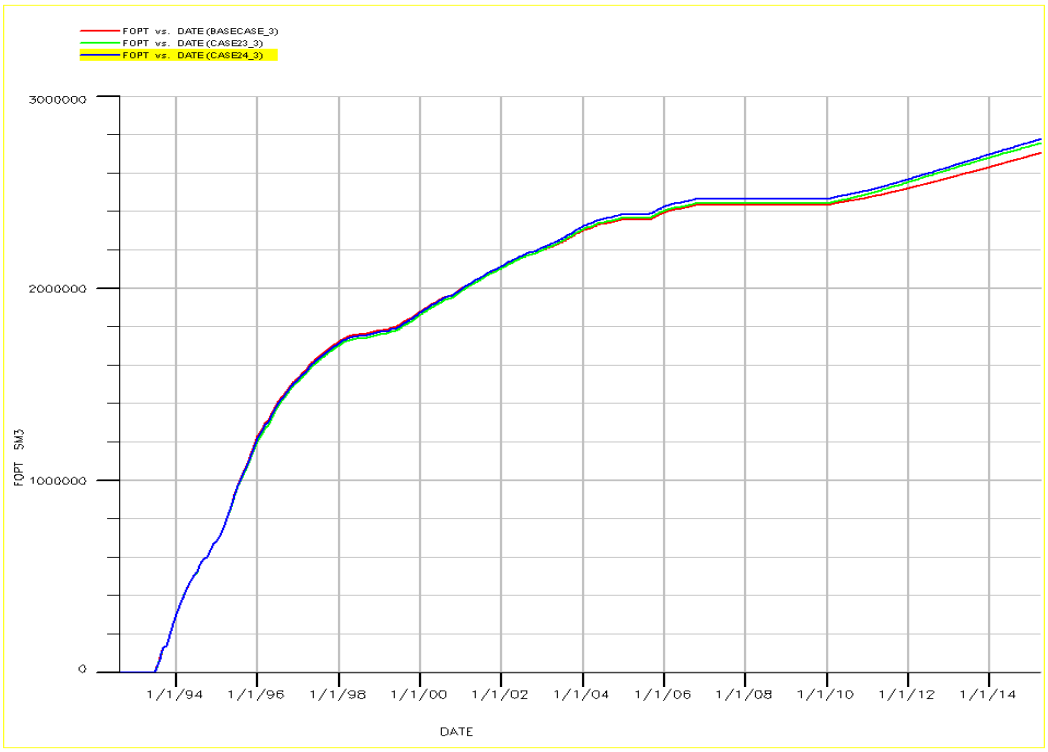

Figure 8-85 Comparison of the total oil production for the different cases

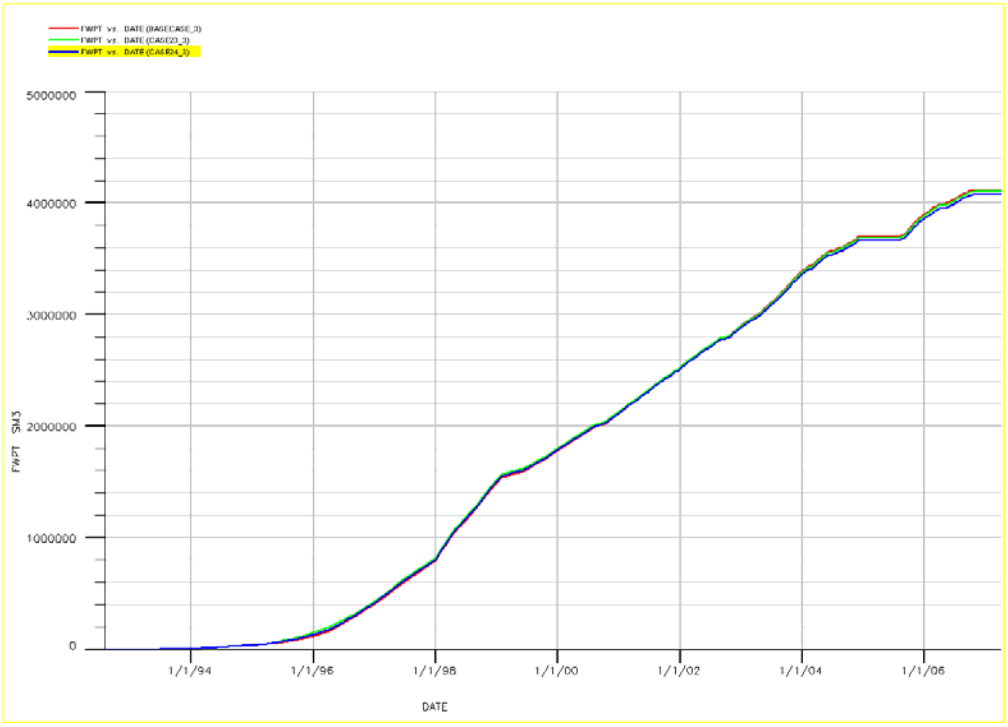

Figure 8-86 Comparison of the total water production for the different cases

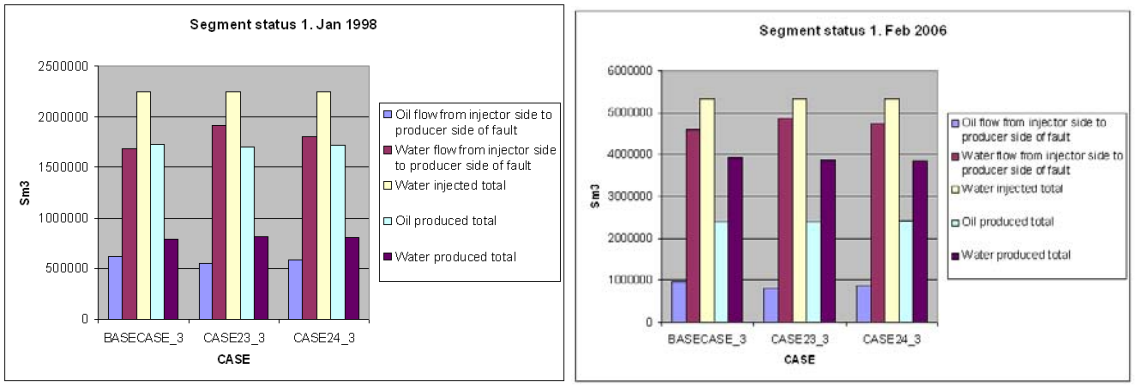

Figure 8-87 Segment status at two different times (1. Jan 1998 and 1. Feb 2006)

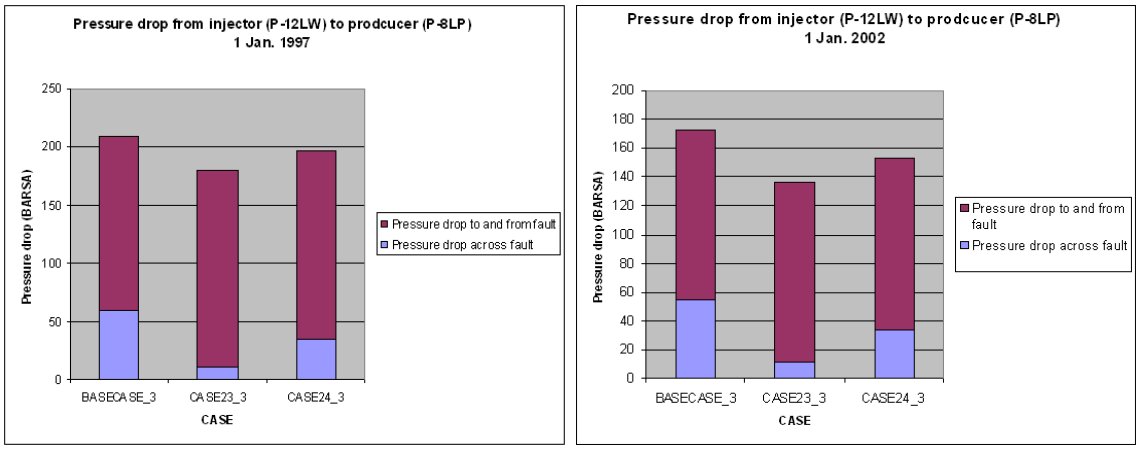

Figure 8-88 Pressure drop from injector to producer at different times (1. Jan 1997 and 1. Jan 2002)

8.4.2.10 Adjusting Transmissibility across Faults

Adjusting the transmissibility multipliers was performed by using the Eclipse keyword MULTFLT, as described earlier. Both the fault (C230) and the fault elongation were multiplied by the same factor.

The simulation results show that adjusting the transmissibility multipliers will have a significant impact on the total oil and water production from the segment (Figure 8-89 and Figure 8-90). As expected, multiplying of the transmissibility will increase the overall oil production from the segment. On the other hand, when dividing the fault transmissibility by different factors there is a reduction in the total oil production. The tightest case (CASE36_3), where the fault transmissibility is divided by 50, did only produce until the beginning of 1998 before it close due to limited pressure in the reservoir. In CASE35_3, where the fault transmissibility is reduced by a factor of 10, the total oil production matches the reference case very well in the historical period. In the predicted interval this case has nearly no oil production. The two cases with increased fault permeability compared to BASECASE_3 will have a much better pressure maintenance on the producer side because of more effect of water injection. As the prediction show, these cases will give a significantly higher recovery than the reference case. The simulations show that multiplying the fault transmissibility by 100 gives a higher recovery than for instance applying a brittle factor of 100, which is meant to improve the fault permeability with a second order of magnitude.

Figure 8-91 shows the status for the segment at two different time steps (1. Jan 1998 and 1. Feb 2006). CASE33_3 has more oil flowing from the injector to the producer side of the fault and approximately the same amount of water flowing through the fault as BASECASE_3 in January 1998. In February 2006 there is still a higher oil flow across the fault for CASE33_3 compared with the reference case, but now the water volume that has flowed across the fault is lower. The increased flow of oil across the fault for this case is most likely caused by that the transmissibility across the fault elongation has increased as well as the rest of the fault. In the cases where fault seal parameters modified in the RMSfaultseal have given higher fault transmissibility, the elongation of fault C230 has not been modified. In this sensitivity study the transmissibility along the entire fault, included the elongation, is modified. In January 1998, oil and water flow across the fault is lower for CASE35_3 than in the reference case. The trend is the same in February 2006. The reduced transmissibility will prevent both water and oil from flowing across the fault.

Figure 8-92 illustrates the pressure drop from injector to producer for the two cases. BASECASE_3 is included for comparison. The pressure drop for CASE33_3 is lower than in the reference case. The difference in pressure drop between the reference case and CASE33_3 is a result of lower pressure drop across the fault. This is the expected response when increasing the fault transmissibility. CASE35_3 has a very high pressure drop from the injector to the producer (ca. 430 bars) and the fault is dominating the pressure drop between injector and producer for this case. 1. Jan 2002, the pressure drop across the fault has increased for CASE35_3 compared to 1. Jan 1997. The reason for this can be local pressure differences within the grid blocks at this time step.

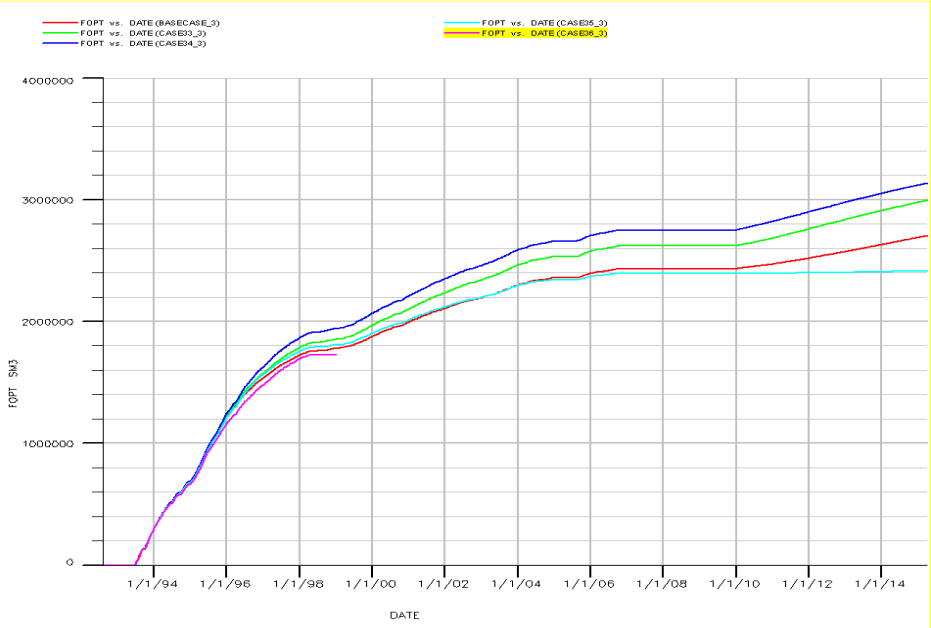

Figure 8-89 Comparison of the total oil production from the different cases

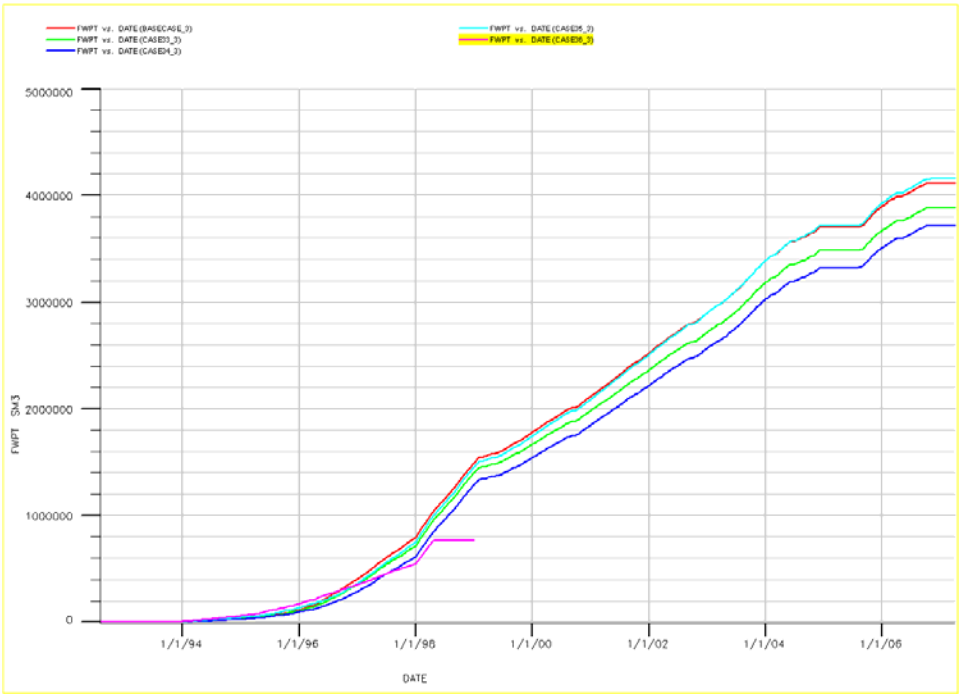

Figure 8-90 Comparison of the total water production from the different cases

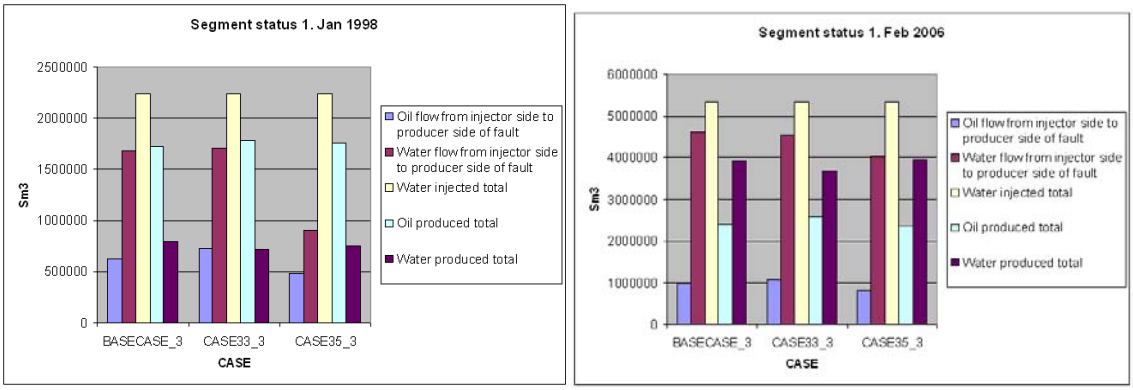

Figure 8-91 Segment status at two different times (1. Jan 1998 and 1. Feb 2006)

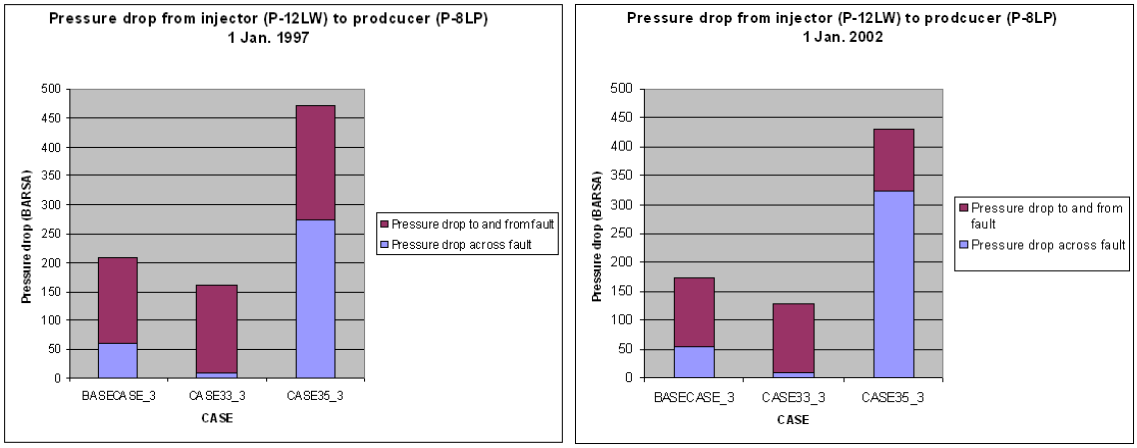

Figure 8-92 Pressure drop from injector to producer at different times (1. Jan 1997 and 1. Jan 2002)

8.4.2.11 No Fault Seal or Transmissibility Adjustments

A case was established in order to see the impact of using transmissibility calculated by Eclipse without any fault transmissibility multipliers included. Figure 8-93 and Figure 8-94 show the oil and water production from this case (CASE37_3) compared with the reference case. The predicted oil production in 2015 is significant higher for CASE37_3 than the reference case. This was expected since there is actually no fault having impact on the flow in this case. The water production is lower than in the reference case, because the high oil production will cause correspondingly lower water production to match the reservoir volume produced. The fault throw is so small that juxtaposition of non-reservoir units against reservoir units is very unlikely to occur.

Figure 8-95 shows the segment status at two different times (1. Jan 1998 and 1. Feb 2006). One can see that there has been higher oil production and more flow of oil from injector to producer side of the fault for CASE37_3 at both times. The flow pattern of oil and water will be totally different for this case since there are no fault restrictions to fluid flow. Both in January 1998 and February 2006 the reference case produces larger amount of water and less oil than CASE37_3.

Figure 8-96 shows that there is no pressure drop occurring across the fault. The pressure drop in CASE37_3 is only caused by fluid flow to and from the fault.

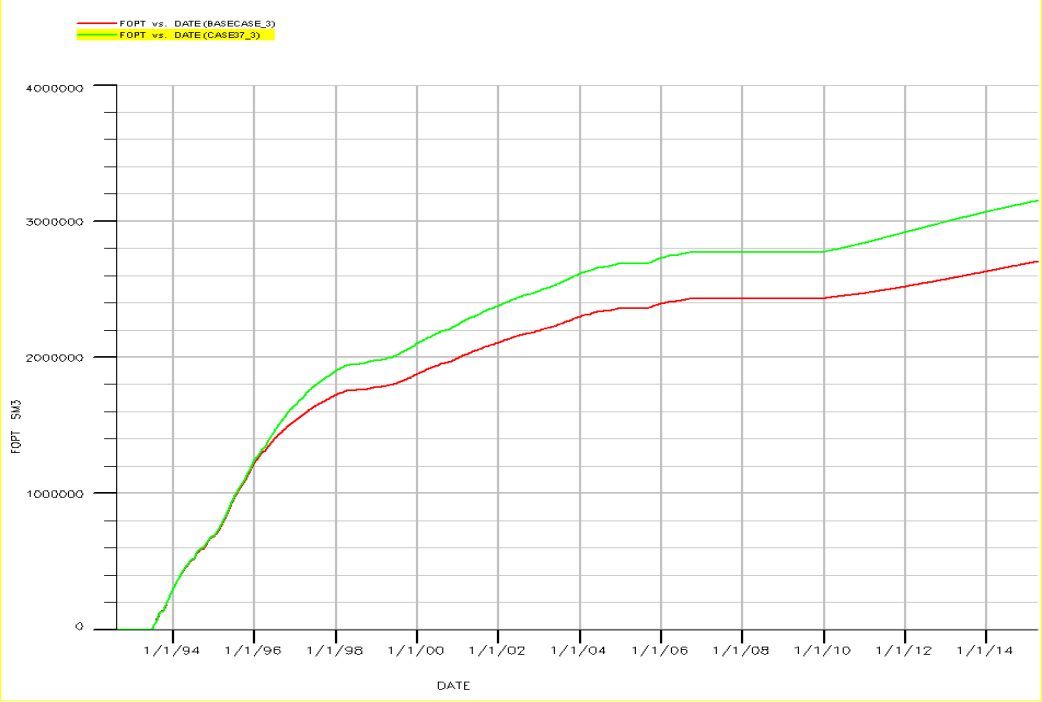

Figure 8-93 Comparison of the total oil production for the different cases

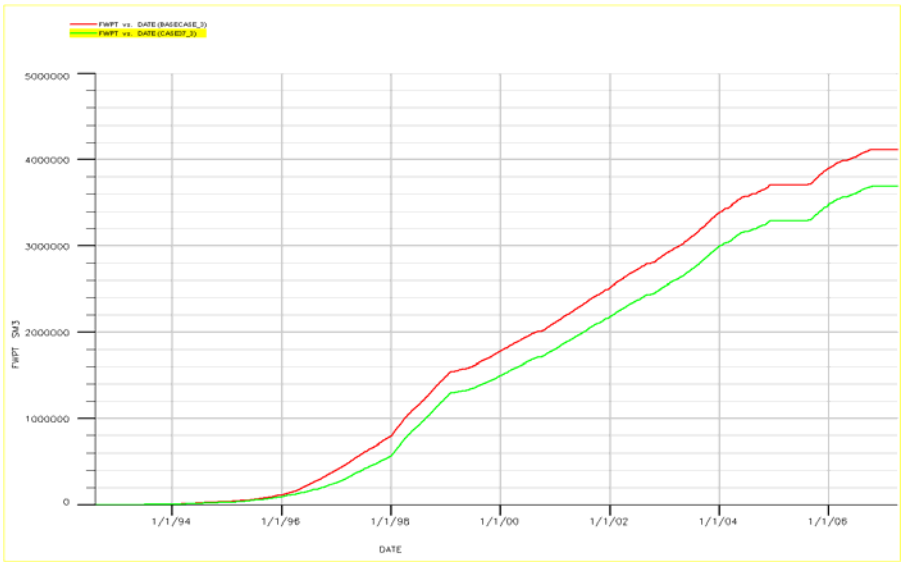

Figure 8-94 Comparison of the total water production for the different cases

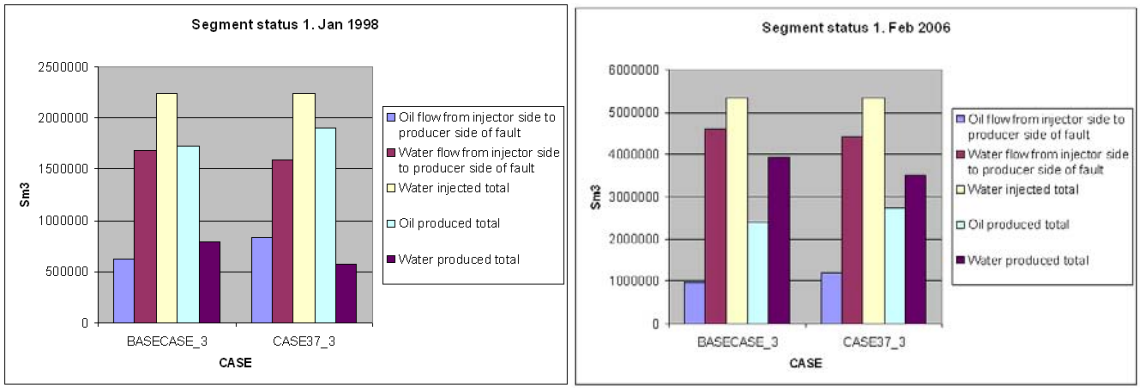

Figure 8-95 Segment status at two different times (1. Jan 1998 and 1. Feb 2006)

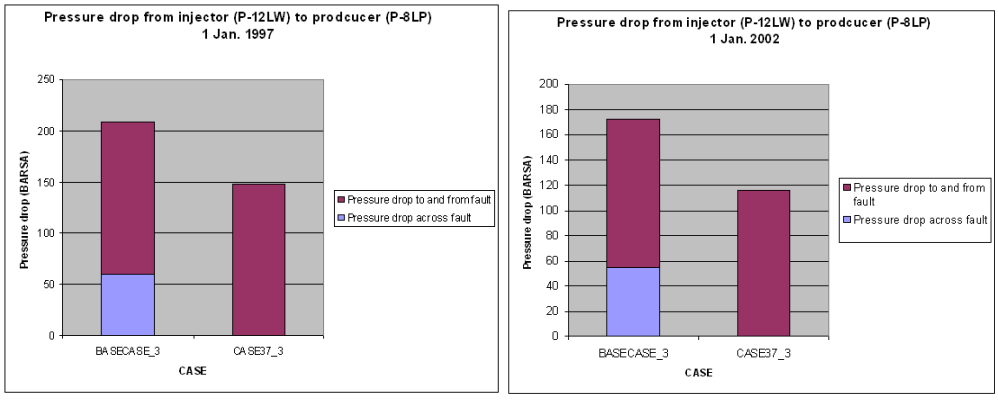

Figure 8-96 Pressure drop from injector to producer at different times (1. Jan 1997 and 1. Jan 2002)

8.5 Summary of Results

Figure 8-97 and Figure 8-98 represent the difference in oil production (%) for historical and predicted period for the different cases compared with the reference case. The cases where the SGR-curves are modified seem to have small effect on the oil production in the segment. In CASE4_3 where the fault permeability is reduced by a factor 10 well P-8LP produce some percent less oil than the reference case, both for the historical and predicted period.

The figures reveal that the cases where the fault throw is increased have the largest difference from the reference case. For the case where the throw is increased with 100 m the difference in total oil production is almost 80% less than the reference case (BASECASE_3). The reason for the limited oil production in these cases is that some of the oil on the injector side of fault becomes unavailable because of the juxtaposition.

In CASE12_3, where the displacement-thickness ratio is set to 1 (geological unrealistic) the oil production will be some percent less compared with BASECASE_3. This is caused by the reduced fault transmissibility.

Oil production from CASE21_3 and CASE22_3, where different geological realizations are applied, is also significant lower than in the reference case. The difference is most significant in CASE22_3 where a different channel direction is applied. Both of these alternative geological realizations give to poor communication in the segment and P-8LP is not able to produce enough oil in these cases. The way sands are modelled stochastically will have very high impact on the performance of the segment. Even though realization #3 (used in the reference case) gives the best match to historical data, there can be other distributions of sands that may give a better match. When it comes to the direction of the sand channels, it seems like it is very difficult to produce the same amount of oil because of the limited communication. The difference is as big as 35% compared with the reference case in the historical period and even higher in the prediction.

In CASE23_3 and CASE24_3 the Manzocchi and Sperrevik algorithm is used to calculate the fault permeability. Both cases will give a higher predicted oil production than the reference case because of increased fault permeability.

In CASE33_3, CASE34_3, CASE35_3 and CASE36_3 there are significant changes in the oil production. In these cases different multipliers have been applied to increase and decrease the transmissibility across the fault. In CASE33_3 and CASE34_3 the transmissibility across the fault is increased, by factor 10 and 100 respectively. The entire fault are multiplied by these values include the elongation of the fault. This will result in higher oil production from the segment because of more fluid flow across the fault.

At the end of the prediction run the differences in oil production will be larger than at the end of the historical period. The reason for this is that the P-8LP has another mode of control in the predicted period. In the predicted period the well is controlled by pressure and not on reservoir volume rate. For this reason the well are able to produce at higher rates as long as it can deliver a certain tubing head pressure. In the cases where the fault transmissibility is

increased there will be higher predicted oil production than in the reference case. The cases where change of fault seal parameters has reduced the fault transmissibility there will be lower oil production at this time compared with the reference case. This is because the effect of the injector is lower in these cases because of the reduced transmissibility across the fault, and there will be a lower bottom hole pressure available in the well.

Five cases (C38, C39, C40, C41 and C42) were established to investigate how much fluid is flowing from the injector side to producer side in the elongation. The results are represented in Figure 8-99. The elongation of fault C230 to fault CSF_1 was, as already mentioned, made in the history matching of the model. Different fault transmissibility multipliers were applied in the vertical direction of the elongation. The elongation is tightened by different factors (100 (C38), 1000 (C39), 10000 (C40) and 100000 (C41). In the last of the cases, C42, the transmissibility of the fault elongation was set to zero. BASECASE_3 was used for comparison. This study showed that the majority of the oil is flowing through the fault elongation. When closing the eastern part of the fault the oil from injector side to producer side of the fault is almost zero. The flow of water across the fault is still high and is most likely to flow through the other parts of the fault. By performing a visual inspection of the SGR-values along the fault (App C) it is revealed that some parts of the fault has relatively low SGR-values, which indicate that fault permeability is higher.

Applying different fault seal parameters are either opening or closing the fault, dependent on the parameter adjusted. In the cases where the fault transmissibility is reduced the effect of the injector will be less. Less water will in these cases flow through the fault and act as pressure maintenance when reservoir fluid is produced. The pressure on the producer side of the fault will for this reason be lower in these cases. Well P-12LP is injecting with constant rate in all cases and there will be a pressure build – up on the injector side when the fault is sealed. In the cases with reduced fault transmissibility the fluid flow across the fault will mainly occur through the fault elongation. This means that larger amount of oil will flow across the fault for these cases, because the pressure on the injector side becomes very high and the pressure on the producer will decrease. In other words, the pressure depletion on the producer side is compensated by oil and water flow through the fault elongation. In thigh cases the oil on the injector side will be produced faster and much of the oil on the producer side will not be produced, due to the fact that pressure maintenance is not high enough on this side of the fault.

Performing similar studies as the one discussed here for other parts of the model can give useful information about the dynamic properties of the faults. It is for instance, important to know if the fault transmissibility is high or low when planning new wells. It is also useful to define a region on each side of the fault to control how much fluid is flowing from injector to producer side of fault for different cases. If the fault is dominating the pressure drop from injector to producer, the effect of a new injector may not be so efficient. Such studies are though a time consuming process and it must be considered how much time that can be prioritized to perform studies like this.

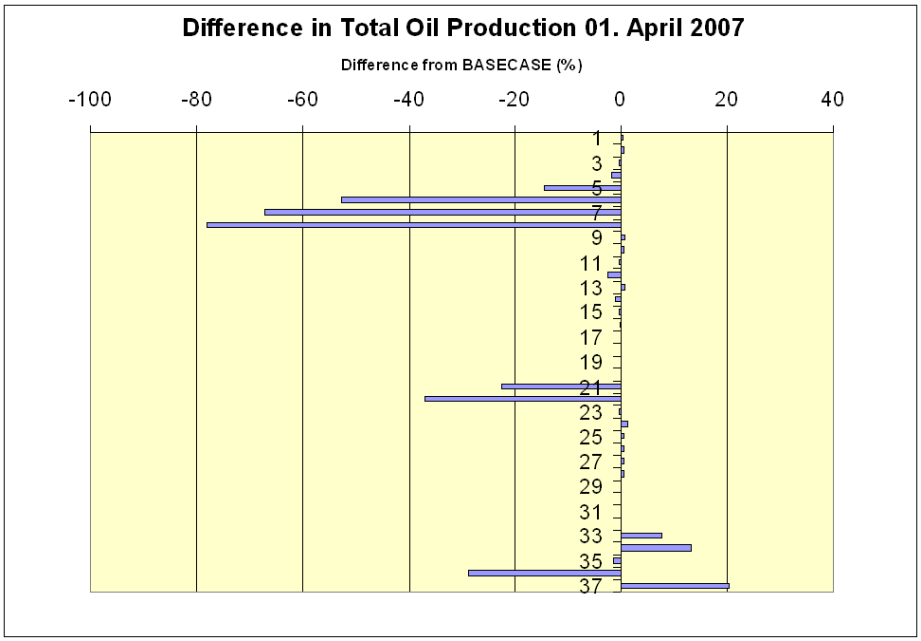

Figure 8-97 Difference (%) in total oil production at the end of the historical period for the different cases compared with the reference case (BASECASE_3)

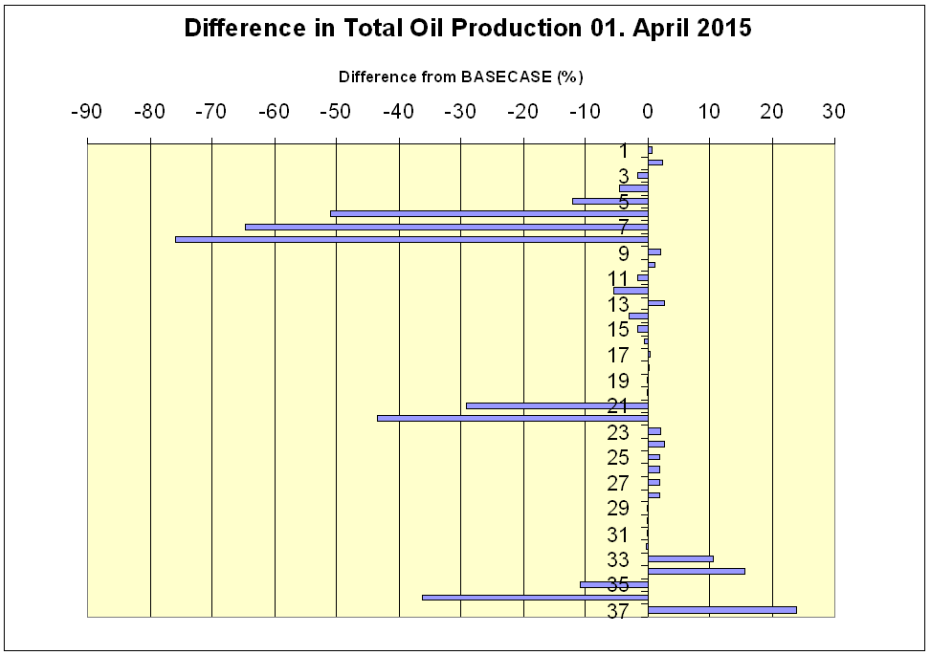

Figure 8-98 Difference (%) in predicted total oil production in 2015 for the different cases compared with the reference case (BASECASE_3)

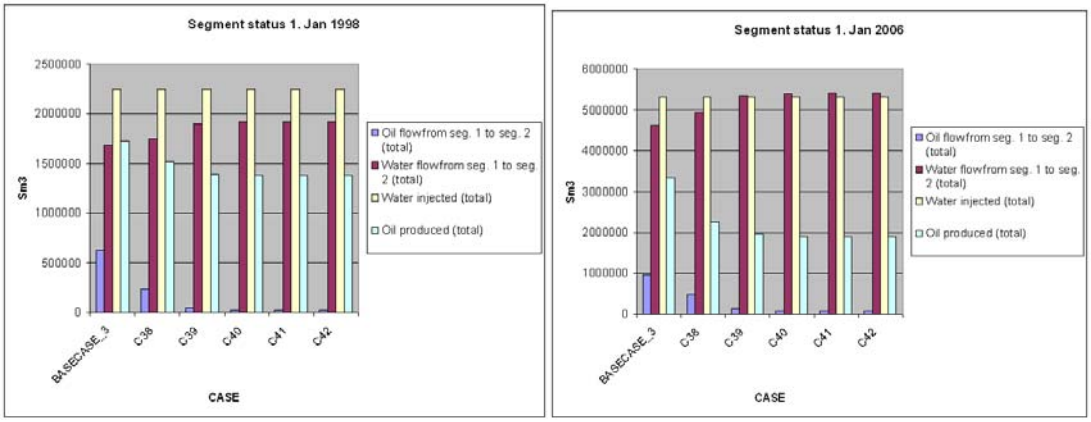

Figure 8-99 Segment status at two different times (1. of Jan 1998 and 1. of Feb 2006)

9 Conclusions

- Applying different fault transmissibility multipliers in the A-Lu model will have impact on the predicted Snorre performance. It is possible to achieve a satisfying history match for the different parts of the A-Lu model regarding RFT pressure and oil-, water- and gas production, when multiplying or dividing the fault transmissibility by different factors. This indicates that there is high uncertainty in the prediction runs for the A-Lu model.

- Increasing the fault transmissibility had largest impact in the NCFB, indicating that many fault are affecting the production from this area. In the EFB multiplying the fault transmissibility by a factor 5 had very small impact on the predicted performance of the fault block, compared with the expected case (A-Lu model)

- Predicted oil production until 2030 from the A-Lu model was compared with an alternative case, where fault transmissibility multipliers in the different fault blocks are modified by different factors. The difference in predicted oil production from the two cases was about 1.4 million Sm^3.

- Different parameters in RMSfaultseal can be used to change the transmissibility across the fault. The parameters are either increasing or reducing the fault zone permeability. Changeing of parameters like the SGR-curve, cementation factor, brittle factor and displacement-thickness ratio will all result in differences in predicted oil production from the segment compared with the reference case.

- The oblique slip angle will not have impact on the fault zone thickness for faults with small displacement. Large fault displacement and large oblique slip angles are needed to see the effect of this parameter on fault transmissibility.

- Using a cementation factor value of zero, which is supposed to make the fault sealing, did not have the effect as expected. It actually had the opposite effect and made the fault more open. No good explanation can be given to this behaviour.

- The fault throw has significant impact on the oil production from the segment. Increasing the fault throw will make much of the oil on the injector side of the fault unavailable, and this gives very limited oil production in these cases.

- The geological realizations used in the model will have high impact on the performance of the segment. Realization #5 which has a different stochastic distribution of sand in the channels gives almost 30 % lower predicted oil production than the reference case in 2015. Realization #10 where an alternative channel direction is applied also gives a dramatic reduction in predicted performance of the segment. In 2015 the predicted oil production differs with more than 40 % from the reference case. Realization #3, used in the models today, is the best alternative at the moment. The choice of geological realization is uncertain and testing of different realizations is required to find the one that matches the area/model the best.

- The algorithm used for predicting fault zone permeability will influence the predicted oil production. The Sperrevik algorithm and Manzocchi algorithm gave both higher predicted oil productions from the segment than the reference case. Both algorithms give a lower pressure drop across the fault than the reference case (Manzocchi algorithm gives the lowest). This indicates that these methods generate higher fault transmissibility than the SGR-curve method, which is applied in the reference case.

10 Nomenclature

10.1 Abbreviations

10.1.1 Eclipse keywords

Keyword	Operation
ADDZCORN	Changing the vertical position of grid blocks
ACTNUM	Used to indicate which grid blocks are active and which are inactive
AQUNUM	Used to incorporate one- dimensional numerical aquifers
BPR	Block Pressure
EDITNNC	Keyword used to modify fault generated non – neighbour connections
FGOR	Field Gas-Oil Ratio
FGORH	Field Gas-Oil Ratio History
FGPT	Field Gas Production Total
FGPTH	Field Gas Production Total History
FOPR	Field Oil Production Rate
FOPRH	Field Oil Production Rate History
FOPT	Field Oil Production Total
FOPTH	Field Oil Production Total History
FPR	Field Pressure
FWPR	Field Water Production Rate
FWPRH	Field Water Production Rate History
FWPT	Field Water Production Total
FWPTH	Field Water Production Total History
GOPR	Group Oil Production Rate
GOPRH	Group Oil Production Rate History
GOPT	Group Oil Production Total
GOPTH	Group Oil Production Total History
GWPR	Group Water Production Rate
GWPRH	Group Water Production Rate History
GWPT	Group Water Production Total
GWPTH	Group Water Production Total History
MINPV	Minimum pore volume a cell can have before it is inactivated
MULTFLT	Used to modify fault transmissibility (fault transmissibility multiplier)
MULTPV	Multiplier used on the pore volume to make the model match official 2D HCPV
MULTZ-	Transmissibility multiplier used to modify vertical transmissibility
PERMX	Permeability in x – direction
TRANX	Transmissibility in x - direction
TRANY	Transmissibility in y - direction
TZONE	Used to modify the water mobility in the transition zone.
WBHP	Well Bottom Hole Pressure
WGOR	Well GOR
WGORH	Well GOR History
WOPR	Well Oil Production Rate
WOPRH	Well Oil Production Rate History
WOPT	Well Oil Production Total
WOPTH	Well Oil Production Total History
WWPR	Well Water Production Rate
WWPRH	Well Water Production Rate History
WWPT	Well Water Production Total
WWPTH	Well Water Production Total History

10.1.2 Others

ALU-OLP-C3-FINAL-3	Official history matched A-Lunde model
4D	4 dimensional
BV	Bulk volume
CFB	Central Fault Block
ECFB	East Central Fault Block
EFB	Eastern Fault Block
EOR	Enhanced Oil Recovery
FW	Foot Wall
FWL	Free Water Level
FZ	Fault Zone
HCPV	Hydrocarbon Pore Volume
HW	Hanging Wall
IOR	Improved Oil Recovery
MSL	Mean Sea Level
NCFB	North Central Fault Block
NEFB	North Eastern Fault Block
NFB	Northern Fault Block
NTG	Net to Gross
OOIP	Oil Original In Place
PHID	Porosity
PI	Productivity Index
PLT	Production Logging Tool
PV	Pore volume
PVT	Pressure, Volume, Temperature
RFT	Repeat Formation Tester
SCAL	Special Core Analysis
SGR	Shale Gouge Ratio
SSF	Shale Smear Factor
SSP	Shale Smear Potential
TVD	True Vertical Depth
WFB	Western Fault block

10.2 Symbols

k_f : Fault zone permeability

P_c : Capillary pressure

P_t : Capillary entry pressure

V_f : Fault rock clay content

$z_{\max}$: Maximum burial depth

z_f : Depth at time of deformation

ρ_w : Density of wetting phase

ρ_{nw} : Density on non – wetting phase

σ : Interfacial tension

r_c : Radius of capillary

g : Gravitational constant

S_w : Water saturation

S_{wirr} :	Irreducible water saturation
$S_w(J)$:	J – function.
$CapillaryS_w$:	Capillary bound water
T_{mult} :	Fault transmissibility multiplier
K_{fw} :	Permeability of footwall cell
K_{hw} :	Permeability of hanging wall cell
W_{fz} :	Fault zone thickness
L_{fw} :	Grid cell dimension for footwall
L_{hw} :	Grid cell dimension for hanging wall
K_{fz} :	Fault zone permeability
SWL :	Connate water saturation
$SWCR$:	Critical water saturation
$SGCR$:	Critical gas saturation
D :	Fault displacement
S_{orw} :	Residual oil saturation to water
S_{org} :	Residual oil saturation to gas
T :	Transmissibility
k_{rw} :	Relative water permeability
h :	Heave
t :	Throw
BV_{up} :	Up scaled bulk volume
SV_{up} :	Up scaled sand volume
PV_{up} :	Up scaled pore volume
BV_{fine} :	Fine scale bulk volume
SV_{fine} :	Fine scale sand volume
PV_{fine} :	Fine scale pore volume
NTG_{up} :	Up scaled Net to Gross
$PORO_{up}$:	Up scaled porosity
H_{fine} :	Fine scale gross thickness
kh :	Permeability - thickness
θ :	Contact angle
K :	Cell Permeability
R :	Net to Gross ratio
S :	Contact area between grid blocks
SGR^{fw} :	SGR foot wall
SGR^{hw} :	SGR hanging wall
K_{fz}^{hw} :	Fault zone permeability hanging wall
K_{fz}^{fw} :	Fault zone permeability foot wall

11 References

Written references:

1. Agaev, G.S. et al. (2008): “Best Practice - 3D Reservoir Modelling”, version 1, internal report, StatoilHydro.

2. Amyx, J. W, Bass, D.M and Whiting, R. L (1988).: “Petroleum Reservoir Engineering”, New York, McGraw-Hill Book Company.

3. Aziz, K. & Settari, A (2002).: “Petroleum Reservoir Simulation”, Calgary, Alberta, Blitzprint Ltd.

4. Bø, Ø.: “Reservoir Model of the Snorre Field 2006, Fault - and Stratigraphic modelling on the Snorre Field” report RA-SNORRE-00262, Statoil

5. Cerveny, K. et al. (winter 2004/2005). “Reducing Uncertainty with Fault-Seal Analysis”. Oilfield Review, from http://www.slb.com/media/services/resources/oilfieldreview/ors04/win04/04_fault_seal_analysis.pdf.

6. Dake, L.P (1978). “Fundamentals of reservoir engineering”. Amsterdam, Elsevier Science Publishers B.V.

7. Eclipce (2008) Simulation Software Manuals 2008.1, Schlumberger

8. Fisher, Q.J., Jolley, S.J. (2007). “Treatment of faults in production simulation models”. Geological Society, London, Special Publications, **292**, 219-233

9. Fisher, Q.J. et al. (Jan. 2006). ”Microstructural and Petrophysical Properties of Fault Rocks from the Snorre Field”, Rock Deformation Research Group, report 9454.

10. Freeman, B et. al. (1998). “Fault seal prediction: the gouge ratio method”. In *Structural Geology in Reservoir Characterization* (edited by Coward, M.P., Daltaban, T.S. and Johnson, H.). Geological Society, London, Special Publications, **127**, 19-25.

11. Fristad, T. et al. (1997). “Quantitative fault seal prediction: a case study from Oseberg Syd”, In: *Hydrocarbon Seals: Importance for Exploration and Production* (edited by Møller-Pedersen, P. and Koestler, A.G), NPF Special Publications 7, pp 107-124.

12. Færseth, R.B. et al. (Sept. 2007).”Methodology for risking fault seal capacity: Implications of fault zone architecture”, American Association of Petroleum Geologists Bulletin, v. 91, no. 9, 1231 – 1246.

13. Harris, D. et al. (2002). “Using Shale Gouge Ratio (SGR) to model faults as transmissibility barriers in reservoirs: an example from the Strathspey Field, North Sea”, Petroleum Geoscience, Vol. 8, p. 167-176.

14. Håland, T.S. (2003) “Representation of Transmissibilities in Faulted Gas Reservoirs”, Department of Petroleum Technology. University of Stavanger.

15. Kleppe, H. (2008). Course compendium in reservoir simulation, University of Stavanger.

16. Knai, T.A. and Knipe, R.J. (1998). “The impact of faults on fluid flow in the Heidrun Field”. In: *Faulting, Fault Sealing and Fluid Flow in Hydrocarbon Reservoirs* (edited by Jones, G., Fisher, Q.J. and Knipe, R.J). Geological Society, London, Special Publications, **147**, 269 -282.

17. Knipe R.J. et al. (1997). “Fault seal analysis: successful methodologies, application and future directions”, In: *Hydrocarbon Seals: Importance for Exploration and Production* (edited by Møller-Pedersen, P. and Koestler, A.G), NPF Special Publications 7, pp 15-40.

18. Knipe, R.J, Jones, G and Fisher, Q.J (1998). “Faulting, fault sealing and fluid flow in hydrocarbon reservoirs: an introduction”. In: *Faulting, Fault Sealing and Fluid Flow in Hydrocarbon Reservoirs* (edited by Jones, G., Fisher, Q.J. and Knipe, R.J). Geological Society, London, Special Publications, **147**, vii -xxi.

19. Knott, S.D. (1993). “Fault Seal Analysis in the North Sea”. American Association of Petroleum Geologists Bulletin v. 77, No 5, pp 778-792.

20. Lescoffit, G. and Townsend, C. (2005). “Quantifying the Impact of Fault Modeling Parameters on Production Forecasting for Clastic Reservoirs”, In: *Evaluating Fault and Cap Rock Seals* (edited by Boult, P and Kaldi, J.). *AAPG Hedberg Series*, no 2, p 137-149.

21. Manzocchi, T. et al. (1999). “Fault transmissibility multipliers for flow simulation models”, Petroleum Geoscience, Vol. 5, pp. 53-63

22. Ottesen, S., Townsend, C. and Øverland K.M (2005). “Investigating the Effect of Varying Fault Geometry and Transmissibility on Recovery: Using a New Workflow for Structural Uncertainty Modeling in a Clastic Reservoir”, In: *Evaluating Fault and Cap Rock Seals* (edited by Boult, P and Kaldi, J.). *AAPG Hedberg Series*, no 2, p 125-136.

23. Reime, Mona. S. (2009). “Snorre Full field models-overview, products and use”, Presentation at “Geologiens dag”, 21.01.09 on Snorre.

24. ROXAR Software Solutions. (2008). Irap RMS Maintenance Release User Guide.

25. Seldal, M. et al (Nov. 2008). “Snorre Reservoir Development Plan 2008”, internal report, StatoilHydro.

26. Seldal, M. et al. (Oct. 2008). “Reservoir Model of the Snorre Field 2006, Simulation Models and History Matching”, report RA-SNORRE-00262, StatoilHydro.

27. Sperrevik, S. et al. (2002). “Empirical estimation of fault rock properties”, In: *Hydrocarbon Seal Quantification* (edited by Koestler, A.G and Hunsdale, R), NPF Special Publication 11, pp 109 -125.

28. Stromback, A. et al. “Reservoir Model of the Snorre Field 2006, Stochastic Modelling” report RA-SNORRE-00262, Statoil.

29. Sverdrup, E., Helgesen, J. and Vold, J. (Sept. 2003). ”Sealing properties of faults and their influence on water-alternating-gas injection effiency in the Snorre field, northern North Sea”. American Association of Petroleum Geologists Bulletin, **87**, 1437-1458

30. Vavra, C. L., Kaldi J.G. and Sneider R.M (1992). ”Geological Applications of Capillary Pressure: A Review”. American Association of Petroleum Geologists Bulletin v. 76, No 6, p 840-850.

31. Vølstad, A.M. (2006). “Fault impact on fluid flow simulation in different depositional settings – A quantitative sensitivity study”, Masterthesis, Department of Earth Science, University of Bergen.

32. Vølstad, A.M., Stromback, A. and Eik, S. (Feb. 2007) “Use of heterogeneous fault seal data in reservoir simulation and history matching of the Snorre Field”, abstract to Production Geoscience.

33. Welbon, A.I. et al. (1997). “Fault seal analysis in hydrocarbon exploration and appraisal: examples from offshore mid-Norway”, In: *Hydrocarbon Seals: Importance for Exploration and Production* (edited by Møller-Pedersen, P. and Koestler, A.G), NPF Special Publication 7, pp 125-138.

34. Yielding, G. (2002). “Shale Gouge Ratio – calibration by geohistory”, In: *Hydrocarbon Seal Quantification* (edited by Koestler, A.G and Hunsdale, R), NPF Special Publication 11, pp 1-15.

35. Yielding, G., Freeman, B. and Needham, D.T. (1997). “Quantitative Fault Seal Prediction”. American Association of Petroleum Geologists Bulletin, **81**, 897-917

36. Yielding, G., Øverland, J.J. and Byberg, G. (1999). “Characterization of Fault Zones for Reservoir Modeling: An Example from the Gullfaks Field, Northern North Sea”. American Association of Petroleum Geologists Bulletin, **83**, 925-951

Internet references:

37. Wikipedia. (2009). “Fault (geology)”. From http://en.wikipedia.org/wiki/Geologic_fault

Personal Communication:

38. Steinar Ekrann (2009), personal communication

12 Appendix

App A Faults and Fault Transmissibility Multipliers used in The A-Lu model

1st PRIORITY	
Fault name	Multiplier
'CSF_1'	1,0000
'CSF_2'	1,0000
'EWFC'	1,0000
'EWF_1'	1,0000
'EWF_2'	1,0000
'MNSF_1'	1,0000
'MNSF_2'	1,0000
'NB_2'	1,0000
'OSF_1'	1,0000
'WNSF_1'	0,0010
'WNSF_2'	1,0000
'W120'	1,0000
'C220'	1,0000
'W108'	1,0000
'W134'	1,0000
'W140'	1,0000
'W124'	1,0000
'C230'	0,0500
'W161'	0,0010
'W181'	1,0000
'OSF_3'	300,0000
'C226'	0,0100
'C260'	1,0000
'C280'	1,0000
'E301'	1,0000
'E306'	0,0001
'E310'	1,0000
'C243'	1,0000
'W185'	1,0000
'CSF_1a'	0,0001
'NC690'	1,0000
'N822'	1,0000
'EC445'	1,0000
'EC499'	1,0000
'EC450'	1,0000
'EC435'	1,0000
'NE545'	1,0000
'EC465'	1,0000
'EC445'	1,0000
'NW740'	1,0000
'NW750'	1,0000
'NW715'	1,0000
'NE515'	1,0000
'EC455'	1,0000
'E308'	0,0100
'NE510'	1,0000
'NC610'	1,0000
'E352'	100,0000
'E350'	1,0000
'NE515'	1,0000
'E328'	1,0000
'NC650'	1,0000
'E338'	1,0000
'E340'	1,0000
'N821'	1,0000
'W180'	0,0100
'W190'	1,0000
'C240'	1,0000
'C234'	0,0100
'W116'	1,0000
'OSF_2'	1,0000
'C250'	1,0000
'C222'	1,0000
'NC642'	1,0000
'NW725'	1,0000
'EC440'	1,0000
'W131'	1,0000
'W129'	1,0000
'W122'	1,0000
'C242'	1,0000
'E307'	1,0000
'W196'	1,0000
'W118'	1,0000
'W176'	1,0000
'E325'	0,0100

3rd PRIORITY	
Fault name	Multiplier
'C209'	1,0000
'C223'	1,0000
'C224'	0,0100
'C236'	1,0000
'C238'	0,0100
'C244'	1,0000
'C251'	1,0000
'C252'	1,0000
'C253'	1,0000
'C254'	1,0000
'C256'	1,0000
'C261'	1,0000
'C262'	1,0000
'E305'	1,0000
'E309'	1,0000
'E312'	0,0100
'E314'	1,0000
'E317'	1,0000
'E318'	0,1000
'E322'	1,0000
'E324'	1,0000
'E326'	1,0000
'E329'	1,0000
'E336'	1,0000
'E337'	1,0000
'E339'	1,0000
'E346'	1,0000

1st PRIORITY taken out from grid generation	
Fault name	Multiplier
'W182'	1,0000
'C232'	1,0000
'C241'	1,0000
'E354'	1,0000
'E348'	0,0000
'E334'	1,0000
'E360'	1,0000
'E358'	1,0000
'E316'	1,0000
'E333'	1,0000
'E370'	1,0000
'E327'	1,0000
'EC460'	1,0000
'NC680'	1,0000
'NC630'	1,0000
'NC629'	1,0000

Fault elongation/or division	
Fault name	Multiplier
'MNSF_1_1'	0,0200
'MNSF_1_2'	0,1000
'MNSF_1_3'	0,1000
'MNSF_1_4'	1,0000
'MNSF_1_5'	1,0000
'E328_1'	1,0000
'E328_2'	0,0000
'E328_3'	0,0000
'E325_1'	1,0000
'E325_2'	0,0100
'E325_3'	0,0100
'EWFC_1'	1000,0000
'EWFC_2'	10,0000
'EWFC_3'	0,2000
'EWFC_4'	0,0000
'EWF_1_NC'	1000,0000
'WNSF_1_1'	0,0010
'CSF_1_TO'	0,1000
'P9CH2'	0,1000
'E308_1'	0,0001
'W180_1'	0,0001
'C226_1'	0,0100
'C230_1'	0,5000
'C230_1B'	0,0030
'C230_2'	1,0000
'C230_3'	0,0100
'CSF_1A_1'	10000,0000

MEPO Adjusted faults	
Fault name	Multiplier
'OSF_1'	100,000000
'W120'	13,887031
'W134'	1,438050
'W161'	0,003369
'W181'	1,140127
'OSF_3'	613,119041
'W180'	0,079254
'W190'	0,515367
'W116'	7,811628
'OSF_2'	0,778978
'W131'	0,248008
'W129'	16,272472
'W180_1'	0,000142
'W132'	0,201041
'W159'	1,704987

App B Cases run on segment

(CASE11_3_1 = CASE11_3 and CASE24_3_1 = CASE24_3)

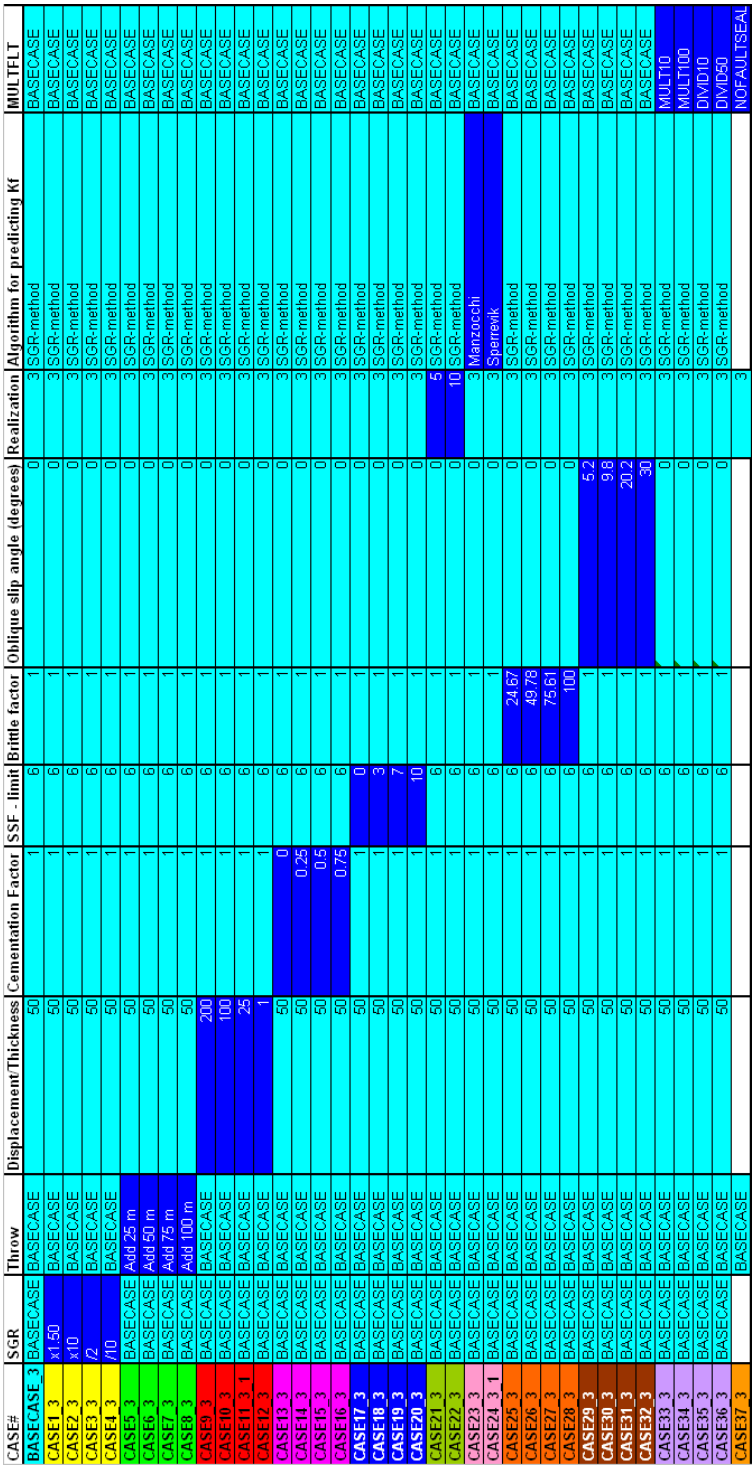

CASE#	SGR	Throw	Displacement Thickness	Cementation Factor	SSF - limit	Brittle factor	Oblique slip angle (degrees)	Realization	Algorithm for predicting Kf	MULTFLT
BASECASE_3	BASECASE	BASECASE	50	1	6	1	0	3	SGR-method	BASECASE
CASE1_3	x1.50	BASECASE	50	1	6	1	0	3	SGR-method	BASECASE
CASE2_3	x10	BASECASE	50	1	6	1	0	3	SGR-method	BASECASE
CASE3_3	/2	BASECASE	50	1	6	1	0	3	SGR-method	BASECASE
CASE4_3	/10	BASECASE	50	1	6	1	0	3	SGR-method	BASECASE
CASE5_3	Add 25 m	BASECASE	50	1	6	1	0	3	SGR-method	BASECASE
CASE6_3	Add 50 m	BASECASE	50	1	6	1	0	3	SGR-method	BASECASE
CASE7_3	Add 75 m	BASECASE	50	1	6	1	0	3	SGR-method	BASECASE
CASE8_3	Add 100 m	BASECASE	50	1	6	1	0	3	SGR-method	BASECASE
CASE9_3	BASECASE	BASECASE	200	1	6	1	0	3	SGR-method	BASECASE
CASE10_3	BASECASE	BASECASE	100	1	6	1	0	3	SGR-method	BASECASE
CASE11_3_1	BASECASE	BASECASE	25	1	6	1	0	3	SGR-method	BASECASE
CASE12_3	BASECASE	BASECASE	1	1	6	1	0	3	SGR-method	BASECASE
CASE13_3	BASECASE	BASECASE	50	0	6	1	0	3	SGR-method	BASECASE
CASE14_3	BASECASE	BASECASE	50	0.25	6	1	0	3	SGR-method	BASECASE
CASE15_3	BASECASE	BASECASE	50	0.5	6	1	0	3	SGR-method	BASECASE
CASE16_3	BASECASE	BASECASE	50	0.75	6	1	0	3	SGR-method	BASECASE
CASE17_3	BASECASE	BASECASE	50	1	0	1	0	3	SGR-method	BASECASE
CASE18_3	BASECASE	BASECASE	50	1	3	1	0	3	SGR-method	BASECASE
CASE19_3	BASECASE	BASECASE	50	1	7	1	0	3	SGR-method	BASECASE
CASE20_3	BASECASE	BASECASE	50	1	10	1	0	3	SGR-method	BASECASE
CASE21_3	BASECASE	BASECASE	50	1	6	1	0	5	SGR-method	BASECASE
CASE22_3	BASECASE	BASECASE	50	1	6	1	0	10	SGR-method	BASECASE
CASE23_3	BASECASE	BASECASE	50	1	6	1	0	3	Manzocchi	BASECASE
CASE24_3_1	BASECASE	BASECASE	50	1	6	1	0	3	Sperrevik	BASECASE
CASE25_3	BASECASE	BASECASE	50	1	6	24.67	0	3	SGR-method	BASECASE
CASE26_3	BASECASE	BASECASE	50	1	6	49.78	0	3	SGR-method	BASECASE
CASE27_3	BASECASE	BASECASE	50	1	6	75.61	0	3	SGR-method	BASECASE
CASE28_3	BASECASE	BASECASE	50	1	6	100	0	3	SGR-method	BASECASE
CASE29_3	BASECASE	BASECASE	50	1	6	1	5.2	3	SGR-method	BASECASE
CASE30_3	BASECASE	BASECASE	50	1	6	1	9.8	3	SGR-method	BASECASE
CASE31_3	BASECASE	BASECASE	50	1	6	1	20.2	3	SGR-method	BASECASE
CASE32_3	BASECASE	BASECASE	50	1	6	1	30	3	SGR-method	BASECASE
CASE33_3	BASECASE	BASECASE	50	1	6	1	0	3	SGR-method	MULT10
CASE34_3	BASECASE	BASECASE	50	1	6	1	0	3	SGR-method	MULT100
CASE35_3	BASECASE	BASECASE	50	1	6	1	0	3	SGR-method	DIVD10
CASE36_3	BASECASE	BASECASE	50	1	6	1	0	3	SGR-method	DIVD50
CASE37_3		BASECASE						3		NOFAULTSEAL

App C SGR – values for fault C230 (P-70)

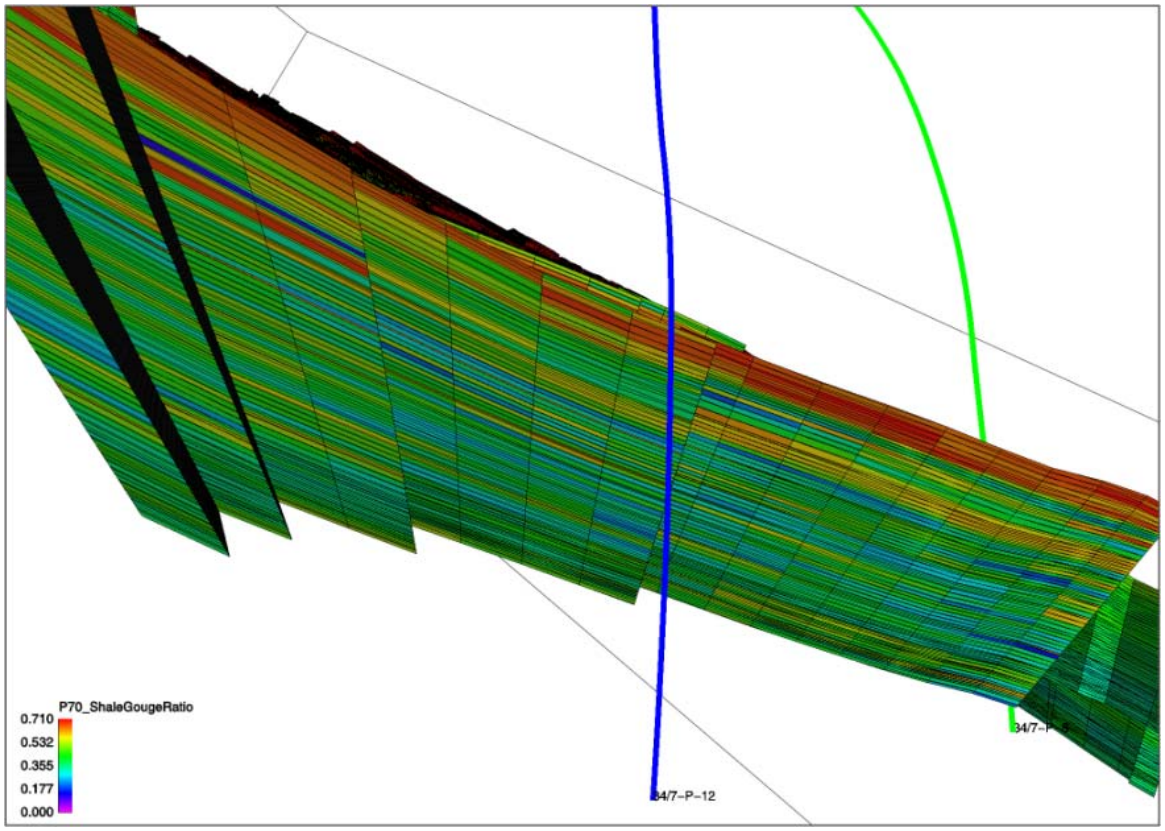

App D SGR-curves Used in Sensitivity Study

Phyllosilicate content host rock (%)	Fault permeability BASECASE (P-70)	Fault permeability x1.5	Fault permeability x10	Fault permeability /2	Fault permeability /10
0	3,16	4,74	31,6	1,58	0,316
2	2,21	3,315	22,1	1,105	0,221
5	1,26	1,89	12,6	0,63	0,126
7	0,87	1,305	8,7	0,435	0,087
10	0,4	0,6	4	0,2	0,04
15	0,08	0,12	0,8	0,04	0,008
20	0,01	0,015	0,1	0,005	0,001
25	0,0029	0,00435	0,029	0,00145	0,00029
30	0,0011	0,00165	0,011	0,00055	0,00011
35	0,0004	0,0006	0,004	0,0002	0,00004
40	0,00017	0,000255	0,0017	0,000085	0,000017
45	0,00008	0,00012	0,0008	0,00004	0,000008
50	0,00003	0,000045	0,0003	0,000015	0,000003
55	0,00002	0,00003	0,0002	0,00001	0,000002
100	0,00001	0,000015	0,0001	0,000005	0,000001

Table used to generate SGR curves

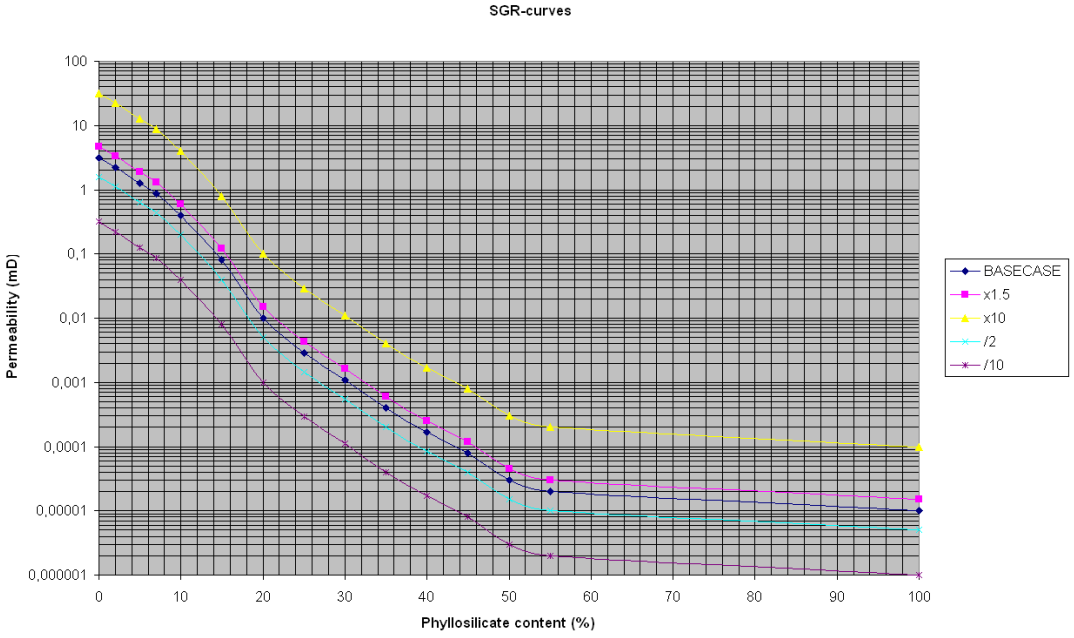

SGR-curves

App E Net to Gross Distribution for Realization #5 and Realization #10

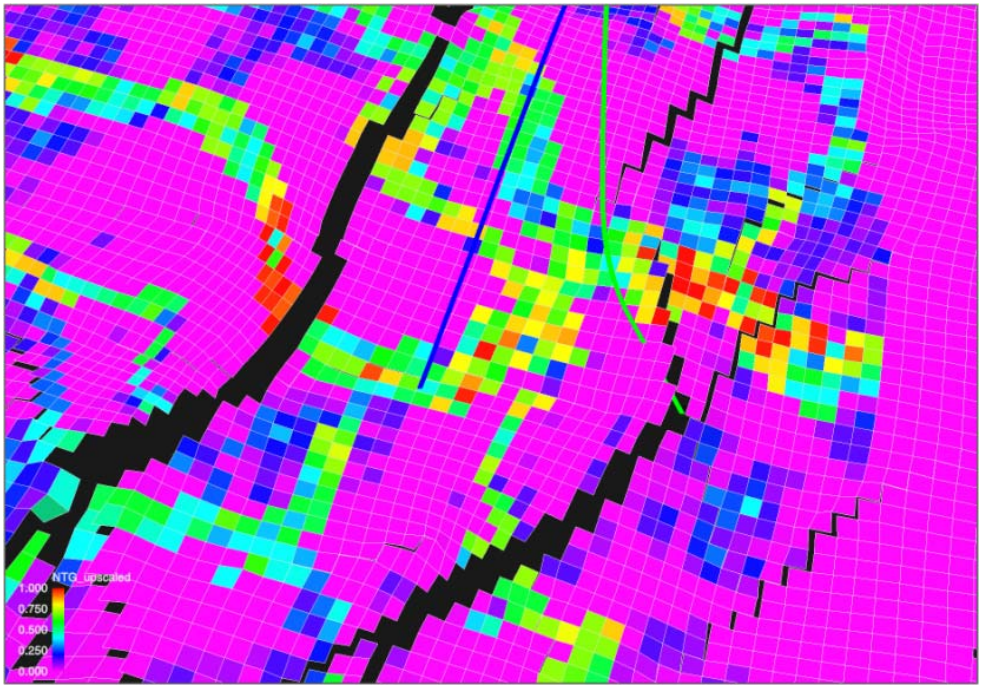

Realization #5

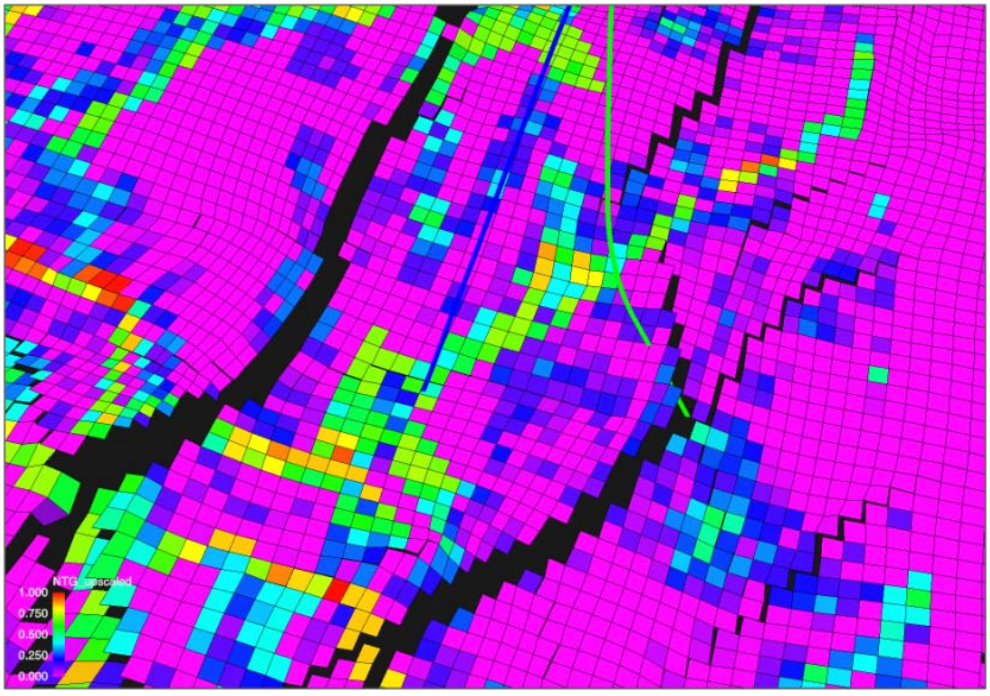

Realization #10